Multiple scales Analysis of the impact of a bending beam on a rigid surface

Auteur : Delcourt, Arnaud
Promoteur(s) : Denoel, Vincent
Faculté : Faculté des Sciences appliquées
Diplôme : Master en ingénieur civil physicien, à finalité approfondie
Année académique : 2018-2019
URI/URL : http://hdl.handle.net/2268.2/6716

University of Liege
Faculty of Applied Sciences
Academic Year 2018 - 2019

Multiple scales Analysis of the impact of a bending beam on a rigid surface

Supervisors: Vincent Denoël & Olivier Bruls

Graduation Studies conducted for obtaining the Master's degree in Physical Engineering by Arnaud Delcourt

June 6, 2019

Acknowledgements

First of all, I would like to thanks my supervisor Vincent Denoël for proposing me that interesting subject to work on. Thanks also to him and to Olivier Bruls for the weekly meetings we had together, they were very constructive and helpful to realize this thesis for both theoretical and simulations aspects.

A big thank-you also to Céline for her careful review of this paper and for her daily inducement.

Finally, I would like to thanks all my family for their sincere encouragement throughout this work.

Abstract

The purpose of this master thesis is to study the behavior of a bent beam impacting a rigid wall with the vibrating dynamics generated. This problem is recurrent in different fields of engineering. One example is the drilling in petroleum industry.

Two approaches are investigated: the analytical and numerical fields. The first objective is to study the leading order. Then, the purpose is to study the properties of the behavior at the second order.

In the analytical part, the perturbation method is used to separate the slow (natural vibration mode) and fast (impact of an infinitely long beam) dynamics. To solved separately these two dynamics, the multiple scales method is introduced and the matching will occur to satisfy the complementary condition of no penetration.

In the numerical simulations, a nonsmooth solver is used to represent the discontinuity. Indeed, with the activation of the unilateral constraint, a temporal discontinuity appears. Moreover, at the borders of the contact, a spatial discontinuity occurs. After an analysis on the numerical parameters, the results obtained by simulations are compared to those obtained theoretically.

For the majority of the results at leading order, the results obtained with both analytical and numerical approaches are consistent. The high order have also been introduced. However, we met troubles because of numerical errors and thus the only the tendencies could be observed. The tracks given in the end of this document may be investigated to get the matching.

Contents

1 Introduction

This report takes place in the context of a master thesis in physical engineering.

The problem to be investigated is a bent beam impacting a rigid wall with the vibrating dynamics generated.

In this part, the motivations and objectives will be investigated. For the analytic part, some related works will be used to develop the report as explained in the part "Related works". Finally, the organization of the document will be explained.

1.1 Motivations and objectives

This type of problem is present in different fields of engineering. One example is the drilling in petroleum industry. For the drilling structure, the drillstring impacts on the walls of the borehole provoking fatigue failure. The impact on theses walls are seen as a non-penetration condition which is kinematic compatibility. The dynamics effects due to the impact are source of vibrations of the beam. The flat wall during the impact will induce a modification of the geometry to satisfy the condition of no-penetration.

In this document, to model this dynamic, two approaches are investigated. The first approach is a semi-analytic which will use two time scales to represent the solution. By solving the fundamental solution with an impulsive force, the complementary condition can be written as function of the type of contact encountered. The second one is the numerical approach. A nonsmooth solver, including the unilateral constraints, will be used. Thus, the unilateral contact will characterized the impact between the beam and the wall by introducing an impact law.

Analytically, the goals are to verify the leading order and to continue at high order. Moreover, the second main goal was to apply a numerical approach to valid these results.

1.2 Related works

The subject was selected with the professor Vincent Denoël which has a scientific orientation for the research. Having taken the course "Perturbation methods", I was interested by this approach semi-analytic. M. Denoël proposed me to go deeper in this field for my master thesis.

In the analytic part, we restart with the information given in the paper [1]. The computation of the leading order are checked and slightly modified in this work. Then, the development to the second order analysis will be extended from that basis.

Concerning the numerical part, the non-smooth solver provided by the department of Olivier Brüls will be used. This solver includes a discretization model of the Euler-Bernoulli beam, the explicit time integration, the unilateral constraint. More details about this solver will be given in the appropriate sections.

1.3 Organization of the document

Firstly, the analytic approach is developed. A correct definition of the problem statement, including the assumptions made, is presented. A description of the perturbation methods and multiple scales is effectuated with one example to show the efficiency of this method. Then, the perturbation method is applied on the problem. The different types of contact will also be investigated. After that, the analysis can investigate the leading and high order in purpose to differentiate all the possible cases.

The main objective of the second part is to validate these results numerically. With a description on the discretization and the nonsmooth generalized-α method with the impact law. A numerical analysis is performed on the numerical parameters to see their influence on the results and the accuracy. Finally, the matching at the leading order and high order is made.

2 Analytic Part

In this first part, the problem statement is explained. Then, the complete development of the analytic solution will be realized until the second order by taking into account all the possible cases. To apply the analysis, the perturbation method will be introduced to solve the problem by multiple scales. To facilitate the task for the comparison with the numerical results, the analysis will be dimensionless. Before starting, the context must be set up to understand the studied situation. As explained in the introduction, the goal fixed with the supervisor Vincent Denoël for the analytic part is to restart with the information given in the paper [1] and to extend the development to the second order analysis.

2.1 Problem statement

The problem is to solve a naturally bent beam. This beam impacts an infinity rigid surface, *i.e.* there is no deformation nor displacement of the wall surface. The situation of the problem is represented in Figure 2.1.

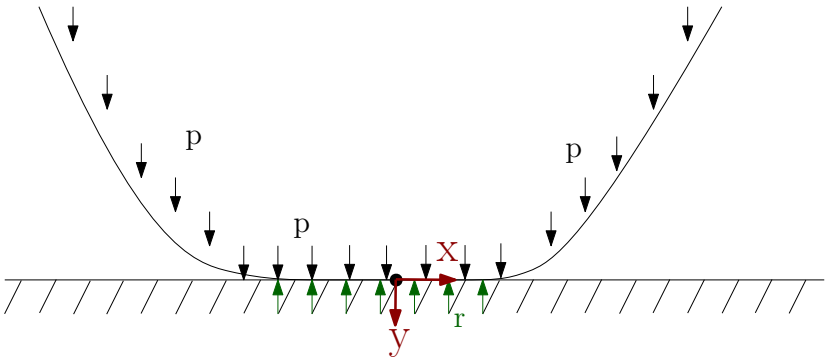

Figure 2.1: General representation of the problem.

For the representation of the model, the Euler–Bernoulli beam theory is applied. This theory does not take into account shear deformation compared to the Timoshenko theory. The Euler-Bernoulli is valid when the dimension lengths of the section are small compared to the length of the beam. For the Euler-Bernoulli model, the cross section orientation θ is matched with the gradient displacement dw/dx. Moreover, for the analytic part, the linearity of the equation is a major advantage to develop a semi-analytic approach. The governing equation is

$$\mu\partial_t^2 y + EI\partial_x^4 y = p(x,t) - r(x,t) \tag{2.1.1}$$

where t corresponds to the time, x is the abscissa and y the transverse displacement of the beam. The distributed external forces applied on the beam are represented by $p(x,t)$. When the beam impacts the horizontal rigid surface, a reaction force $r(x,t)$ occurs on the beam. Concerning the physical parameters, μ is the mass per unit length, EI the bending stiffness and the total length of the beam is L.

In this problem, gravity effect is neglected. Moreover, one should consider the fact that the problem is completely symmetric between the positive and negative x. The complementary condition of the no-penetration on the rigid surface is

$$0 \leq r(x,t) \perp y(x,t) \leq 0 \tag{2.1.2}$$

which represents the unilateral contact, called Signorini condition.

As shown in Figure 2.1, by convention, the origin of the axis is located at the level of the wall and at the middle of the beam (where the first contact occurs during the impact). For the y-axis, the positive convention is directed downwards. The uniform loading is positive in this direction. For the reaction force, the positive convention is in the up direction. Consequently, in Equation (2.1.1), a negative sign appears in front of the reaction force to be consistent with the convention. Considering the linear nature of the piece, the impact and the general movement of the beam due to uniform loading will be solved separately and combined to satisfy the complementary condition of no-penetration.

Two configurations are possible for the position x at time t:

- no contact between the beam and the surface: so no reaction force $r(x,t) = 0$ with $y(x,t) > 0$;
- contact between the beam and the surface: so reaction force $r(x,t) \neq 0$ with $y(x,t) = 0$.

To solve the problem, the concept of the multiple scales will used. It is introduced in the next section.

2.2 Perturbations methods- Multiple scales

Before going deeper in the problem, here is a reminder on perturbations methods and multiple scales [2] and [3].

The perturbation method allows to simplify complex problem to have shortest expressions and to have a better understanding of the problem. Perturbation methods are methods which rely on a dimensionless parameter ε. This parameter is very small ($0 < \varepsilon \ll 1$) and the purpose is to find an approximate solution for any problem. The ansatz solution of the problem, which is a perturbation series, can be written as

$$A = A_0 + \varepsilon A_1 + \varepsilon^2 A_2 + \mathcal{O}(\varepsilon^3) \tag{2.2.1}$$

where A_0 is the leading solution which solves the problem without perturbation and A_1, A_2,... are the solutions at higher order (they take into account the perturbation term).

A simple example is given by the following problem

$$x^2 - \varepsilon x - 1 = 0 \tag{2.2.2}$$

where $0 < \varepsilon \ll 1$. The two asymptotic roots of this equation are

$$x_1 = 1 + \frac{\varepsilon}{2} + \frac{\varepsilon^2}{8} + \mathcal{O}(\varepsilon^3) \qquad x_2 = -1 + \frac{\varepsilon}{2} - \frac{\varepsilon^2}{8} + \mathcal{O}(\varepsilon^3) \tag{2.2.3}$$

Moreover, the notion of multiple scales is introduced when the solution depends simultaneously on different scales. One interesting example is the Duffing's Oscillator where the governing equation is

$$\frac{d^2y}{dt^2} + y + \varepsilon y^3 = 0 \tag{2.2.4}$$

where ε is very small ($0 < \varepsilon \ll 1$) with the initial conditions $y(0) = 1$ and $y'(0) = 0$. A classical approach can be performed to find an asymptotic solution with the ansatz

$$y(t) = y_0(t) + \varepsilon y_1(t) + \mathcal{O}(\varepsilon^2) \tag{2.2.5}$$

giving at leading order (ε^0) and at first high order (ε^1)

$$(\varepsilon^0) : y_0'' + y_0 = 0 \qquad \text{with} \;\; y_0(0) = 1 \;\text{and}\; y_0'(0) = 0 \tag{2.2.6}$$
$$(\varepsilon^1) : y_1'' + y_1 + y_0^3 = 0 \;\; \text{with} \;\; y_1(0) = 0 \;\text{and}\; y_1'(0) = 0 \tag{2.2.7}$$

The solution can easily be determined

$$y(t) = \cos(t) + \varepsilon\left[\frac{1}{32}\big(\cos(3t) - \cos(t)\big) - \frac{3}{8}t\sin(t)\right] + \mathcal{O}(\varepsilon^2) \tag{2.2.8}$$

where the angular velocity ω_0 is equal to 1 ($\omega = 2\pi/T$).

The problem with this solution is that the last term evolves linearly with the time t. Consequently, when t is of the order ε, the high term becomes important and is not a small correction to the unperturbed solution.

To solve this problem, a new characteristic time must be introduced. Indeed, the solution $y(t)$ oscillates with a period of $T^{fast} \sim 1/\omega$ and the envelope of the solution is varying on the much longer timescale $T^{slow} = T^{fast}/\varepsilon$. Thus, we have

$$y(t, \tau) \qquad \text{and} \qquad \tau = \omega(\varepsilon)t \tag{2.2.9}$$

Using the asymptotic expansion of the form

$$y(\tau) = y_0(\tau) + \varepsilon y_1(\tau) + \mathcal{O}(\varepsilon^2) \tag{2.2.10}$$
$$\omega(\varepsilon) = \omega_0 + \varepsilon\omega_1 + \mathcal{O}(\varepsilon^2) \tag{2.2.11}$$

After calculations, the solution obtained is

$$y(\tau) = \cos(\tau) + \frac{1}{32}\varepsilon\big(\cos(3\tau) - \cos(\tau)\big) + \mathcal{O}(\varepsilon^2) \tag{2.2.12}$$

giving

$$y(t) = \cos(\omega t) + \frac{1}{32}\varepsilon\big(\cos(3\omega t) - \cos(\omega t)\big) + \mathcal{O}(\varepsilon^2) \tag{2.2.13}$$
$$\omega = 1 + \frac{3}{8}\varepsilon + \mathcal{O}(\varepsilon^2) \tag{2.2.14}$$

In Figure 2.2, with the classical ansatz solution using one time scale, the amplitude of oscillations increases due to the term $t\sin(t)$ which has a period of oscillation ω_0. With the multiple scales method, the solution can catch the behavior of the oscillator without amplification and the oscillation period is smaller than the classical ansatz solution.

In our impact beam problem, the multiple scales method will be applied by introducing two timescales:

- large timescale representing the natural vibrations mode of the beam.
- small timescale representing the propagation wave due to the impact of the beam on the rigid wall with uniform rigid body motion.

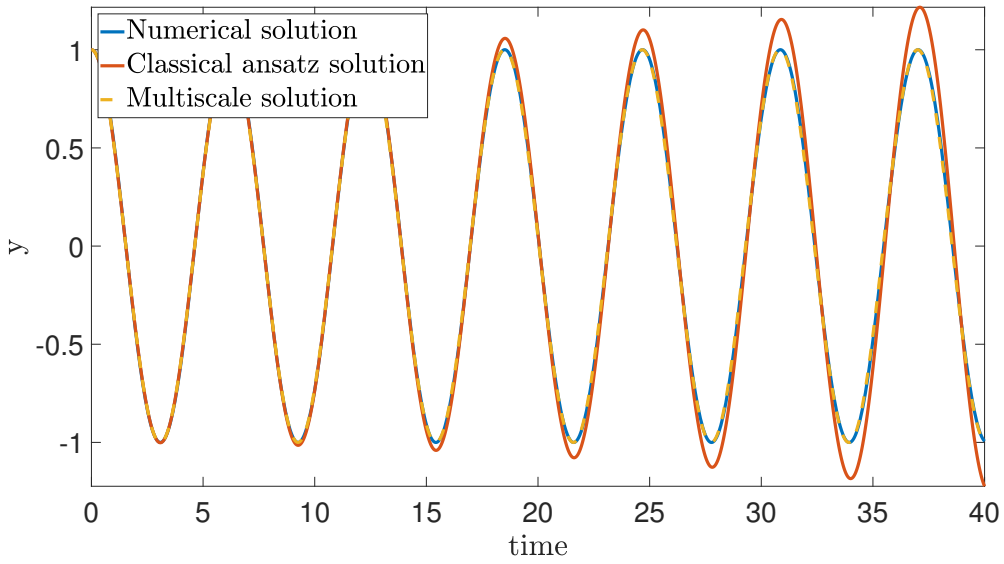

Figure 2.2: Duffing's Oscillator: numerical solution, classical ansatz solution and multiple scales solution.

2.2.1 Slow dynamics

As explained before, the period of the beam oscillations are present at a timescale which is large compared to the timescale of the wave propagation due to the impact. Before the impact on the rigid surface, the governing equation reads

$$\mu\partial_t^2 y_0 + EI\partial_x^4 y_0 = p(x,t) \tag{2.2.15}$$

where $y_0(x,t)$ is the slow dynamic solution. The reaction $r(x,t)$ on the wall is not present yet. A slow timescale can be introduced using the macroscopic properties

$$T^* = \sqrt{\frac{\mu L^{*4}}{EI}} \tag{2.2.16}$$

where

- $L^* = L/2$ is the half length of the beam $[m]$
- μ is the mass per unit length $[kg/m]$
- EI is the bending stiffness $[N \cdot m^2]$

A dimensional analysis can easily be applied

$$[T^*] = \sqrt{\frac{kg/m \cdot m^4}{N \cdot m^2}} = s \tag{2.2.17}$$

where $N = kg \cdot m/s^2$.
The dimensionless transverse displacement of the beam can be written as

$$\Gamma\left(\frac{x}{L^*}, \frac{t}{T^*}\right) = \frac{y_0(x,t)}{y^*} \tag{2.2.18}$$

where y^* is a scaling of the transverse displacement $y^* = p^* L^{*4}/EI$ obtained by defining a characteristic load per unit length p^*. This load represents $p(x,t)$. Γ is a function of order

1 (because $y \sim y^*$ and $p \sim p^*$) which characterizes the dimensionless displacement of the slow dynamic. This function Γ will be determined by applying the matching between the slow and fast dynamics. A dimensionless length and time can be defined by x/L^* and t/T^*, respectively. The slow dynamic involves important displacement and uniform loading, of order y^* and p^*, respectively.

2.2.2 Fast Dynamics

The fast dynamics occurs during the impact of the beam on the surface. The complementary condition must be applied on the governing equation. Using the piecewise linear nature of the problem, the complete solution is the sum of the slow and fast dynamics: $y(x,t) = y_0(x,t) - z(x,t)$. The minus sign is present due to the convention applied on the reaction force. Injecting the development of the total solution $y(x,t)$ in the governing equation, we have

$$\mu\partial_t^2(y_0 - z) + EI\partial_x^4(y_0 - z) = p(x,t) - r(x,t) \tag{2.2.19}$$

and using the equation (2.2.15) at slow dynamic, the governing equation at fast dynamic level is obtained

$$\mu\partial_t^2 z + EI\partial_x^4 z = r(x,t) \tag{2.2.20}$$

where the fast dynamics will take into account the complementary condition.

A timescale t^*, which is smaller than the timescale T^*, must be introduced in the slow dynamics by using the dimensionless parameter ε: $t^* = \varepsilon T^*$. As explained previously, the parameter ε is included in the interval $0 < \varepsilon \ll 1$. For the length scale, by comparing the differentiation orders with respect to time and space in the equation, a correct choice is $l^* = \sqrt{\varepsilon}L^*$. A dimensionless time and space are introduced in the fast dynamics

$$\tau = \frac{t}{t^*} \qquad \text{and} \qquad \xi = \frac{x}{l^*} \tag{2.2.21}$$

where $\partial_\tau = t^*\partial_t$ and $\partial_\xi = l^*\partial_x$. Using all theses definitions, the governing equation for the fast dynamics can be made dimensionless by the next steps

$$\frac{\mu}{\varepsilon^2 T^{*2}}\partial_\tau^2 z + \frac{EI}{\varepsilon^2 L^{*4}}\partial_\xi^4 z = r \tag{2.2.22}$$

$$\frac{\mu L^{*4}}{EI}\frac{1}{\varepsilon^2 T^{*2}}\partial_\tau^2 z + \frac{1}{\varepsilon^2}\partial_\xi^4 z = \frac{ry^*}{p^*} \tag{2.2.23}$$

$$\partial_\tau^2\left(\frac{z}{\varepsilon y^*}\right) + \partial_\xi^4\left(\frac{z}{\varepsilon y^*}\right) = \frac{r\varepsilon}{p^*} \tag{2.2.24}$$

Thus, the dimensionless displacement and reacting pressure on the wall can be deduced

$$\eta(\xi,\tau) = \frac{z(x,t)}{\varepsilon y^*} \qquad \text{and} \qquad \tilde{r} = \frac{r(x,t)\varepsilon}{p^*} \tag{2.2.25}$$

giving the dimensionless equation

$$\partial_\tau^2\eta + \partial_\xi^4\eta = \tilde{r} \tag{2.2.26}$$

Consequently, the fast dynamics is characterized by small displacements of order εy^* and high reaction pressure of order p^*/ε.

2.2.3 Matching of the solution

In perturbation methods, to solve problem with inner and outer solution, the technique is to solve the sub-problems separately and the limit cases between inner and outer solution are applied to match the two solutions together. Here, the idea is to develop, with a Taylor expansion, the function Γ around (0,0), meaning at the instant t=0, and at the middle of the beam, where the first contact occurs. Using the fact that $x/L^* = \sqrt{\varepsilon}\xi$ and $t/T^* = \varepsilon\tau$

$$y_0 = y^*\Gamma(\sqrt{\varepsilon}\xi, \varepsilon\tau) \tag{2.2.27}$$

$$= y^*\left[\Gamma(0,0) + \sqrt{\varepsilon}\xi\Gamma'(0,0) + \varepsilon\left(\frac{\xi^2}{2}\Gamma''(0,0) + \tau\dot{\Gamma}(0,0)\right) + \varepsilon\sqrt{\varepsilon}\left(\frac{\xi^3}{6}\Gamma'''(0,0) + \xi\tau\dot{\Gamma}'(0,0)\right)\right. \tag{2.2.28}$$

$$\left. + \varepsilon^2\left(\frac{\xi^4}{24}\Gamma''''(0,0) + \frac{\xi^2\tau}{2}\dot{\Gamma}''(0,0) + \frac{\tau^2}{2}\ddot{\Gamma}(0,0)\right) + \mathcal{O}(\varepsilon^{5/2})\right] \tag{2.2.29}$$

The convention taken are the followings: the prime symbol (') refers to differentiation with respect to the variable ξ and the dot ($\dot{}$) refers to differentiation with respect to the variable τ. Logically, $\Gamma(0,0) = \Gamma'(0,0) = 0$ because the position and the slope are null at the contact level to satisfy the complementary with the wall. At the instant of the impact, the velocity is positive ($\dot{\Gamma}(0,0) > 0$) meaning the beam moves in the downwards. Moreover, due to the convention of y, the curvature must be concave or null in this axis meaning $\Gamma''(0,0) \leq 0$. Using the fact that the problem is totally symmetric, the powers which are odd must be cancelled. Using all these conditions, the transverse displacement of the slow dynamic becomes

$$y_0 = y^*\left[\varepsilon\left(\frac{\xi^2}{2}\Gamma''(0,0) + \tau\dot{\Gamma}(0,0)\right) + \varepsilon^2\left(\frac{\xi^4}{24}\Gamma''''(0,0) + \frac{\xi^2\tau}{2}\dot{\Gamma}''(0,0) + \frac{\tau^2}{2}\ddot{\Gamma}(0,0)\right) + \mathcal{O}(\varepsilon^6)\right] \tag{2.2.30}$$

The idea is now to scale the slow dynamics into the same as the fast dynamic by dividing by εy^*

$$\frac{y_0}{\varepsilon y^*} = \frac{\Gamma(\sqrt{\varepsilon}\xi, \varepsilon\tau)}{\varepsilon} = \tau\nu - \frac{\xi^2}{2}\kappa + \varepsilon\left(\frac{\xi^4}{24}\psi + \frac{\xi^2\tau}{2}\chi + \frac{\tau^2}{2}\alpha\right) + \mathcal{O}(\varepsilon^2) \tag{2.2.31}$$

The variables are introduced by using the transverse displacement definition $y_0(x,t) = y^*\Gamma(x/L^*, t/T^*)$. The dimensionless curvature of the beam is

$$\kappa := -\Gamma''(0,0) = -\frac{\partial_x^2 y_0(0,0)L^{*2}}{y^*} \tag{2.2.32}$$

By simplicity to have the variable $\kappa \geq 0$, a minus sign is put. Then, the dimensionless velocity reads

$$\nu := \dot{\Gamma}(0,0) = \frac{\partial_t y_0(0,0)T^*}{y^*} \tag{2.2.33}$$

This dimensionless velocity must be positive because the beam moves in the direction of the wall to have the impact. If $\nu \leq 0$, no impact will occur on the wall which is not

the problem statement. Then, the dimensionless variable ψ is the fourth derivative with respect to the variable ξ

$$\psi := \Gamma''''(0,0) = \frac{\partial_x^4 y_0(0,0) L^{*4}}{y^*} \tag{2.2.34}$$

The dimensionless rate of change of the curvature χ reads

$$\chi := \dot{\Gamma}''(0,0) = \frac{\partial_x^2 \partial_t y_0(0,0) L^{*2} T^*}{y^*} \tag{2.2.35}$$

And finally, the dimensionless acceleration α is

$$\alpha := \ddot{\Gamma}(0,0) = \frac{\partial_t^2 y_0(0,0) T^{*2}}{y^*} \tag{2.2.36}$$

A matching must be applied between the slow and fast dynamic in the far field of the contact by cancelling the term $z(x,t)$ to obtain the solution $y(x,t) = y_0(x,t)$. The effect of the contact at infinity must not be present. Thus, the fast dynamic behavior must be

$$\lim_{\xi \to \pm\infty} \eta(\xi,t) = 0 \qquad \text{and} \qquad \lim_{\xi \to \pm\infty} \partial_\xi \eta(\xi,t) = 0 \tag{2.2.37}$$

These assumption will be verified later in the next section (Section 2.3).

The complementary condition of no-penetration can be written taking into account the fact that the total solution y must be equal to zero ($y(x,t) = y_0(x,t) - z(x,t) = 0$). It gives

$$y_0(x,t) = z(x,t) \tag{2.2.38}$$

$$\Leftrightarrow \quad y^* \Gamma(\sqrt{\varepsilon}\xi, \varepsilon\tau) = \varepsilon y^* \eta(\xi,\tau) \tag{2.2.39}$$

$$\Leftrightarrow \quad \eta(\xi,\tau) = \frac{\Gamma(\sqrt{\varepsilon}\xi, \varepsilon\tau)}{\varepsilon} \tag{2.2.40}$$

$$= \nu\tau - \kappa\frac{\xi^2}{2} + \varepsilon\left(\psi\frac{\xi^4}{24} + \chi\frac{\xi^2\tau}{2} + \alpha\frac{\tau^2}{2}\right) + \mathcal{O}(\varepsilon^2) \tag{2.2.41}$$

In the same way, the slope where the contact occurs must be equal to zero: $\partial_x y(x,t) = \partial_x y_0(x,t) - \partial_x z(x,t) = 0$ giving

$$\partial_\xi \eta(\xi,\tau) = \frac{\Gamma'(\sqrt{\varepsilon}\xi, \varepsilon\tau)}{\varepsilon} \tag{2.2.42}$$

$$= -\kappa\xi + \varepsilon\left(\psi\frac{\xi^3}{6} + \chi\tau\xi\right) + \mathcal{O}(\varepsilon^2) \tag{2.2.43}$$

Likewise, for the curvature, at the contact level, this physical parameter must be zero to follow the straight of the wall

$$\partial_\xi^2 \eta(\xi,\tau) = \frac{\Gamma''(\sqrt{\varepsilon}\xi, \varepsilon\tau)}{\varepsilon} \tag{2.2.44}$$

$$= -\kappa + \varepsilon\left(\psi\frac{\xi^2}{2} + \chi\tau\right) + \mathcal{O}(\varepsilon^2) \tag{2.2.45}$$

A timescale can be introduced for the fast dynamics using the dimensional macroscopic properties of the problem

$$t^* = \frac{1}{v_0^2}\sqrt{\frac{EI}{\mu}} \tag{2.2.46}$$

where a dimensional analysis is performed

$$[t^*] = \frac{1}{m^2/s^2}\sqrt{\frac{N \cdot m^2}{kg/m}} = s \tag{2.2.47}$$

where $N = kg \cdot m/s^2$. Knowing that $t^* = \varepsilon T^*$, a physical meaning can be found for the dimensionless parameter ε

$$\varepsilon = \frac{t^*}{T^*} = \frac{\frac{1}{V_0^2}\sqrt{\frac{EI}{\mu}}}{\sqrt{\frac{\mu L^{*4}}{EI}}} = \left(\sqrt{\frac{EI}{\mu}}\frac{1}{V_0 L^*}\right)^2 \tag{2.2.48}$$

To validate the assumption of multiple scales, parameter ε must be $\varepsilon \ll 1$ ($t^* \ll T^*$). Thus, it implies either the impact velocity V_0 is high or the beam L^* is long or heavy μ or very flexible EI. During the numerical part, this assumption will be verified to obtain correct results.

2.3 Fundamental Solution of the problem

To solve the impact beam problem as a function of the contact reaction type, the fundamental problem with an impulsive force at time τ at position ξ must be solved. The equation to solve is

$$\partial_\tau^2 \mathcal{K} + \partial_\xi^4 \mathcal{K} = \delta(\tau)\delta(\xi) \tag{2.3.1}$$

Using the frequency domain like in [4] and [5] where the complete development of calculation is effectuated, the solution of this problem can be written as

$$\mathcal{K}(\xi, \tau) = \sqrt{\frac{\tau}{2\pi}}\mathcal{H}\left(\frac{|\xi|}{\sqrt{\tau}}\right) \tag{2.3.2}$$

where the function $\mathcal{H}$ is defined as

$$\mathcal{H}(\beta) = \sqrt{\frac{\pi}{2}}\beta\left[\mathcal{S}\left(\frac{\beta}{\sqrt{2\pi}}\right) - \mathcal{C}\left(\frac{\beta}{\sqrt{2\pi}}\right)\right] + \sqrt{2}\sin\left(\frac{\pi + \beta^2}{4}\right) \tag{2.3.3}$$

The functions $\mathcal{S}$ and $\mathcal{C}$ are the Fresnel integrals which are defined as follow

$$\mathcal{C}(x) = \int_0^x \cos\left(\frac{\pi t^2}{2}\right)dt$$
$$\mathcal{S}(x) = \int_0^x \sin\left(\frac{\pi t^2}{2}\right)dt$$

In Figure 2.3, the function $\mathcal{H}$ is represented. At the infinity, the solution tends to zero. The derivative behaves in the same way at infinity with the solution going to zero. It allows to validate the matching between the fast and slow solution with $\lim_{\xi \to \pm\infty} \eta(\xi, t) = 0$ and $\lim_{\xi \to \pm\infty} \partial_\xi \eta(\xi, t) = 0$. Indeed, the fast solution η will be obtained by the convolution using the fundamental solution and the contact type reaction.

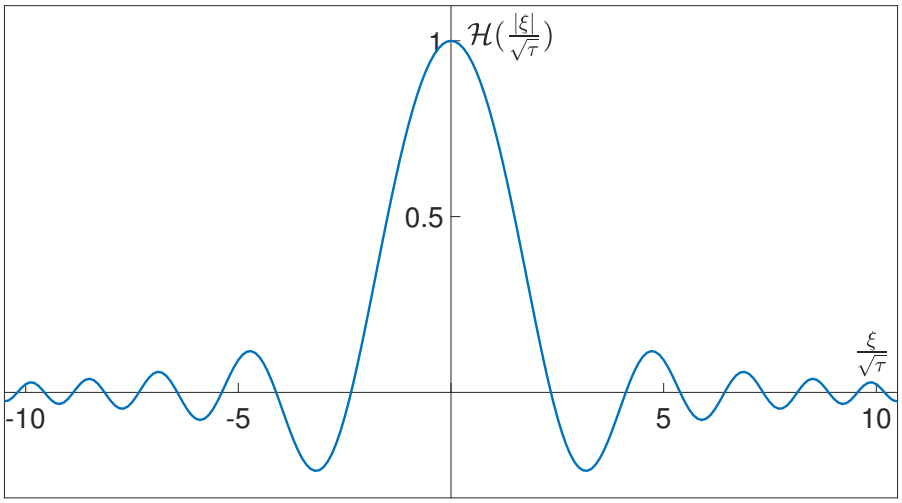

Figure 2.3: Function $\mathcal{H}(|\xi|/\sqrt{\tau})$.

2.4 Types of contact

Before solving directly the beam impact problem, one important factor to study is the kind of reaction contact that will occur between the two bodies. The complementary condition depends strongly to these contact reactions to avoid gap in the wall in order to obtain correct solution.

The three types of contact reaction are: discrete contact reaction, double contact reaction and continuous contact reaction.

2.4.1 Discrete contact reaction

Firstly, with the discrete contact reaction (Figure 2.4), only a reaction contact occurs at the middle of the beam, *i.e.* at $\xi = 0$ during all the impact time. Thus, at the position level, the reaction is characterized by a Dirac function $\delta(\xi)$. The reaction can be written as $\tilde{r}(\tau) = \tilde{R}(\tau)\delta(\xi)$ where the function $\tilde{R}$ evolves with time. Injecting in the fast dynamics to satisfy the condition, the problem to solve is

$$\partial_\tau^2 \eta + \partial_\xi^4 \eta = \tilde{R}(\tau)\delta(\xi). \tag{2.4.1}$$

By applying the convolution with the fundamental solution $\mathcal{K}$ until the time τ, the complementary condition can be written as

$$\eta(\xi,\tau) = \int_0^\tau \tilde{R}(\bar{\tau})\,\mathcal{K}(\xi,\tau-\bar{\tau})d\bar{\tau} = \frac{1}{\sqrt{2\pi}}\int_0^\tau \tilde{R}(\bar{\tau})\sqrt{\tau-\bar{\tau}}\,\mathcal{H}\left(\frac{|\xi|}{\sqrt{\tau-\bar{\tau}}}\right)d\bar{\tau}. \tag{2.4.2}$$

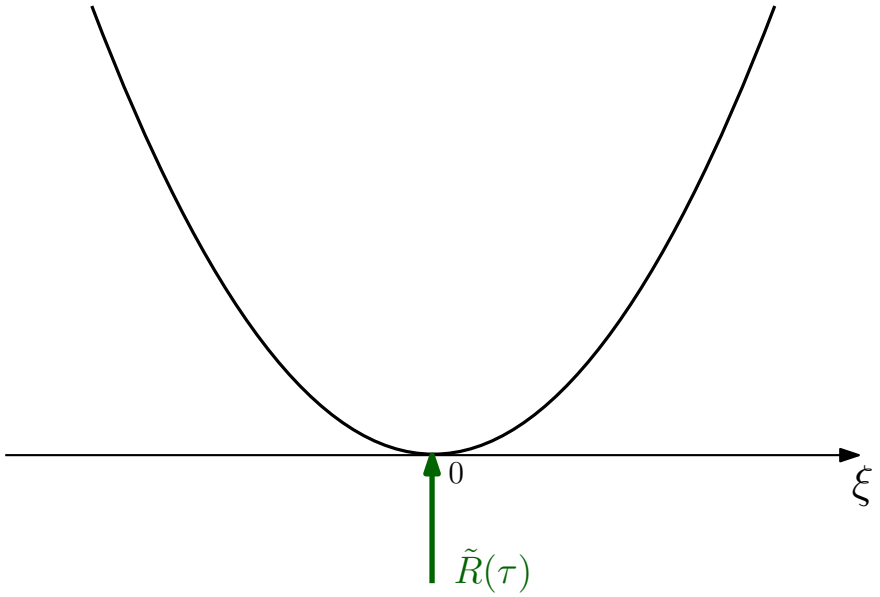

Figure 2.4: Discrete contact at $\xi = 0$ with the reaction contact $\tilde{R}(\tau)$.

2.4.2 Double contact reaction

The second contact is the double contact which propagates along the beam symmetrically from each side (Figure 2.5). This situation results from the discrete contact reaction which evolves with time. Indeed, all the beam starts to embed against the wall and consequently a propagation occurs at each side from the middle of the contact with a reaction. At any instant τ, the positions of the reaction of the contact are $\xi = \pm\lambda_c(\tau)$. In the same way than the discrete contact, the total reaction is the sum of the two reactions at $\xi = \pm\lambda_c(\tau)$: $\tilde{R}_T = 0.5 \cdot \tilde{R}(\tau)\delta(\xi - \lambda_c(\tau)) + 0.5 \cdot \tilde{R}(\tau)\delta(\xi + \lambda_c(\tau))$. Taking $\tau = 0$, the total reaction is logically identical to the discrete contact initially ($\tilde{R}_T(0) = \tilde{R}(0)\delta(0)$). With this contact reaction, the governing Euler equation is

$$\partial_\tau^2\eta + \partial_\xi^4\eta = \frac{1}{2}\tilde{R}(\tau)\delta\big(\xi - \lambda_c(\tau)\big) + \frac{1}{2}\tilde{R}(\tau)\delta\big(\xi + \lambda_c(\tau)\big). \tag{2.4.3}$$

Again, applying the convolution on the fundamental solution $\mathcal{K}$ with the new reaction contact at two points, the solution reads

$$\eta(\xi,\tau) = \frac{1}{2}\int_0^\tau \tilde{R}(\bar{\tau})\big[\mathcal{K}(\xi - \lambda_c(\bar{\tau}), \tau - \bar{\tau}) + \mathcal{K}(\xi + \lambda_c(\bar{\tau}), \tau - \bar{\tau})\big]d\bar{\tau} \tag{2.4.4}$$

$$= \frac{1}{2\sqrt{2\pi}}\int_0^\tau \tilde{R}(\bar{\tau})\sqrt{\tau - \bar{\tau}}\left[\mathcal{H}\left(\frac{|\xi - \lambda_c(\bar{\tau})|}{\sqrt{\tau - \bar{\tau}}}\right) + \mathcal{H}\left(\frac{|\xi + \lambda_c(\bar{\tau})|}{\sqrt{\tau - \bar{\tau}}}\right)\right]d\bar{\tau} \tag{2.4.5}$$

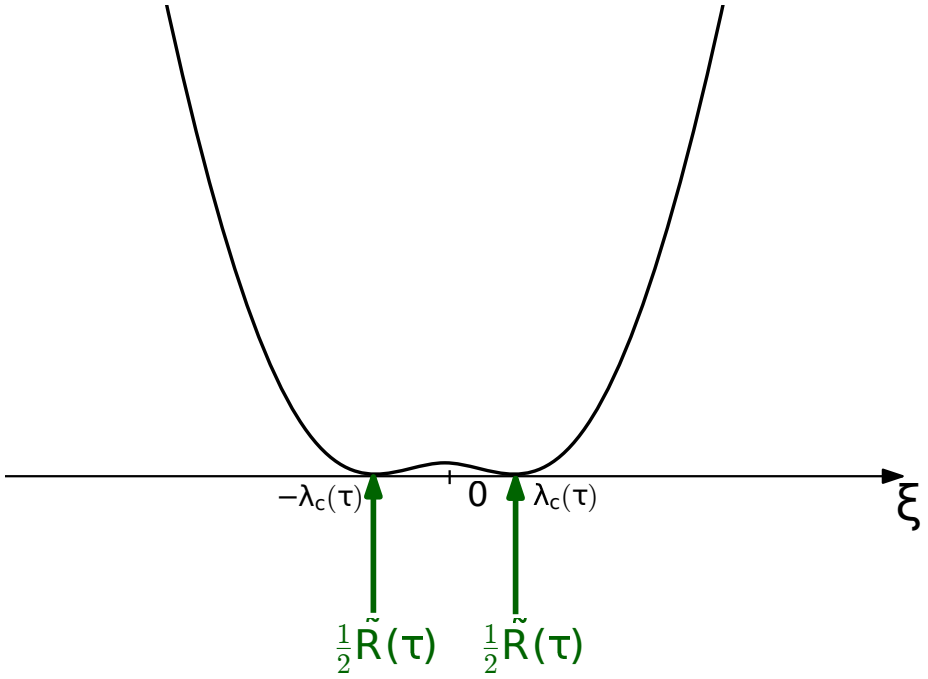

Figure 2.5: Double contact at $\xi = \pm\lambda_c(\tau)$ with the total reaction contact $\tilde{R}(\tau)$.

2.4.3 Continuous contact reaction

The last configuration corresponds to a continuous contact on the domain contact $\mathcal{D} = [-\lambda_c(\tau); \lambda_c(\tau)]$ which evolves with time τ (Figure 2.6). The reaction pressure $\tilde{r}(\xi, \tau)$ on the domain is assumed constant in time and space. The Euler equation is written as

$$\partial_\tau^2 \eta + \partial_\xi^4 \eta = \tilde{r}\big[H(\xi + \lambda_c(\tau)) - H(\xi - \lambda_c(\tau))\big] \tag{2.4.6}$$

where H is the Heaviside function.
The solution $\eta(\xi, \tau)$ is calculated with the convolution of the fundamental solution $\mathcal{K}$ until the time τ and on the domain contact $\mathcal{D}$

$$\eta(\xi, \tau) = \tilde{r} \int_0^\tau \int_{-\lambda_c(\bar{\tau})}^{\lambda_c(\bar{\tau})} \mathcal{K}(\xi - \bar{\xi}, \tau - \bar{\tau}) d\bar{\xi} d\bar{\tau} \tag{2.4.7}$$

$$= \tilde{r} \int_0^\tau \sqrt{\frac{\tau - \bar{\tau}}{2\pi}} \int_{-\lambda_c(\bar{\tau})}^{\lambda_c(\bar{\tau})} \mathcal{H}\left(\frac{|\xi - \bar{\xi}|}{\sqrt{\tau - \bar{\tau}}}\right) d\bar{\xi} d\bar{\tau} \tag{2.4.8}$$

where $\tilde{r}$ is independent of time and space in the domain contact $\mathcal{D}$.

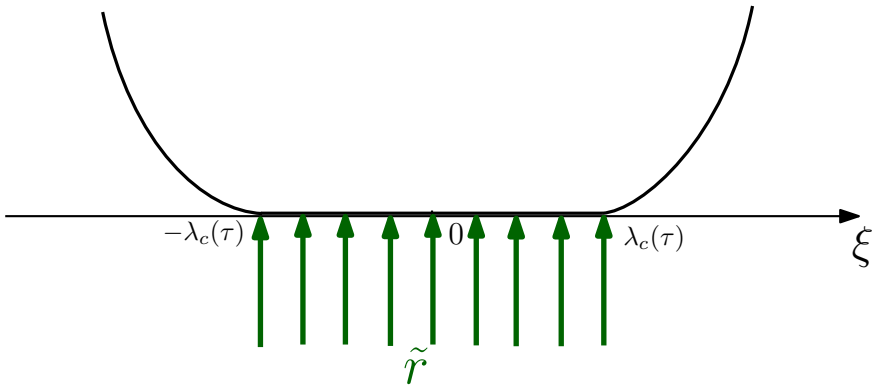

Figure 2.6: Continuous contact on domain $\mathcal{D} = [-\lambda_c(\tau); \lambda_c(\tau)]$ with the continuous reaction $\tilde{r}$.

2.5 Perturbation method- Ansatz

As it was previously explained in Section 2.2, the parameter ε will allow to separate the two time scales (*i.e.* the slow dynamics with the vibrating beam and the fast dynamics due to the impact). Using the usual ansatz, the fast solution is written as

$$\eta = \eta_0 + \varepsilon\eta_1 + \varepsilon^2\eta_2^2 + ... \tag{2.5.1}$$

$$= \nu\tau - \kappa\frac{\xi^2}{2} + \varepsilon\left(\psi\frac{\xi^4}{24} + \chi\frac{\xi^2\tau}{2} + \alpha\frac{\tau^2}{2}\right) + \mathcal{O}(\varepsilon^2) \tag{2.5.2}$$

For the continuous reaction, we will assume that the contact reaction $\tilde{r}$ is constant in time and space in the contact domain. It can be decomposed with the same ansatz

$$\tilde{r} = \tilde{r}_0 + \varepsilon\tilde{r}_1 + \varepsilon^2\tilde{r}_2 + ... \tag{2.5.3}$$

For the concentrated contact reaction $\tilde{r}$, the power separation is made using the usual ansatz as follows

$$\tilde{R}(\tau) = \tilde{R}_0(\tau) + \varepsilon\tilde{R}_1(\tau) + \varepsilon^2\tilde{R}_2(\tau) + ... \tag{2.5.4}$$

Injecting all these developments in the fast governing equation

$$\partial_\tau^2(\eta_0 + \varepsilon\eta_1 + ...) + \partial_\xi^4(\eta_0 + \varepsilon\eta_1 + ...) = r_0(\tilde{r}_0, \tilde{R}_0) + \varepsilon r_1(\tilde{r}_1, \tilde{R}_1) + ... \tag{2.5.5}$$

where r_0, r_1, ... regroup the continuous and concentrated reaction. Applying the perturbation method and balancing the similar power of ε yields to the following set of equations

$$\text{ord}(\varepsilon^0): \qquad \partial_\tau^2\eta_0 + \partial_\xi^4\eta_0 = r_0(\tilde{r}_0, \tilde{R}_0) \tag{2.5.6}$$

$$\text{ord}(\varepsilon^1): \qquad \partial_\tau^2\eta_1 + \partial_\xi^4\eta_1 = r_1(\tilde{r}_1, \tilde{R}_1) \tag{2.5.7}$$

Using the slow dynamics, the complementary condition is also decomposed into ε power

$$\text{ord}(\varepsilon^0): \qquad \eta_0(\xi, \tau) = \nu\tau - \kappa\frac{\xi^2}{2} \tag{2.5.8}$$

$$\text{ord}(\varepsilon^1): \qquad \eta_1(\xi, \tau) = \psi\frac{\xi^4}{24} + \chi\frac{\xi^2\tau}{2} + \alpha\frac{\tau^2}{2} \tag{2.5.9}$$

2.6 Leading order solution

The leading order equation will be investigated (ε^0). One interesting thing is to determine $\tilde{r}_0$ (which is constant in time and uniform in the contact domain) by injecting the solution η_0 in the governing equation at the order (ε^0)

$$\tilde{r}_0 = \partial_\tau^2\left(\nu\tau - \kappa\frac{\xi^2}{2}\right) + \partial_\xi^4\left(\nu\tau - \kappa\frac{\xi^2}{2}\right) \tag{2.6.1}$$

$$= 0 \tag{2.6.2}$$

Indeed, the total reaction r_0 is the sum of the continuous reaction $\tilde{r}_0$ (independent of the time and space) and the concentrated reaction $\tilde{R}_0$ which evolves in time and space. Consequently, at the leading order, no continuous reaction is induced by the fast dynamics to avoid the penetration in the wall. As a consequence, the continuous contact reaction is eliminated. Only concentrated reaction is possible in the problem which evolves with time and space. The two possible cases are the discrete contact reaction at $\xi = 0$ or the double contact reaction at $\xi = \pm\lambda_c(\tau)$. The following analysis uses the dimensionless parameters (ν, κ, ψ, χ and α) to find a criterion to distinguish discrete contact and continuous contact. The methodology is to study the cases separately and then to find the difference to obtain this condition.

2.6.1 Discrete contact reaction

The discrete case is firstly studied to find the function $\tilde{R}(\tau)$ to satisfy the complementary condition. After, the same analysis will be performed for the double contact reaction.
One can start from the general solution obtained for discrete contact reaction Equation (2.4.2) with $\xi = 0$ and using the ansatz on $\tilde{R}$

$$\eta_0(0,\tau) = \frac{1}{\sqrt{2\pi}}\int_0^\tau \tilde{R}_0(\bar{\tau})\sqrt{\tau - \bar{\tau}}d\bar{\tau}, \tag{2.6.3}$$

where the function $\mathcal{H}(0) = 1$. To satisfy the complementary condition, this contribution must be equal to the slow dynamics equation at the leading order at $\xi = 0$. It gives

$$\frac{1}{\sqrt{2\pi}}\int_0^\tau \tilde{R}_0(\bar{\tau})\sqrt{\tau - \bar{\tau}}d\bar{\tau} = \nu\tau \tag{2.6.4}$$

This equation is a general form of Abel integral equation. The complete resolution of this type of integral is effectuated in Appendix Appendix A.1. The solution $\tilde{R}_0$ is

$$\tilde{R}_0(\tau) = 2\sqrt{\frac{2}{\pi}}\frac{r_0}{\sqrt{\tau}} \tag{2.6.5}$$

The only way to satisfy the equation is to have $r_0 = \nu$ for discrete contact. With double reaction contact, the value r_0 will depend on others parameters than ν.

2.6.2 Double contact reaction

For the double contact reaction, the reaction contact occurs at $\xi = \pm\lambda_c(\tau)$. A continuous contact between the wall and the beam occurs on the domain $\mathcal{D} = [-\lambda_c(\tau); \lambda_c(\tau)]$. By simplicity of calculation, the complementary condition is written in $\xi = 0$. Using Equation (2.4.5), the governing equation of the fast dynamics at $\xi = 0$ is

$$\eta_0(0,\tau) = \frac{1}{2}\int_0^\tau \tilde{R}_0(\bar{\tau})\big[\mathcal{K}(-\lambda_c(\bar{\tau}), \tau-\bar{\tau}) + \mathcal{K}(\lambda_c(\bar{\tau}), \tau-\bar{\tau})\big]d\bar{\tau} \tag{2.6.6}$$

$$= \frac{1}{\sqrt{2\pi}}\int_0^\tau \tilde{R}_0(\bar{\tau})\sqrt{\tau-\bar{\tau}}\mathcal{H}\bigg(\frac{\lambda_c(\bar{\tau})}{\sqrt{\tau-\bar{\tau}}}\bigg)d\bar{\tau} \tag{2.6.7}$$

The complementary condition at $\xi = 0$ can be written as

$$\frac{1}{\sqrt{2\pi}}\int_0^\tau \tilde{R}_0(\bar{\tau})\sqrt{\tau-\bar{\tau}}\mathcal{H}\bigg(\frac{\lambda_c(\bar{\tau})}{\sqrt{\tau-\bar{\tau}}}\bigg)d\bar{\tau} = \nu\tau \tag{2.6.8}$$

With the solution obtained for $\tilde{R}_0$ (see Equation (2.6.5)), the complementary condition is

$$\frac{2r_0}{\pi}\int_0^\tau \sqrt{\frac{\tau-\bar{\tau}}{\bar{\tau}}}\mathcal{H}\bigg(\frac{\lambda_c(\bar{\tau})}{\sqrt{\tau-\bar{\tau}}}\bigg)d\bar{\tau} = \nu\tau \tag{2.6.9}$$

The contact evolution λ_c is a function of the parameter $\bar{\tau}$. However, the evolution of the law is unknown at this stage. A change of variable which is $u = \sqrt{(\tau-\bar{\tau})/\bar{\tau}}$ will be effectuated. It can be written as $\bar{\tau} = \tau/(1+u^2)$, the equation becomes

$$\frac{2r_0}{\pi}\int_0^\tau \sqrt{\frac{\tau-\bar{\tau}}{\bar{\tau}}}\mathcal{H}\bigg(\frac{\lambda_c(\bar{\tau})}{\sqrt{\tau-\bar{\tau}}}\bigg)d\bar{\tau} = -\frac{4r_0}{\pi}\int_*^* \frac{u^2\tau}{(1+u^2)^2}\mathcal{H}\bigg(\frac{\sqrt{1+u^2}}{\sqrt{\tau}u}\lambda_c\big(\frac{\tau}{1+u^2}\big)\bigg)du \tag{2.6.10}$$

$$= \frac{4r_0}{\pi}\int_0^{+\infty} \frac{u^2\tau}{(1+u^2)^2}\mathcal{H}\bigg(\frac{\sqrt{1+u^2}}{\sqrt{\tau}u}\lambda_c\big(\frac{\tau}{1+u^2}\big)\bigg)du \tag{2.6.11}$$

where $d\bar{\tau} = -2u\tau/(1+u^2)^2du$, $\bar{\tau} = 0 \to u = +\infty$ and $\bar{\tau} = \tau \to u = 0$. To satisfy the complementary in power τ, no dependence in τ must appear in the function $\mathcal{H}$. Consequently, the contact evolution λ_c is in the form

$$\lambda_c(\tau) = \lambda_0\sqrt{\tau} \tag{2.6.12}$$

where λ_0 is a coefficient to determine. λ_0 and r_0 are two unknowns which will be determined with the complementary condition at $\xi = 0$ at the level position and at the curvature level in order to obtain a system to solve.
The second derivative of η with respect to ξ is

$$\partial_\xi^2\eta_0(\xi,\tau) = \frac{r_0}{\pi}\int_0^\tau \frac{1}{\sqrt{\bar{\tau}(\tau-\bar{\tau})}}\bigg[\mathcal{H}''\bigg(\frac{|\xi-\lambda_c(\bar{\tau})|}{\sqrt{\tau-\bar{\tau}}}\bigg) + \mathcal{H}''\bigg(\frac{|\xi+\lambda_c(\bar{\tau})|}{\sqrt{\tau-\bar{\tau}}}\bigg)\bigg]d\bar{\tau} \tag{2.6.13}$$

At $\xi = 0$, the curvature of the beam can be determined

$$\partial_\xi^2 \eta_0(0,\tau) = \frac{2r_0}{\pi} \int_0^\tau \frac{1}{\sqrt{\bar{\tau}(\tau-\bar{\tau})}} \mathcal{H}''\left(\lambda_0 \sqrt{\frac{\bar{\tau}}{\tau-\bar{\tau}}}\right) d\bar{\tau} \tag{2.6.14}$$

The complementary condition can be written at the curvature level as

$$\partial_\xi^2 \eta_0(0,\tau) = \frac{2r_0}{\pi} \int_0^\tau \frac{1}{\sqrt{\bar{\tau}(\tau-\bar{\tau})}} \mathcal{H}''\left(\lambda_0 \sqrt{\frac{\bar{\tau}}{\tau-\bar{\tau}}}\right) d\bar{\tau} = -\kappa \tag{2.6.15}$$

which is independent of ξ with the slow dynamics. The system of two equations with 2 unknowns λ_0 and r_0 is formed.
By simplicity, we will introduce a parameter β for the analysis. Starting Equation (2.6.9), the change of variable $\beta = \lambda_0 \sqrt{\bar{\tau}/(\tau-\bar{\tau})}$ is applied

$$r_0 \varphi_\nu(\lambda_0)\tau = \nu\tau \tag{2.6.16}$$

$$\Leftrightarrow \quad r_0 \varphi_\nu(\lambda_0) = \nu \tag{2.6.17}$$

where $\varphi_\nu(\lambda)$ is defined as

$$\varphi_\nu(\lambda) := \frac{4}{\pi} \int_0^{+\infty} \frac{\lambda^3 \mathcal{H}(\beta)}{(\beta^2+\lambda^2)^2} d\beta \tag{2.6.18}$$

For the curvature beam condition, with the same change of variable $\beta = \lambda_0 \sqrt{\bar{\tau}/(\tau-\bar{\tau})}$, the complementary of no-penetration at the curvature level is

$$r_0 \varphi_\kappa(\lambda_0) = \kappa \tag{2.6.19}$$

where $\varphi_\nu(\lambda)$ is defined as

$$\varphi_\kappa(\lambda) := -\frac{4}{\pi} \int_0^{+\infty} \frac{\lambda \mathcal{H}''(\beta)}{\beta^2+\lambda^2} d\beta = \frac{-4}{\pi} \int_0^{+\infty} \frac{2\lambda\beta}{(\beta^2+\lambda^2)^2} \mathcal{H}'(\beta) d\beta = \frac{4}{\pi} \int_0^{+\infty} \frac{2\lambda(\lambda^2-3\beta^2)\mathcal{H}(\beta)}{(\beta^2+\lambda^2)^3} d\beta \tag{2.6.20}$$

where an integration by parts is effectuated (see Appendix A.2).

To avoid to solve completely the system, λ_0 can be obtained by applying the ratio of Equations (2.6.17) and (2.6.19) which cancels the dependence on r_0

$$\frac{\varphi_\kappa(\lambda_0)}{\varphi_\nu(\lambda_0)} = \frac{\kappa}{\nu} \tag{2.6.21}$$

Having λ_0 and using (2.6.17), the value r_0 is determined as follows

$$r_0 = \frac{\nu}{\varphi_\nu(\lambda_0)} \tag{2.6.22}$$

In Figure 2.7a, when the ratio $\varphi_\kappa/\varphi_\nu$ tends to 1, λ_0 tends to 0. It corresponds to the discrete contact because the contact zone does not evolve with time τ. In Figure 2.7b,

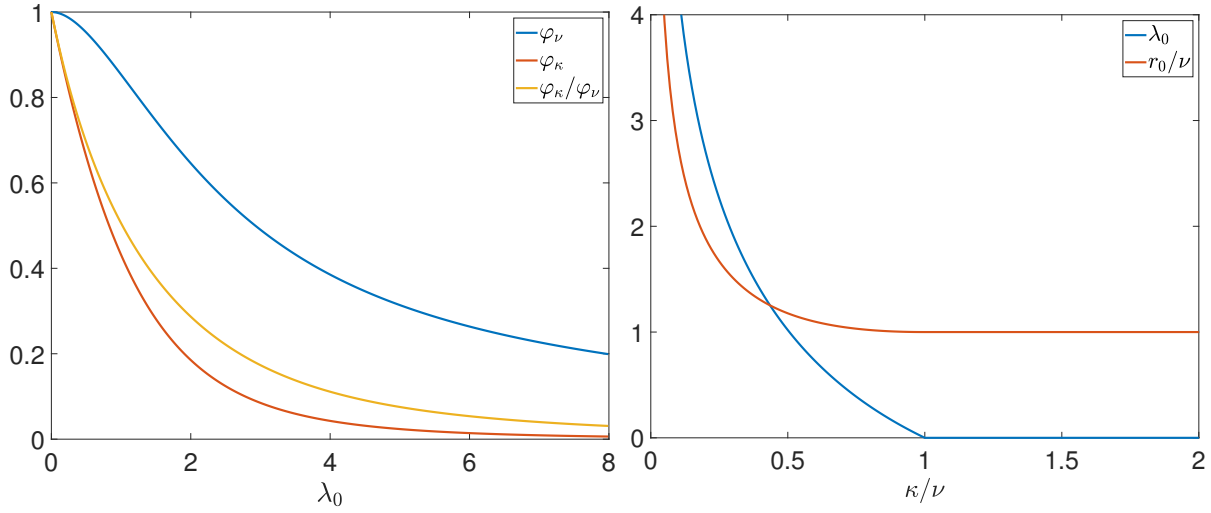

(a) Functions φ_ν, φ_κ and $\varphi_\kappa/\varphi_\nu$.

(b) Solutions λ_0 and r_0/ν.

Figure 2.7: Functions and solutions at leading order.

when the ratio κ/ν tends to 1, r_0/ν tends to 1, meaning at $\lambda_0 = 0$, the reaction r_0 is equal to ν which is totally in adequation with the solution from Abel equation. Thus, the reaction is nonzero at $\xi = 0$ in the discrete contact. Indeed, a force must be applied to avoid the penetration of the beam in the rigid surface. When the ratio κ/ν tends to 0, meaning either the speed of the impact ν tends to infinity either the beam is completely flat (no curvature). At the instant of impact, in this configuration, the contact zone propagates to infinity ($\lambda_0 \to \infty$) in both cases (infinite impact velocity or flat beam). Consequently, because the contact zone tends to infinity, the reaction contact also goes to infinity.

A criterion can easily be established to distinguish discrete contact and continuous contact

$$\frac{\kappa}{\nu} = \begin{cases} < 1 \Rightarrow & \text{Continuous contact} \\ \geq 1 \Rightarrow & \text{Discrete contact} \end{cases} \tag{2.6.23}$$

The complementary condition of no-penetration of the wall was applied at $\xi = 0$. The idea is now to check if the criterion is correct on the domain $\mathcal{D} = [-\lambda_c(\tau); \lambda_c(\tau)]$. The analytic demonstration will be applied at $\xi = \lambda_c(\tau)$. Then, a numerical approach will be made to prove the validity of the criteria on the entire domain $\mathcal{D}$ because of some problems are encountered to prove it analytically.

For the demonstration, at the position $\xi = \lambda_c(\tau) = \lambda_0\tau$ and using Equation (2.6.5), the solution of the governing equation is

$$\eta_0(\lambda_0\sqrt{\tau}, \tau) = \frac{r_0}{\pi} \int_0^\tau \sqrt{\frac{\tau - \bar{\tau}}{\bar{\tau}}} \left[\mathcal{H}\left(\lambda_0 \frac{\sqrt{\tau} - \sqrt{\bar{\tau}}}{\sqrt{\tau - \bar{\tau}}} \right) + \mathcal{H}\left(\lambda_0 \frac{\sqrt{\tau} + \sqrt{\bar{\tau}}}{\sqrt{\tau - \bar{\tau}}} \right) \right] \tag{2.6.24}$$

The integrand is split into two parts in order to apply a change of variable which is $\beta_\pm = \lambda_0 \dfrac{\sqrt{\tau} \pm \sqrt{\bar{\tau}}}{\sqrt{\tau - \bar{\tau}}}$. The complete development of this change of variable is made in

Appendix Appendix A.3. The fast solution becomes

$$\eta_0(\lambda_0\sqrt{\tau},\tau) = 16\lambda_0^3\tau \int_{\lambda_0}^{+\infty} \frac{\beta_+^2\mathcal{H}(\beta_+)}{(\beta_+^2+\lambda_0^2)^3}d\beta_+ \; + \; 16\lambda_0^3\tau \int_0^{\lambda_0} \frac{\beta_-^2\mathcal{H}(\beta_-)}{(\beta_-^2+\lambda_0^2)^3}d\beta_- \tag{2.6.25}$$

$$= 16\lambda_0^3\tau \int_0^{+\infty} \frac{\beta^2\mathcal{H}(\beta)}{(\beta^2+\lambda_0^2)^3}d\beta \tag{2.6.26}$$

where the two terms have the same integrand with different integration limits. They are complementary to cover the domain $[0;+\infty]$. The slow solution at first order at the position $\xi = \lambda_0\sqrt{\tau}$ and time τ is

$$\eta_0(\lambda_0\sqrt{\tau},\tau) = \nu\tau - \kappa\frac{\lambda_0^2\tau}{2} = r_0\tau\left(\varphi_\nu(\lambda_0) - \varphi_\kappa(\lambda_0)\frac{\lambda_0^2}{2}\right) \tag{2.6.27}$$

using the relations Equation (2.6.17) and Equation (2.6.19). With the definition of these 2 functions φ_ν and φ_κ, the slow solution becomes

$$\eta_0(\lambda_0\sqrt{\tau},\tau) = r_0\tau\left(\frac{4}{\pi}\int_0^{+\infty}\frac{\lambda_0^3\mathcal{H}(\beta)}{(\beta^2+\lambda_0^2)^2}d\beta - \frac{\lambda_0^2}{2}\frac{4}{\pi}\int_0^{+\infty}2\lambda_0\frac{(\lambda_0^2-3\beta^2)\mathcal{H}(\beta)}{(\beta^2+\lambda_0^2)^3}d\beta\right) \tag{2.6.28}$$

$$= r_0\tau\frac{16}{\pi}\int_0^{+\infty}\frac{\lambda_0^3\beta^2\mathcal{H}(\beta)}{(\beta^2+\lambda_0^2)^3}d\beta \tag{2.6.29}$$

The fast and slow solutions are identical, which proves that the no-penetration is also verified at the end of the contact zone.

To generalize to the domain $\mathcal{D}$, the parameter a is introduced. It varies inside the interval $[-1;1]$ to be in the domain

$$\xi = a\lambda_0\sqrt{\tau} \tag{2.6.30}$$

The slow solution reads

$$\eta_0(a\lambda_0\sqrt{\tau},\tau) = \nu\tau - \kappa\frac{a^2\lambda_0^2\tau}{2} = r_0\tau\left(\varphi_\nu(\lambda_0) - \frac{a^2\lambda_0^2}{2}\varphi_\kappa(\lambda_0)\right) \tag{2.6.31}$$

For the fast solution, the solution becomes

$$\eta_0(a\lambda_0\sqrt{\tau},\tau) = \frac{r_0}{\pi}\int_0^\tau\sqrt{\frac{\tau-\bar{\tau}}{\bar{\tau}}}\left[\mathcal{H}\left(\lambda_0\frac{|a\sqrt{\tau}-\sqrt{\bar{\tau}}|}{\sqrt{\tau-\bar{\tau}}}\right) + \mathcal{H}\left(\lambda_0\frac{|a\sqrt{\tau}+\sqrt{\bar{\tau}}|}{\sqrt{\tau-\bar{\tau}}}\right)\right]d\bar{\tau} \tag{2.6.32}$$

For the particular case of the discrete contact with the parameter $\lambda_0 = 0$, the terms in brackets of Equation (2.6.32) becomes $2\mathcal{H}(0)$. Thus, the fast and slow solutions at $\xi = 0$ satisfy the no-penetration condition

$$\eta_0(0,\tau) = \nu\tau \tag{2.6.33}$$

$$= \frac{r_0}{\pi}\int_0^\tau\sqrt{\frac{\tau-\bar{\tau}}{\bar{\tau}}}2\mathcal{H}(0)d\bar{\tau} = r_0\tau \tag{2.6.34}$$

where $\int_0^\tau\sqrt{(\tau-\bar{\tau})/\bar{\tau}}d\bar{\tau} = \pi\tau/2$. The relation $r_0 = \nu$ is recovered.

In Figure 2.8, the superposition of the slow (2.6.31) and fast dynamics (2.6.32) are shown numerically for different cases of continuous contact. In the contact domain which is $\mathcal{D} = [-1; 1]$, the two solutions are as expected identical meaning that the no-penetration condition is satisfied on the entire contact domain $\mathcal{D}$.

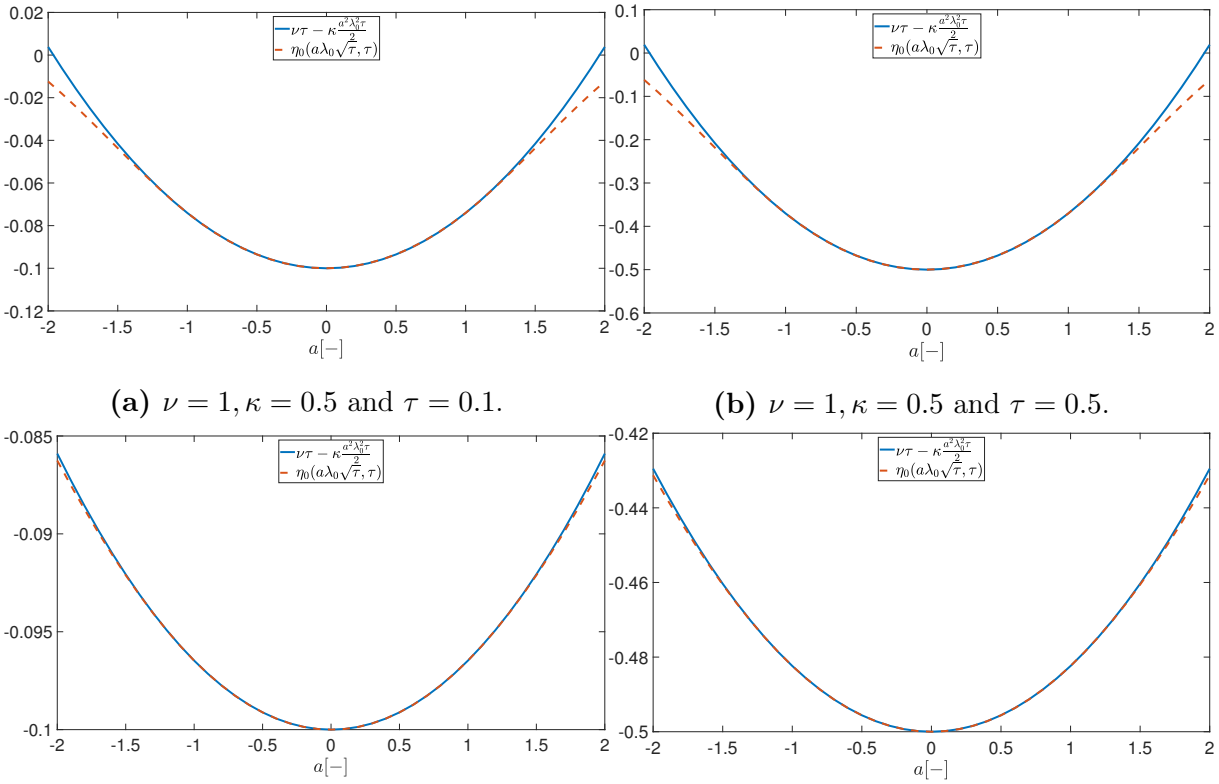

(a) $\nu = 1, \kappa = 0.5$ and $\tau = 0.1$.

(b) $\nu = 1, \kappa = 0.5$ and $\tau = 0.5$.

(c) $\nu = 1, \kappa = 0.8$ and $\tau = 0.1$.

(d) $\nu = 1, \kappa = 0.8$ and $\tau = 0.5$.

Figure 2.8: Complementary condition expressed as function of a for different values ν, κ and instant times τ for the leading order.

As a reminder, the slow solution of the bent beam at leading order is

$$\eta_0(\xi, \tau) = \nu\tau - \kappa\frac{\xi^2}{2} \tag{2.6.35}$$

Knowing the dimensionless velocity ν and curvature κ, the type contact can easily be determined by the ratio of these 2 parameters. In the discrete contact case, the complementary solution to satisfy the no-penetration is

$$\eta_0(\xi, \tau) = \frac{2\nu}{\pi}\int_0^\tau \sqrt{\frac{\tau - \bar{\tau}}{\bar{\tau}}}\mathcal{H}\left(\frac{|\xi|}{\sqrt{\tau - \bar{\tau}}}\right)d\bar{\tau} \tag{2.6.36}$$

and for the continuous contact, the solution becomes

$$\eta_0(\xi, \tau) = \frac{r_0}{\pi}\int_0^\tau \sqrt{\frac{\tau - \bar{\tau}}{\bar{\tau}}}\left[\mathcal{H}\left(\frac{|\xi - \lambda_c(\bar{\tau})|}{\sqrt{\tau - \bar{\tau}}}\right) + \mathcal{H}\left(\frac{|\xi + \lambda_c(\bar{\tau})|}{\sqrt{\tau - \bar{\tau}}}\right)\right]d\bar{\tau} \tag{2.6.37}$$

In both cases, the parameters λ_0 and r_0 can be determined and then injected in the fast dynamics to satisfy the complementary condition.

In Figure 2.9, the resolution of the analytic problem is effectuated in the two cases. On the left column of the Figure, the continuous reaction with a double reaction contact is represented for $\kappa = 0.5$ and $\nu = 1$ at different time τ. As expected, the beam impacts the wall with the propagation of the contact domain. On the right column of the Figure, this situation illustrates clearly the discrete contact and reaction with $\kappa = 2$ and $\nu = 1$ at the same instants of time τ. In both cases, when the time increases, the fast dynamics solution increases logically to compensate the gap in the wall that the slow solution generates.

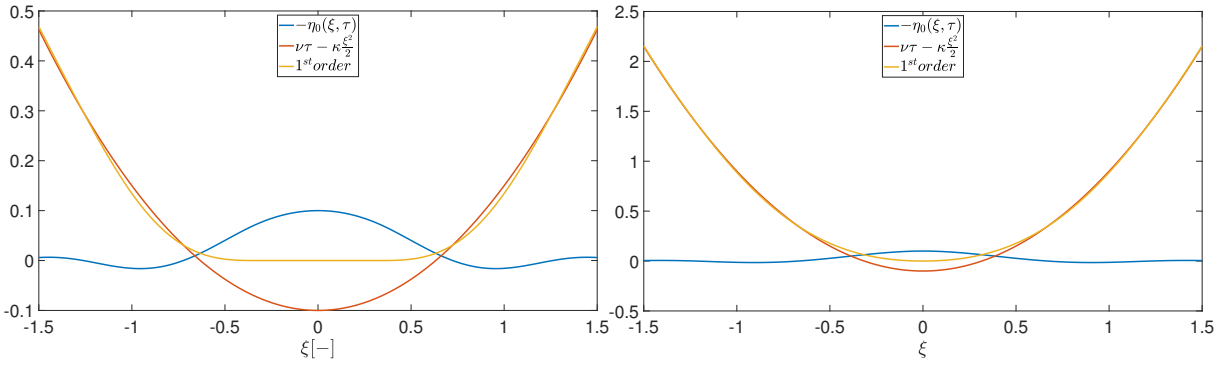

(a) $\kappa = 0.5$, $\nu = 1$ and $\tau = 0.1$.

(b) $\kappa = 2$, $\nu = 1$ and $\tau = 0.1$.

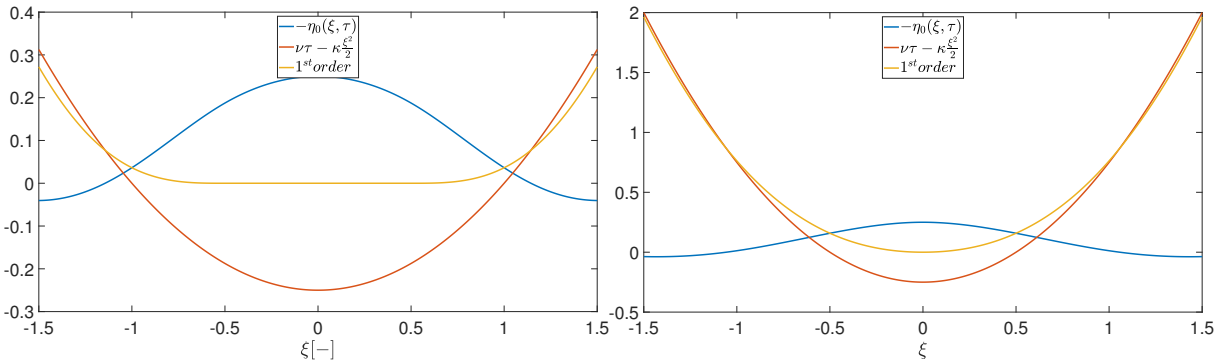

(c) $\kappa = 0.5$, $\nu = 1$ and $\tau = 0.25$.

(d) $\kappa = 2$, $\nu = 1$ and $\tau = 0.25$.

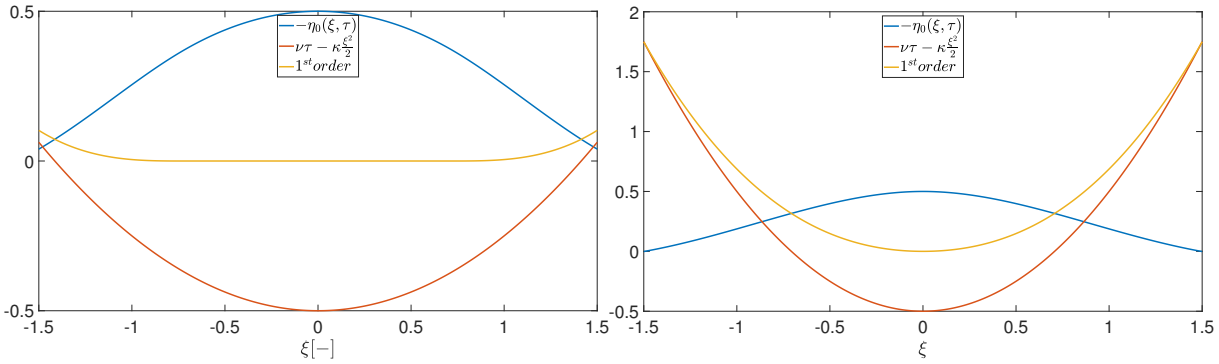

(e) $\kappa = 0.5$, $\nu = 1$ and $\tau = 0.5$.

(f) $\kappa = 2$, $\nu = 1$ and $\tau = 0.5$.

Figure 2.9: Beam impacting a rigid surface as function the parameters κ, ν at different times τ for the leading order. On the left column, a continuous contact impact and on the right column a discrete contact at the middle of the beam.

2.7 High order solution

The high order equation would be investigated by using the results obtained at leading order. Like it was the case at leading order, we verify firstly if there is an uniform reaction on the contact domain (which is the term $\tilde{r}_1$). Injecting the usual ansatz of fast dynamics at the high order η_1 in the governing equation

$$\tilde{r}_1 = \partial_\tau^2\left(\psi\frac{\xi^4}{24} + \chi\frac{\xi^2\tau}{2} + \alpha\frac{\tau^2}{2}\right) + \partial_\xi^4\left(\psi\frac{\xi^4}{24} + \chi\frac{\xi^2\tau}{2} + \alpha\frac{\tau^2}{2}\right) \tag{2.7.1}$$

$$= \alpha + \psi \tag{2.7.2}$$

A constant reacting pressure $\tilde{r}_1$ is applied along the contact zone which depends only on the second derivative of the curvature ψ and the acceleration α. If $\alpha + \psi > 0$, a positive reaction occurs meaning that the external loading is applied in the opposite direction of the movement of the beam to avoid penetration in the wall. In the other case, $\alpha+\psi < 0$, no uniform reaction must be take into account to avoid the penetration in the fast dynamics because a progressive detachment of the beam will occur in the middle. Consequently, the dynamics can be completely different as a function of the sign of the sum of these two terms.

2.7.1 Continuous contact with double reaction forces and continuous reaction

To obtain a continuous contact, the condition $\nu > \kappa$ must be respected (this result comes from the leading order) provoking a double reaction forces at the contact zone extremity $\lambda_c(\tau)$ and the distributed reaction because to $\alpha + \psi > 0$. The general fast dynamics response $\eta(\xi, \tau)$ including the leading and the high order is

$$\eta(\xi,\tau) = \eta_0(\xi,\tau) + \varepsilon\eta_1(\xi,\tau) = \tilde{r}\int_0^\tau \sqrt{\frac{\tau-\bar{\tau}}{2\pi}} \int_{-\lambda_c(\bar{\tau})}^{\lambda_c(\bar{\tau})} \mathcal{H}\left(\frac{|\xi-\bar{\xi}|}{\sqrt{\tau-\bar{\tau}}}\right) d\bar{\xi}d\bar{\tau}$$

$$+\frac{1}{2\sqrt{2\pi}}\int_0^\tau \tilde{R}(\bar{\tau})\sqrt{\tau-\bar{\tau}}\left[\mathcal{H}\left(\frac{|\xi-\lambda_c(\bar{\tau})|}{\sqrt{\tau-\bar{\tau}}}\right) + \mathcal{H}\left(\frac{|\xi+\lambda_c(\bar{\tau})|}{\sqrt{\tau-\bar{\tau}}}\right)\right] d\bar{\tau} \tag{2.7.3}$$

where the first term corresponds to the continuous reaction and the second to the double contact reaction. As explained previously, the uniform reaction is written as the usual ansatz

$$\tilde{r} = \tilde{r}_0 + \varepsilon\tilde{r}_1 \tag{2.7.4}$$

$$= \varepsilon(\alpha + \psi) \tag{2.7.5}$$

At leading order, to satisfy the evolution in order τ, the contact length must be at order $\sqrt{\tau}$ as developed previously with the change of variable u. At high order, the evolution is in τ^2, consequently the contact length is at the order $\tau^{3/2}$. Because the contact length must be the same whatever the scales, the total length for the contact is the contribution of the leading and high orders. Thus, the contact length can be expressed by the domination of the leading order which is perturbed (ε) by the contribution of the high order which is in the form $\tau^{3/2}$.

$$\lambda_c(\tau) = \sqrt{\tau}(\lambda_0 + \varepsilon\lambda_1\tau) \tag{2.7.6}$$

The usual ansatz can be applied on the double contact reaction

$$\tilde{R}(\tau) = 2\sqrt{\frac{2}{\pi}}\frac{1}{\sqrt{\tau}}(r_0 + \varepsilon r_1 \tau) \tag{2.7.7}$$

This assumption is checked by solving another Abel equation. For the case of a discrete contact $\kappa/\nu > 1$, the complementary condition at the high order (ε^1) can be written as

$$\int_0^\tau \tilde{R}_1(\bar{\tau})\sqrt{\frac{\tau-\bar{\tau}}{2\pi}}d\bar{\tau} = \frac{\alpha\tau^2}{2} \tag{2.7.8}$$

In Appendix Appendix A.1, the resolution is made. It proves that the ansatz for the concentrated reaction $\tilde{R}$ is correct where the parameter r_1 is equal to 2α. This result will be rediscovered later.
The complementary condition is written in $\xi = 0$ by simplicity of calculations

$$\begin{aligned}\eta(0,\tau) &= \varepsilon\tilde{r}_1 \int_0^\tau \sqrt{\frac{\tau-\bar{\tau}}{2\pi}}2 \int_0^{\lambda_c(\bar{\tau})} \mathcal{H}\left(\frac{\bar{\xi}}{\sqrt{\tau-\bar{\tau}}}\right)d\bar{\xi}d\bar{\tau} \\ &+ \frac{1}{2\sqrt{2\pi}}\int_0^\tau \tilde{R}(\bar{\tau})\sqrt{\tau-\bar{\tau}}2\mathcal{H}\left(\frac{\lambda_c(\bar{\tau})}{\sqrt{\tau-\bar{\tau}}}\right)d\bar{\tau} \qquad (2.7.9)\\ &= \frac{2\tilde{r}_1\varepsilon}{\sqrt{2\pi}}\int_0^\tau (\tau-\bar{\tau})\mathcal{P}\left(\frac{\lambda_c(\bar{\tau})}{\sqrt{\tau-\bar{\tau}}}\right)d\bar{\tau} \\ &+ \frac{1}{\sqrt{2\pi}}\int_0^\tau \tilde{R}(\bar{\tau})\sqrt{\tau-\bar{\tau}}\mathcal{H}\left(\frac{\lambda_c(\bar{\tau})}{\sqrt{\tau-\bar{\tau}}}\right)d\bar{\tau} \qquad (2.7.10)\end{aligned}$$

where the function $\mathcal{P}$ can be defined as

$$\mathcal{P}(\beta) = \int_0^\beta \mathcal{H}(\beta')d\beta' \tag{2.7.11}$$

$$\mathcal{P}(\beta) = \sqrt{\frac{\pi}{2}}\left[\left(\frac{\beta^2+2}{2}\right)\mathcal{S}\left(\frac{\beta}{\sqrt{2\pi}}\right) - \left(\frac{\beta^2-2}{2}\right)\mathcal{C}\left(\frac{\beta}{\sqrt{2\pi}}\right)\right] + \frac{\beta}{2}\left(\sin\left(\frac{\beta^2}{4}\right) + \cos\left(\frac{\beta^2}{4}\right)\right) \tag{2.7.12}$$

using trigonometric and Fresnel functions.
Due to the complexity of the solution and to be able to continue to develop a semi-analytic approach, a Taylor series must be effectuated around $\lambda_0\sqrt{\bar{\tau}}/\sqrt{\tau-\bar{\tau}}$ giving

$$\mathcal{P}\left(\frac{\lambda_0\sqrt{\bar{\tau}} + \varepsilon\lambda_1\sqrt{\bar{\tau}}^3}{\sqrt{\tau-\bar{\tau}}}\right) = \mathcal{P}\left(\frac{\lambda_0\sqrt{\bar{\tau}}}{\sqrt{\tau-\bar{\tau}}}\right) + \frac{\varepsilon\lambda_1\sqrt{\bar{\tau}}^3}{\sqrt{\tau-\bar{\tau}}}\mathcal{P}'\left(\frac{\lambda_0\sqrt{\bar{\tau}}}{\sqrt{\tau-\bar{\tau}}}\right) \tag{2.7.13}$$

This assumption corresponds to the fact that the contact length λ_c is dominated by the contribution at leading order compared to high order. Using this Taylor series, the first

term of $\eta(0,\tau)$ can be written as

$$\frac{2(\alpha+\psi)\varepsilon}{\sqrt{2\pi}}\int_0^\tau(\tau-\bar{\tau})\mathcal{P}\left(\frac{\lambda_0\sqrt{\bar{\tau}}}{\sqrt{\tau-\bar{\tau}}}\right)d\bar{\tau}+\mathcal{O}(\varepsilon^2) \tag{2.7.14}$$

$$=\frac{(\alpha+\psi)\varepsilon\tau^2}{2}\frac{4}{\tau^2\sqrt{2\pi}}\int_0^\tau(\tau-\bar{\tau})\mathcal{P}\left(\frac{\lambda_0\sqrt{\bar{\tau}}}{\sqrt{\tau-\bar{\tau}}}\right)d\bar{\tau} \tag{2.7.15}$$

$$=\frac{(\alpha+\psi)\varepsilon\tau^2}{2}\varphi_p(\lambda_0) \tag{2.7.16}$$

where the function $\varphi_p(\lambda)$ is obtained by applying the change of variable $\beta=\lambda_0\sqrt{\bar{\tau}}/\sqrt{\tau-\bar{\tau}}$ and defined as

$$\varphi_p(\lambda):=\frac{8}{\sqrt{2\pi}}\int_0^{+\infty}\frac{\beta\lambda^4}{(\beta^2+\lambda^2)^3}\mathcal{P}(\beta)d\beta \tag{2.7.17}$$

The second term can be written as

$$\frac{1}{\sqrt{2\pi}}\int_0^\tau\tilde{R}(\bar{\tau})\sqrt{\tau-\bar{\tau}}\mathcal{H}\left(\frac{\lambda_c(\bar{\tau})}{\sqrt{\tau-\bar{\tau}}}\right)d\bar{\tau}=\frac{2}{\pi}\int_0^\tau(r_0+\varepsilon r_1\bar{\tau})\sqrt{\frac{\tau-\bar{\tau}}{\bar{\tau}}}\mathcal{H}\left(\frac{\sqrt{\bar{\tau}}}{\sqrt{\tau-\bar{\tau}}}(\lambda_0+\varepsilon\lambda_1\bar{\tau})\right)d\bar{\tau} \tag{2.7.18}$$

In the same way, a Taylor around $\lambda_0\sqrt{\bar{\tau}}/\sqrt{\tau-\bar{\tau}}$ is applied on the function $\mathcal{H}$ by using simultaneously the change of variable $\beta=\lambda_0\sqrt{\bar{\tau}}/\sqrt{\tau-\bar{\tau}}$

$$\mathcal{H}\left(\frac{\sqrt{\bar{\tau}}}{\sqrt{\tau-\bar{\tau}}}(\lambda_0+\varepsilon\lambda_1\bar{\tau})\right)=\mathcal{H}\left(\beta+\varepsilon\frac{\lambda_1}{\lambda_0}\frac{\beta^3\tau}{\beta^2+\lambda_0^2}\right) \tag{2.7.19}$$

$$=\mathcal{H}(\beta)+\frac{\lambda_1}{\lambda_0}\frac{\varepsilon\beta^3\tau}{\beta^2+\lambda_0^2}\mathcal{H}'(\beta)+\mathcal{O}(\varepsilon^2) \tag{2.7.20}$$

Finally, the second term reads

$$\frac{4}{\pi}\int_0^{+\infty}\lambda_0^3\left(\frac{r_0\tau}{(\beta^2+\lambda_0^2)^2}+\frac{\varepsilon r_1\tau^2\beta^2}{(\beta^2+\lambda_0^2)^3}\right)\left(\mathcal{H}(\beta)+\frac{\lambda_1}{\lambda_0}\frac{\varepsilon\beta^3\tau}{\beta^2+\lambda_0^2}\mathcal{H}'(\beta)\right)d\beta \tag{2.7.21}$$

$$=r_0\varphi_\nu(\lambda_0)\tau+\varepsilon\left[\frac{r_1}{2}\varphi_\alpha(\lambda_0)-r_0\frac{\lambda_1}{\lambda_0}\varphi_\lambda(\lambda_0)\right]\frac{\tau^2}{2}+\mathcal{O}(\varepsilon^2) \tag{2.7.22}$$

where two new functions φ_α and φ_λ are defined as

$$\varphi_\alpha(\lambda)=\frac{16}{\pi}\int_0^{+\infty}\frac{\lambda^3\beta^2\mathcal{H}(\beta)}{(\beta^2+\lambda^2)^3}d\beta\ ;\ \varphi_\lambda(\lambda)=-\frac{8}{\pi}\int_0^{+\infty}\frac{\lambda^3\beta^3\mathcal{H}'(\beta)}{(\beta^2+\lambda^2)^3}d\beta \tag{2.7.23}$$

For the slow solution at $\xi=0$, we have

$$\eta(0,\tau)=\nu\tau+\varepsilon\alpha\frac{\tau^2}{2} \tag{2.7.24}$$

Grouping the terms together by the power on ε to satisfy the complementary condition

$$(\varepsilon^0): \quad r_0\varphi_\nu(\lambda_0) = \nu$$
$$(\varepsilon^1): \quad 2(\alpha+\psi)\varphi_p(\lambda_0) + r_1\varphi_\alpha(\lambda_0) - 2r_0\frac{\lambda_1}{\lambda_0}\varphi_\lambda(\lambda_0) = 2\alpha$$

As expected, at leading order, the same equation is recovered. At the next order, the solutions r_0 and λ_0 from the leading order which are known have a contribution. The new unknowns are r_1 and λ_1. Consequently, the curvature will also be written at $\xi = 0$ by applying the comparison power on ε. With the information at the position and the curvature, it is possible to obtain a set of four equations to find r_0, r_1, λ_0 and λ_1. To solve the system, the solution λ_0 and r_0 are found in the same way than previously. Then, using the high order equation, r_1 and λ_1 can be found. In Figure 2.10, the representation of the functions φ_p, φ_α and φ_λ is shown.

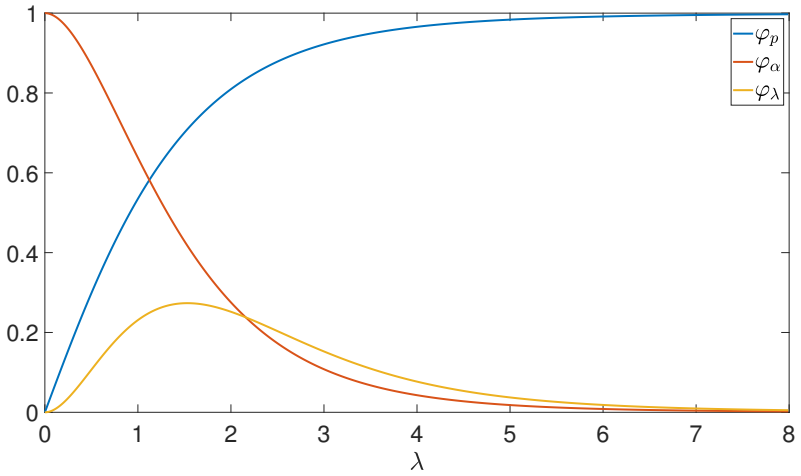

Figure 2.10: Functions φ_p, φ_α and φ_λ.

Consequently, the curvature of the fast solution can be calculated as follow

$$\partial_\xi^2\eta(\xi,\tau) = \partial_\xi^2\eta_0(\xi,\tau) + \varepsilon\partial_\xi^2\eta_1(\xi,\tau) = \tilde{r}\int_0^\tau \sqrt{\frac{1}{2\pi(\tau-\bar{\tau})}}\int_{-\lambda_c(\bar{\tau})}^{\lambda_c(\bar{\tau})} \mathcal{H}''\left(\frac{|\xi-\bar{\xi}|}{\sqrt{\tau-\bar{\tau}}}\right)d\bar{\xi}d\bar{\tau} \tag{2.7.25}$$

$$+\frac{1}{2\sqrt{2\pi}}\int_0^\tau \tilde{R}(\bar{\tau})\frac{1}{\sqrt{\tau-\bar{\tau}}}\left[\mathcal{H}''\left(\frac{|\xi-\lambda_c(\bar{\tau})|}{\sqrt{\tau-\bar{\tau}}}\right) + \mathcal{H}''\left(\frac{|\xi+\lambda_c(\bar{\tau})|}{\sqrt{\tau-\bar{\tau}}}\right)\right]d\bar{\tau} \tag{2.7.26}$$

The solution is examined at $\xi = 0$

$$\partial_\xi^2 \eta(0,\tau) = \varepsilon \tilde{r}_1 \int_0^\tau \sqrt{\frac{1}{2\pi(\tau-\bar{\tau})}} 2 \int_0^{\lambda_c(\bar{\tau})} \mathcal{H}''\left(\frac{\bar{\xi}}{\sqrt{\tau-\bar{\tau}}}\right) d\bar{\xi} d\bar{\tau}$$

$$+ \frac{1}{2\sqrt{2\pi}} \int_0^\tau \tilde{R}(\bar{\tau}) \frac{1}{\sqrt{\tau-\bar{\tau}}} 2\mathcal{H}''\left(\frac{\lambda_c(\bar{\tau})}{\sqrt{\tau-\bar{\tau}}}\right) d\bar{\tau} \tag{2.7.27}$$

$$= 2\varepsilon \tilde{r}_1 \int_0^\tau \sqrt{\frac{1}{2\pi}} \mathcal{H}'\left(\frac{\lambda_c(\bar{\tau})}{\sqrt{\tau-\bar{\tau}}}\right) d\bar{\tau}$$

$$+ \frac{1}{\sqrt{2\pi}} \int_0^\tau \tilde{R}(\bar{\tau}) \frac{1}{\sqrt{\tau-\bar{\tau}}} \mathcal{H}''\left(\frac{\lambda_c(\bar{\tau})}{\sqrt{\tau-\bar{\tau}}}\right) d\bar{\tau} \tag{2.7.28}$$

The Taylor expansion is again applied on this equation assuming that the propagation at leading order is more important than the one at high order with $\beta = \lambda_0\sqrt{\bar{\tau}}/\sqrt{\tau-\bar{\tau}}$

$$\mathcal{H}'\left(\frac{\lambda_c(\bar{\tau})}{\sqrt{\tau-\bar{\tau}}}\right) = \mathcal{H}'(\beta) + \frac{\lambda_1}{\lambda_0} \frac{\varepsilon\beta^3\tau}{\beta^2+\lambda_0^2} \mathcal{H}''(\beta) + \mathcal{O}(\varepsilon^2) \tag{2.7.29}$$

$$\mathcal{H}''\left(\frac{\lambda_c(\bar{\tau})}{\sqrt{\tau-\bar{\tau}}}\right) = \mathcal{H}''(\beta) + \frac{\lambda_1}{\lambda_0} \frac{\varepsilon\beta^3\tau}{\beta^2+\lambda_0^2} \mathcal{H}'''(\beta) + \mathcal{O}(\varepsilon^2) \tag{2.7.30}$$

$$\tag{2.7.31}$$

With this change of variable and Taylor expansion, the first term becomes

$$\frac{2\varepsilon(\alpha+\psi)}{\sqrt{2\pi}} \int_0^\tau \mathcal{H}'\left(\frac{\lambda_0\sqrt{\bar{\tau}}}{\sqrt{\tau-\bar{\tau}}}\right) d\bar{\tau} + \mathcal{O}(\varepsilon^2) \tag{2.7.32}$$

$$= \frac{-\sqrt{2\pi}\varepsilon\tau(\alpha+\psi)}{4} \varphi_{\dot{p}}(\lambda_0) \tag{2.7.33}$$

where the function $\varphi_{\dot{p}}(\lambda_0)$ is defined as

$$\varphi_{\dot{p}}(\lambda_0) = \frac{-8}{\pi} \int_0^{+\infty} \frac{\lambda_0^2 \beta \mathcal{H}'(\beta)}{(\lambda_0^2+\beta^2)^2} d\beta \tag{2.7.34}$$

The second term is now

$$\frac{2}{\pi} \int_0^\tau \frac{r_0 + \varepsilon r_1 \bar{\tau}}{\sqrt{\bar{\tau}(\tau-\bar{\tau})}} \left(\mathcal{H}''(\beta) + \frac{\lambda_1}{\lambda_0} \frac{\varepsilon\beta^3\tau}{\beta^2+\lambda_0^2} \mathcal{H}'''(\beta) \right) d\bar{\tau} + \mathcal{O}(\varepsilon^2) \tag{2.7.35}$$

$$= \frac{2}{\pi} \int_0^\tau \frac{r_0}{\sqrt{\bar{\tau}(\tau-\bar{\tau})}} \mathcal{H}''(\beta) d\bar{\tau} + \frac{2}{\pi} \int_0^\tau \frac{r_0}{\sqrt{\bar{\tau}(\tau-\bar{\tau})}} \frac{\lambda_1}{\lambda_0} \frac{\varepsilon\beta^3\tau}{\beta^2+\lambda_0^2} \mathcal{H}'''(\beta) d\bar{\tau} + \frac{2}{\pi} \int_0^\tau \frac{\varepsilon r_1 \bar{\tau}}{\sqrt{\bar{\tau}(\tau-\bar{\tau})}} \mathcal{H}''(\beta) d\bar{\tau} + \mathcal{O}(\varepsilon^2) \tag{2.7.36}$$

$$= -r_0 \varphi_\kappa(\lambda_0) + \frac{r_0}{4} \frac{\lambda_1}{\lambda_0} \varepsilon\tau \varphi_{\dot{\lambda}}(\lambda_0) - \frac{\varepsilon r_1 \tau}{2} \varphi_{\dot{\kappa}}(\lambda_0) + \mathcal{O}(\varepsilon^2) \tag{2.7.37}$$

where the function $\varphi_{\dot{\lambda}}(\lambda)$ and $\varphi_{\dot{\kappa}}(\lambda)$ are defined as

$$\varphi_{\dot{\lambda}} = \frac{16}{\pi}\int_0^{+\infty} \frac{\beta^3\lambda}{(\lambda^2+\beta^2)^2}\mathcal{H}'''(\beta)d\beta \quad \text{and} \quad \varphi_{\dot{\kappa}} = \frac{-8}{\pi}\int_0^{+\infty} \frac{\beta^2\lambda}{(\lambda^2+\beta^2)^2}\mathcal{H}''(\beta)d\beta \tag{2.7.38}$$

The slow solution taking into account leading and high order at $\xi = 0$ is

$$\partial_\xi^2\eta(0,\tau) = -\kappa + \varepsilon\chi\tau \tag{2.7.39}$$

Grouping the terms together and comparing the power on ε

$$\begin{aligned}
&(\varepsilon^0): \quad r_0\varphi_\kappa(\lambda_0) = \kappa \\
&(\varepsilon^1): \quad -\sqrt{2\pi}(\alpha+\psi)\varphi_{\dot{p}}(\lambda_0) + r_0\frac{\lambda_1}{\lambda_0}\varphi_{\dot{\lambda}}(\lambda_0) - 2r_1\varphi_{\dot{\kappa}}(\lambda_0) = 4\chi
\end{aligned}$$

The functions $\varphi_{\dot{p}}$, $\varphi_{\dot{\kappa}}$ and $\varphi_{\dot{\lambda}}$ can be observed in Figure 2.11.

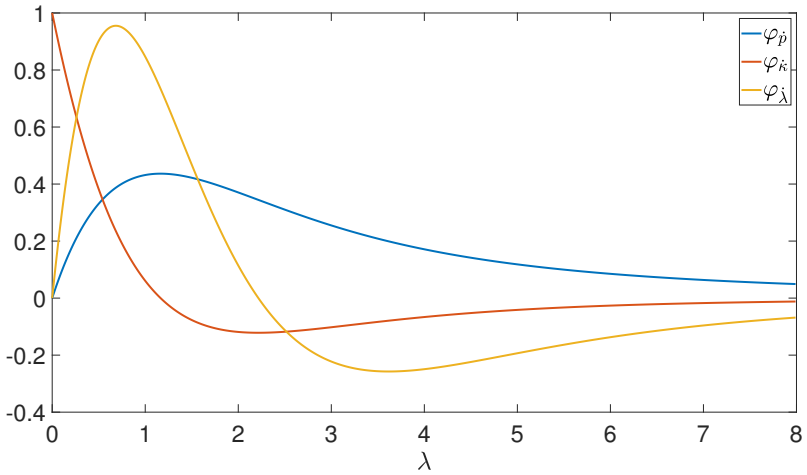

Figure 2.11: Functions $\varphi_{\dot{p}}$, $\varphi_{\dot{\kappa}}$ and $\varphi_{\dot{\lambda}}$.

At leading order, the same solution is found that in (Equation (2.6.19)) at the curvature level. Consequently, because the equations are completely identical at leading order, the solution λ_0 and r_0 are like previously in Section 2.6. This observation allows to prove that the separation of time scaling make sense. At high order, the solutions obtained at leading order must be injected to determine the 2 unknowns r_1 and λ_1. Indeed, the two equations at high order can be rewritten in a matrix problem to solve as following

$$\begin{pmatrix} \varphi_\alpha(\lambda_0) & -2\dfrac{r_0\varphi_\lambda(\lambda_0)}{\lambda_0} \\ -2\varphi_{\dot{\kappa}}(\lambda_0) & \dfrac{r_0\varphi_{\dot{\lambda}}(\lambda_0)}{\lambda_0} \end{pmatrix} \begin{pmatrix} r_1 \\ \lambda_1 \end{pmatrix} = \begin{pmatrix} 2\alpha - 2(\alpha+\psi)\varphi_p(\lambda_0) \\ 4\chi + \sqrt{2\pi}(\alpha+\psi)\varphi_{\dot{p}}(\lambda_0) \end{pmatrix} \tag{2.7.40}$$

The problem is solved in the case of the continuous contact meaning $\kappa/\nu < 1$. The results will be extrapolated in the discrete contact ($\kappa/\nu \geq 1$). In Figure 2.12a and Figure 2.12b, the solution r_1 and λ_1 are shown for different sets of values α, ψ and χ, respectively. In the same way than the leading order, when the ratio κ/ν tends to 0, logically, the reaction becomes infinite and the contact zone propagates to infinity. When $\kappa/\nu > 1$, discrete

contact case, the contact zone corresponds to a discrete point $\xi = 0$. Thus, the λ_1 value is zero. To avoid penetration due to the contribution at high order, a contact reaction r_1 is applied also in the discrete contact which is 2α. In continuous contact, we can observe that for all the cases, the parameter λ_1 is always positive meaning that the high order accelerates the velocity of propagation of the contact domain. For the reaction r_1, the value is positive meaning that a contact reaction is applied to avoid a penetration in the wall due to the effects at the high order except in some cases (for example, with $\alpha = 0$, $\psi = 2$ and $\chi = 0$ at $\kappa/\nu = 0.5$). In this particular case, the reaction r_1 is strictly negative meaning that a contact reaction in the direction of the beam must be applied to avoid a detachment of the wall at $\xi = \pm\lambda(\tau)$ which is completely absurd if the detachment occurs.

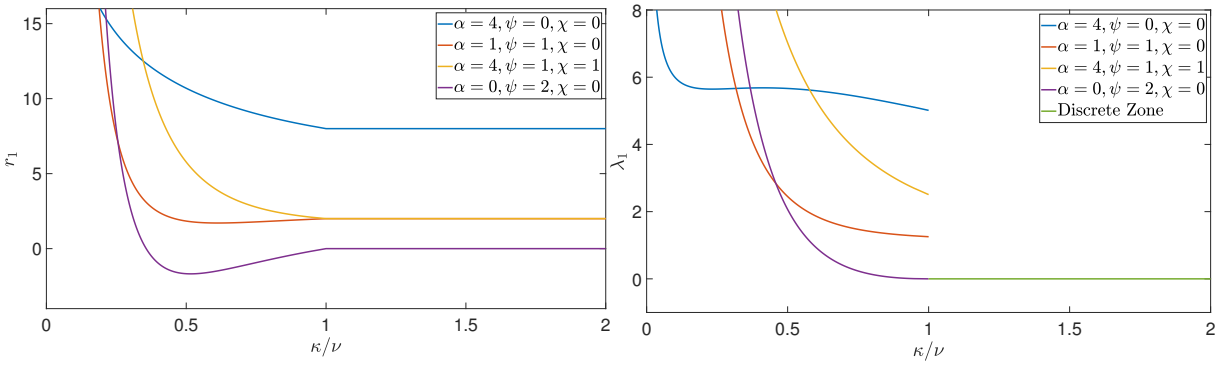

(a) Solution r_1 as function of α, ψ and χ. **(b)** Solution λ_1 as function of α, ψ and χ.

Figure 2.12: Solutions r_1 and λ_1 at high order for $\alpha + \psi > 0$.

The complementary condition is made at $\xi = 0$. As at leading order, the complementary condition can be generalized with the parameter a by keeping only the term in ε^0 and ε^1, neglected at high order such as ε^2.
The slow solution using the fact $\xi = a\sqrt{\tau}(\lambda_0 + \varepsilon\lambda_1\tau)$ can be written as

$$\eta(a\sqrt{\tau}(\lambda_0 + \varepsilon\lambda_1\tau), \tau) = \nu\tau - \frac{\kappa a^2\lambda_0^2\tau}{2} + \varepsilon\bigg(- \kappa a^2\lambda_0\lambda_1\tau^2 + \frac{\psi a^4\lambda_0^4\tau^2}{24} + \frac{\chi a^2\lambda_0^2\tau^2}{2} + \frac{\alpha\tau^2}{2}\bigg) \tag{2.7.41}$$

and the fast dynamics is

$$\begin{aligned}\eta(a\sqrt{\tau}(\lambda_0 + \varepsilon\lambda_1\tau), \tau) = (\alpha + \psi)\varepsilon \int_0^\tau \sqrt{\frac{\tau - \bar{\tau}}{2\pi}} \int_{-\lambda_c(\bar{\tau})}^{\lambda_c(\bar{\tau})} \mathcal{H}\bigg(\frac{|a\sqrt{\bar{\tau}}(\lambda_0 + \varepsilon\bar{\tau}\lambda_1) - \bar{\xi}|}{\sqrt{\tau - \bar{\tau}}}\bigg) d\bar{\xi} d\bar{\tau} \\ \frac{1}{\pi}\int_0^\tau (r_0 + \varepsilon r_1\bar{\tau})\sqrt{\frac{\tau - \bar{\tau}}{\bar{\tau}}}\bigg[\mathcal{H}\bigg(\frac{|a\sqrt{\tau}(\lambda_0 + \varepsilon\tau\lambda_1) - \sqrt{\bar{\tau}}(\lambda_0 + \varepsilon\bar{\tau}\lambda_1)|}{\sqrt{\tau - \bar{\tau}}}\bigg) \\ + \mathcal{H}\bigg(\frac{|a\sqrt{\tau}(\lambda_0 + \varepsilon\tau\lambda_1) + \sqrt{\bar{\tau}}(\lambda_0 + \varepsilon\bar{\tau}\lambda_1)|}{\sqrt{\tau - \bar{\tau}}}\bigg)\bigg] d\bar{\tau}\end{aligned} \tag{2.7.42}$$

At leading order (ε^0) , the generalized complementary equation is completely identical to the complementary obtained at (Eqs. (2.6.31) and (2.6.32)) from the leading analysis.

Injecting the parameters r_0, r_1, λ_0 and λ_1 obtained by the complementary condition at $\xi = 0$, the two previous equations must be identical in the interval $a \in [-1; 1]$ representing the contact domain $\mathcal{D}$. In Figure 2.13, the generalized complementary condition is shown for different sets of parameters. In the interval $[-1; 1]$, as expected, the two solutions overlap. However, some assumptions have been made to establish the relation at $\xi = 0$. Eqs. (2.7.13), (2.7.20), (2.7.29) and (2.7.30), a Taylor expansion have been made around the contact length at leading order. To remember, with the ansatz, the contact length λ_c is $\sqrt{\tau}(\lambda_0 + \varepsilon\lambda_1\tau)$. Thus, if the length λ_1 is not negligible compared to λ_0 or if the time τ becomes important, the Taylor assumption becomes incorrect to develop the semi-analytic solution at high order. For example, with the following set $\nu = 1, \kappa = 0.5$, $\alpha = 4$, $\psi = 0$, $\chi = 0$, the parameter λ_0 is 1.019 and λ_1 5.665. At time $\tau = 0.1$, the Taylor expansions are correct: $\sqrt{0.1} \cdot 1.019 = 0.3222 \gg 0.0179 = \sqrt{0.1} \cdot 0.1 \cdot 5.665 \cdot 0.1$ and we can observe that the complementary condition is satisfied on the domain contact $\mathcal{D}$. However, at time $\tau = 0.5$, the Taylor approximation is not completely correct: $\sqrt{0.5} \cdot 1.019 = 0.7205 > 0.2003 = \sqrt{0.5} \cdot 0.1 \cdot 5.665 \cdot 0.5$ because there is not one order of difference between the leading order and the high order contribution. In Figure 2.13, for this configuration, we can clearly observe that the 2 solutions are not the same in the contact domain.

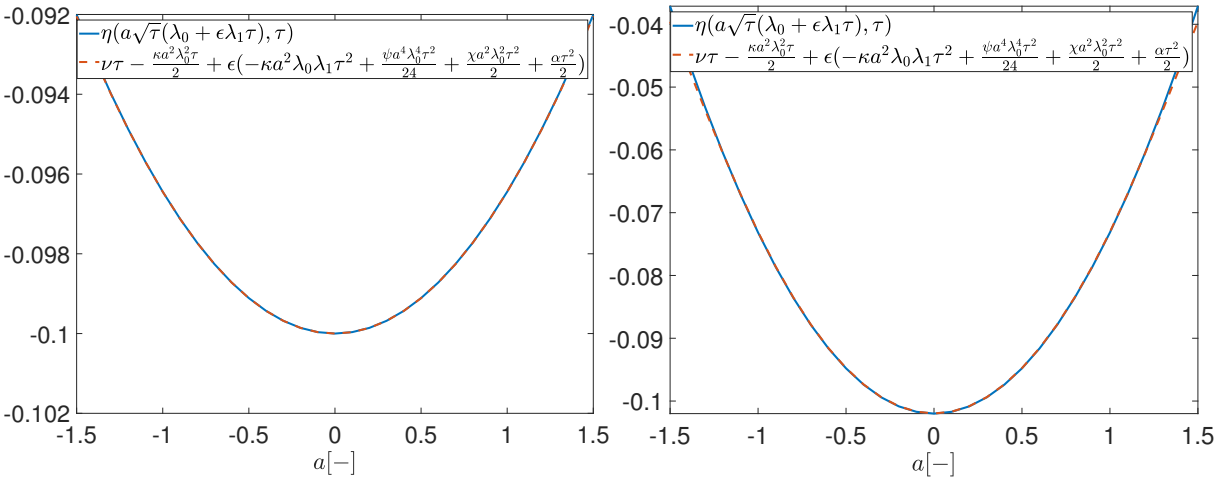

(a) $\nu = 1, \kappa = 0.8$, $\alpha = 0$, $\psi = 2$, $\chi = 0$ and $\tau = 0.1$.

(b) $\nu = 1, \kappa = 0.5$, $\alpha = 4$, $\psi = 0$, $\chi = 0$ and $\tau = 0.1$.

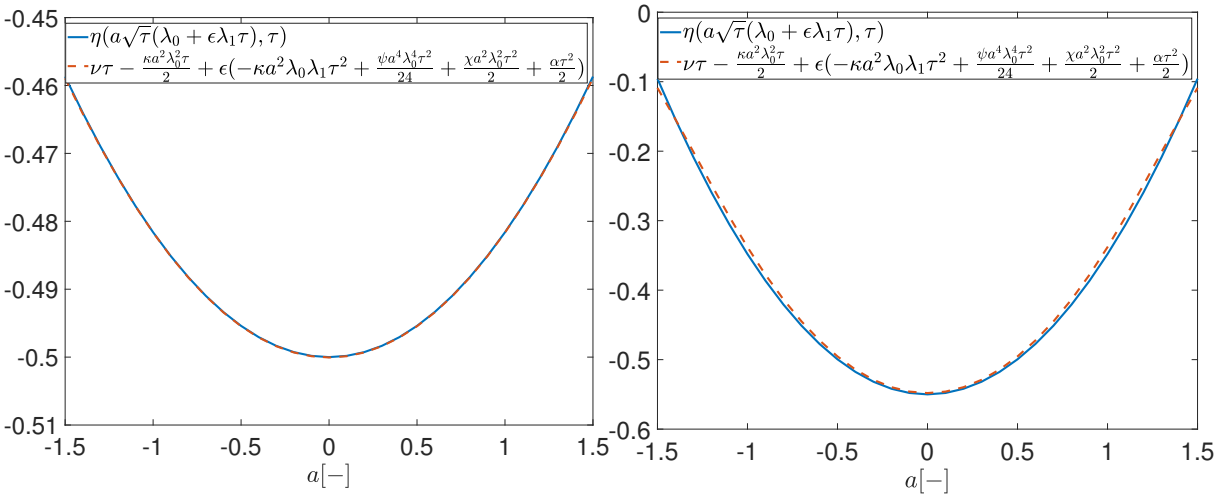

(c) $\nu = 1, \kappa = 0.8$, $\alpha = 0$, $\psi = 2$, $\chi = 0$ and $\tau = 0.5$.

(d) $\nu = 1, \kappa = 0.5$, $\alpha = 4$, $\psi = 0$, $\chi = 0$ and $\tau = 0.5$.

Figure 2.13: Complementary condition expressed as function of a for different values ν, κ, α, ψ, χ and τ with $\varepsilon = 0.1$.

In Figure 2.14, a beam impact is represented with acceleration ($\alpha+\psi > 0$). On the left column of the Figure, in the configuration where the contact is continuous ($\kappa < \nu$), with time, the contact length increases logically. In Appendix A.4 for the continuous contact reaction, to obtain numerically the solution in presence of absolute value, two cases are possible if ξ is in or out the domain. On the right of the Figure, a discrete contact is represented.

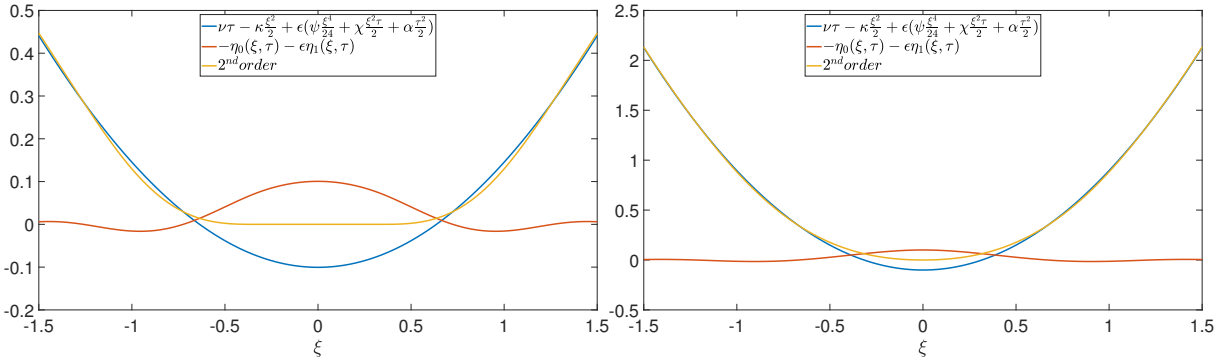

(a) $\nu = 1, \kappa = 0.5$, $\alpha = 1$, $\psi = 1$, $\chi = 0$ and $\tau = 0.1$.

(b) $\nu = 1, \kappa = 2$, $\alpha = 1$, $\psi = 1$, $\chi = 0$ and $\tau = 0.1$.

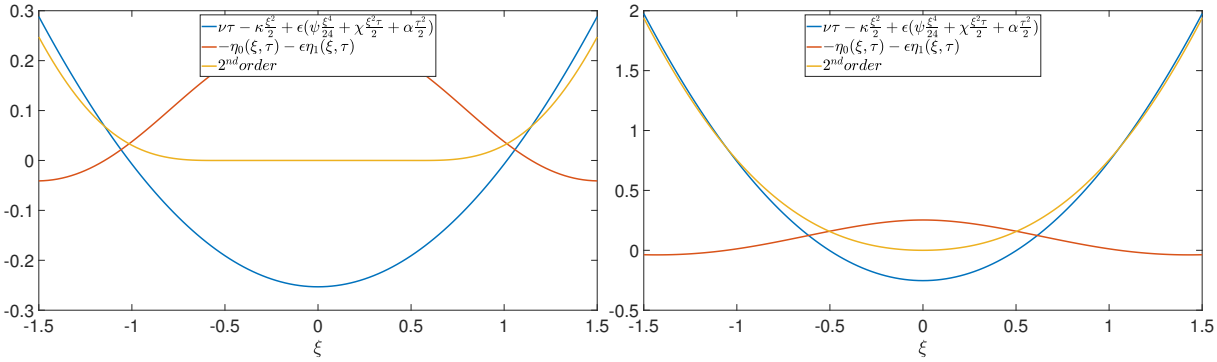

(c) $\nu = 1, \kappa = 0.5$, $\alpha = 1$, $\psi = 1$, $\chi = 0$ and $\tau = 0.25$.

(d) $\nu = 1, \kappa = 2$, $\alpha = 1$, $\psi = 1$, $\chi = 0$ and $\tau = 0.25$.

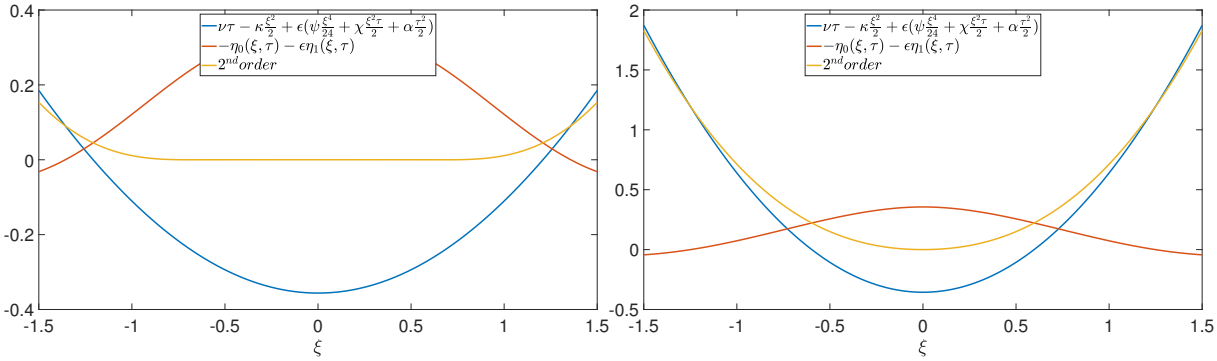

(e) $\nu = 1, \kappa = 0.5$, $\alpha = 1$, $\psi = 1$, $\chi = 0$ and $\tau = 0.35$.

(f) $\nu = 1, \kappa = 2$, $\alpha = 1$, $\psi = 1$, $\chi = 0$ and $\tau = 0.35$.

Figure 2.14: Beam impacting a rigid surface as function the parameters κ, ν, α, ψ, χ for $\varepsilon = 0.1$ at different times τ for the leading and high order. On the left column, a continuous contact occurs and on the left a discrete contact.

2.7.2 Non-continuous contact with double reaction forces

Now, the second case $\alpha + \psi < 0$ will be investigated by following some steps that it have been done for the first case. During the impact of the beam, the contribution at high order provokes a detachment in the middle of the beam. The domain of contact $\mathcal{D}$ is not continuous and corresponds only to 2 contact points at the evolving positions $\xi = \pm\lambda_c(\tau)$. As for $\alpha + \psi$, with the ansatz, the variables λ_1 and r_1 must be deduced using the complementary condition. The general solution of the Euler beam must take into account only the double contact reaction (no uniform reaction on the domain)

$$\eta(\xi,\tau) = \eta_0(\xi,\tau) + \varepsilon\eta_1(\xi,\tau) = \frac{1}{\pi}\int_0^\tau \sqrt{\frac{\tau-\bar{\tau}}{\bar{\tau}}}(r_0 + \varepsilon r_1\bar{\tau})\left[\mathcal{H}\left(\frac{|\xi-\lambda_c(\bar{\tau})|}{\sqrt{\tau-\bar{\tau}}}\right) + \mathcal{H}\left(\frac{|\xi+\lambda_c(\bar{\tau})|}{\sqrt{\tau-\bar{\tau}}}\right)\right]d\bar{\tau} \tag{2.7.43}$$

In this situation, the analysis development can not be performed at $\xi = 0$ due to the detachment occurring with time. Thus, the analysis is performed at $\xi = \lambda_c(\tau)$.
Starting with the slow solution at this position, we obtain

$$\eta(\lambda_c(\tau),\tau) = \tau\left(\nu - \frac{\kappa\lambda_0^2}{2}\right) + \varepsilon\tau^2\left(-\kappa\lambda_0\lambda_1 + \frac{\psi\lambda_0^4}{24} + \frac{\chi\lambda_0^2}{2} + \frac{\alpha}{2}\right) + \mathcal{O}(\varepsilon^2) \tag{2.7.44}$$

For the fast dynamics solution at $\xi = \lambda_c(\tau)$, we have

$$\eta(\lambda_c(\tau),\tau) = \frac{1}{\pi}\int_0^\tau \sqrt{\frac{\tau-\bar{\tau}}{\bar{\tau}}}(r_0 + \varepsilon r_1\bar{\tau})\left[\mathcal{H}\left(\frac{|\lambda_c(\tau)-\lambda_c(\bar{\tau})|}{\sqrt{\tau-\bar{\tau}}}\right) + \mathcal{H}\left(\frac{|\lambda_c(\tau)+\lambda_c(\bar{\tau})|}{\sqrt{\tau-\bar{\tau}}}\right)\right]d\bar{\tau} \tag{2.7.45}$$

The development is applied at $\xi = \lambda_c$ with a Taylor expansion around the contribution at leading order, the two functions $\mathcal{H}$ can be written as

$$\mathcal{H}\left(\frac{|\lambda_c(\tau)-\lambda_c(\bar{\tau})|}{\sqrt{\tau-\bar{\tau}}}\right) = \mathcal{H}\left(\lambda_0\frac{\sqrt{\tau}-\sqrt{\bar{\tau}}}{\sqrt{\tau-\bar{\tau}}}\right) + \varepsilon\lambda_1\frac{\tau\sqrt{\tau}-\bar{\tau}\sqrt{\bar{\tau}}}{\sqrt{\tau-\bar{\tau}}}\mathcal{H}'\left(\lambda_0\frac{\sqrt{\tau}-\sqrt{\bar{\tau}}}{\sqrt{\tau-\bar{\tau}}}\right) + \mathcal{O}(\varepsilon^2) \tag{2.7.46}$$

$$\mathcal{H}\left(\frac{|\lambda_c(\tau)+\lambda_c(\bar{\tau})|}{\sqrt{\tau-\bar{\tau}}}\right) = \mathcal{H}\left(\lambda_0\frac{\sqrt{\tau}+\sqrt{\bar{\tau}}}{\sqrt{\tau-\bar{\tau}}}\right) + \varepsilon\lambda_1\frac{\tau\sqrt{\tau}+\bar{\tau}\sqrt{\bar{\tau}}}{\sqrt{\tau-\bar{\tau}}}\mathcal{H}'\left(\lambda_0\frac{\sqrt{\tau}+\sqrt{\bar{\tau}}}{\sqrt{\tau-\bar{\tau}}}\right) + \mathcal{O}(\varepsilon^2) \tag{2.7.47}$$

Injecting these expansion in the solution and keeping the term until the power ε, the fast solution reads as

$$\begin{aligned}\eta(\lambda_c(\tau),\tau) = {} & \frac{r_0}{\pi}\int_0^\tau \sqrt{\frac{\tau-\bar{\tau}}{\bar{\tau}}}\left[\mathcal{H}\left(\lambda_0\frac{\sqrt{\tau}-\sqrt{\bar{\tau}}}{\sqrt{\tau-\bar{\tau}}}\right) + \mathcal{H}\left(\lambda_0\frac{\sqrt{\tau}+\sqrt{\bar{\tau}}}{\sqrt{\tau-\bar{\tau}}}\right)\right]d\bar{\tau} \\ & + \frac{\varepsilon r_1}{\pi}\int_0^\tau \sqrt{(\tau-\bar{\tau})\bar{\tau}}\left[\mathcal{H}\left(\lambda_0\frac{\sqrt{\tau}-\sqrt{\bar{\tau}}}{\sqrt{\tau-\bar{\tau}}}\right) + \mathcal{H}\left(\lambda_0\frac{\sqrt{\tau}+\sqrt{\bar{\tau}}}{\sqrt{\tau-\bar{\tau}}}\right)\right]d\bar{\tau} \\ & + \frac{\varepsilon r_0\lambda_1}{\pi}\int_0^\tau \left[\frac{\tau\sqrt{\tau}-\bar{\tau}\sqrt{\bar{\tau}}}{\sqrt{\bar{\tau}}}\mathcal{H}'\left(\lambda_0\frac{\sqrt{\tau}-\sqrt{\bar{\tau}}}{\sqrt{\tau-\bar{\tau}}}\right) + \frac{\tau\sqrt{\tau}+\bar{\tau}\sqrt{\bar{\tau}}}{\sqrt{\bar{\tau}}}\mathcal{H}'\left(\lambda_0\frac{\sqrt{\tau}+\sqrt{\bar{\tau}}}{\sqrt{\tau-\bar{\tau}}}\right)\right]d\bar{\tau}\end{aligned} \tag{2.7.48}$$

Now, a double change of variable is applied

$$\beta_- = \lambda_0 \frac{\sqrt{\tau} - \sqrt{\bar{\tau}}}{\sqrt{\tau - \bar{\tau}}} \quad \text{and} \quad \beta_+ = \lambda_0 \frac{\sqrt{\tau} + \sqrt{\bar{\tau}}}{\sqrt{\tau - \bar{\tau}}} \tag{2.7.49}$$

With these changes of variable, the integrals become

$$\begin{aligned}
\eta(\lambda_c(\tau), \tau) = \frac{r_0 \tau}{\pi} \Bigg[& \int_0^{\lambda_0} \frac{16 \beta_-^2 \lambda_0^3}{(\beta_-^2 + \lambda_0^2)^3} \mathcal{H}(\beta_-) d\beta_- + \int_{\lambda_0}^{+\infty} \frac{16 \beta_+^2 \lambda_0^3}{(\beta_+^2 + \lambda_0^2)^3} \mathcal{H}(\beta_+) d\beta_+ \Bigg] \\
& + \frac{\varepsilon r_1 \tau^2}{\pi} \Bigg[\int_0^{\lambda_0} \frac{16 \beta_-^2 \lambda_0^3 (\beta_-^2 - \lambda_0^2)^2}{(\beta_-^2 + \lambda_0^2)^5} \mathcal{H}(\beta_-) d\beta_- + \int_{\lambda_0}^{+\infty} \frac{16 \beta_+^2 \lambda_0^3 (\beta_+^2 - \lambda_0^2)^2}{(\beta_+^2 + \lambda_0^2)^5} \mathcal{H}(\beta_+) d\beta_+ \Bigg] \\
& + \frac{\varepsilon r_0 \lambda_1 \tau^2}{\pi} \Bigg[\int_0^{\lambda_0} \frac{16 \beta_-^3 \lambda_0^2 (\beta_-^4 + 3\lambda_0^4)}{(\beta_-^2 + \lambda_0^2)^5} \mathcal{H}'(\beta_-) d\beta_- + \int_{\lambda_0}^{+\infty} \frac{16 \beta_+^3 \lambda_0^2 (\beta_+^4 + 3\lambda_0^4)}{(\beta_+^2 + \lambda_0^2)^5} \mathcal{H}'(\beta_+) d\beta_+ \Bigg]
\end{aligned} \tag{2.7.50}$$

At each term, the integrand is identical for both β_- and β_+. Only the domain of integration is different. The domains are $[0; \lambda_0]$ and $[\lambda_0; +\infty]$ for β_- and β_+, respectively. The sum of the two contributions gives an integral on the entire domain $[0; +\infty]$ represented by the parameter β. Thus, the 3 integrals can be simplified by

$$\begin{aligned}
\eta(\lambda_c(\tau), \tau) = & \frac{r_0 \tau}{\pi} \int_0^{+\infty} \frac{16 \beta^2 \lambda_0^3}{(\beta^2 + \lambda_0^2)^3} \mathcal{H}(\beta) d\beta \\
& + \frac{\varepsilon r_1 \tau^2}{\pi} \int_0^{+\infty} \frac{16 \beta^2 \lambda_0^3 (\beta^2 - \lambda_0^2)^2}{(\beta^2 + \lambda_0^2)^5} \mathcal{H}(\beta) d\beta \\
& + \frac{\varepsilon r_0 \lambda_1 \tau^2}{\pi} \int_0^{+\infty} \frac{16 \beta^3 \lambda_0^2 (\beta^4 + 3\lambda_0^4)}{(\beta^2 + \lambda_0^2)^5} \mathcal{H}'(\beta) d\beta \qquad (2.7.51) \\
= & \, r_0 \tau \varphi_\alpha(\lambda_0) + \varepsilon \tau^2 \left[r_0 \lambda_1 \varphi_r(\lambda_0) + \frac{1}{4} r_1 \varphi_q(\lambda_0) \right] \qquad (2.7.52)
\end{aligned}$$

where the function φ_α was defined before Equation (2.7.23). The functions $\varphi_r(\lambda)$ and $\varphi_q(\lambda)$ are

$$\varphi_r(\lambda) = \frac{16}{\pi} \int_0^{+\infty} \frac{\beta^3 \lambda^2 (\beta^4 + 3\lambda^4)}{(\beta^2 + \lambda^2)^5} \mathcal{H}'(\beta) d\beta \quad \text{and} \quad \varphi_q(\lambda) = \frac{64}{\pi} \int_0^{+\infty} \frac{\beta^2 \lambda^3 (\beta^2 - \lambda^2)^2}{(\beta^2 + \lambda^2)^5} \mathcal{H}(\beta) d\beta \tag{2.7.53}$$

Comparing the fast and slow solutions in terms of power ε to satisfy the complementary condition

$$(\varepsilon^0): \quad r_0 \varphi_\alpha(\lambda_0) = \nu - \frac{\kappa \lambda_0^2}{2} \tag{2.7.54}$$

$$(\varepsilon^1): \quad r_0 \lambda_1 \varphi_r(\lambda_0) + \frac{1}{4} r_1 \varphi_q(\lambda_0) = -\kappa \lambda_0 \lambda_1 + \frac{\psi \lambda_0^4}{24} + \frac{\chi \lambda_0^2}{2} + \frac{\alpha}{2} \tag{2.7.55}$$

At leading order, the solution is independent of the high order contribution. Using Equation (A.5.9) (Appendix A.5) which expresses φ_α as a function of φ_ν and φ_κ and the relation at leading order for the slope Equation (2.7.69), we have

$$r_0\big(\varphi_\nu(\lambda_0) - \frac{\lambda_0^2}{2}\varphi_\kappa(\lambda_0)\big) = \nu - \kappa\frac{\lambda_0^2}{2} \tag{2.7.56}$$

$$\iff r_0\varphi_\nu(\lambda_0) - \kappa\frac{\lambda_0^2}{2} = \nu - \kappa\frac{\lambda_0^2}{2} \tag{2.7.57}$$

$$\iff \qquad r_0\varphi_\nu(\lambda_0) = \nu \tag{2.7.58}$$

which corresponds totally to Equation (2.6.17) (result obtained at leading order).

In the same way than in the case $\alpha+\psi > 0$, 4 unknowns (r_0, r_1, λ_0 and λ_1) are present. Thus, 4 equations are needed. Previously, the curvature which corresponds to the second derivative was applied. In this case, because the evaluation is made at $\xi = \lambda_c(\tau)$, which is more complex, the second set of equations for the complementary will be by expressing the slope at the contact. Indeed, to express the complementary, the position, the slope, or the curvature can be expressed to satisfy the no-penetration in the wall.
The first derivative of the fast dynamics is

$$\partial_\xi\eta(\xi,\tau) = \frac{1}{\pi}\int_0^\tau \frac{1}{\sqrt{\bar\tau}}(r_0+\varepsilon r_1\bar\tau)\left[\mathcal{H}'\left(\frac{|\xi-\lambda_c(\bar\tau)|}{\sqrt{\tau-\bar\tau}}\right)+\mathcal{H}'\left(\frac{|\xi+\lambda_c(\bar\tau)|}{\sqrt{\tau-\bar\tau}}\right)\right]d\bar\tau \tag{2.7.59}$$

Thus, at $\xi = \lambda_c(\tau)$, the fast dynamics solution at slope level is

$$\partial_\xi\eta\big(\lambda_c(\tau),\tau\big) = \frac{1}{\pi}\int_0^\tau \frac{1}{\sqrt{\bar\tau}}(r_0+\varepsilon r_1\bar\tau)\left[\mathcal{H}'\left(\frac{|\lambda_c(\tau)-\lambda_c(\bar\tau)|}{\sqrt{\tau-\bar\tau}}\right)+\mathcal{H}'\left(\frac{|\lambda_c(\tau)+\lambda_c(\bar\tau)|}{\sqrt{\tau-\bar\tau}}\right)\right]d\bar\tau \tag{2.7.60}$$

and the slow dynamics is

$$\partial_\xi\eta(\xi,\tau) = -\kappa\xi + \varepsilon\left(\frac{\psi\xi^3}{6}+\chi\xi\tau\right) \tag{2.7.61}$$

$$\Rightarrow \partial_\xi\eta(\lambda_c(\tau),\tau) = -\kappa\lambda_0\sqrt{\tau} + \varepsilon\left(-\kappa\lambda_1+\frac{\psi\lambda_0^3}{6}+\chi\lambda_0\right)\tau\sqrt{\tau}+\mathcal{O}(\varepsilon^2) \tag{2.7.62}$$

Applying a Taylor expansion around the leading order, the two functions $\mathcal{H}'$ can be written as

$$\mathcal{H}'\left(\frac{|\lambda_c(\tau)-\lambda_c(\bar\tau)|}{\sqrt{\tau-\bar\tau}}\right) = \mathcal{H}'\left(\lambda_0\frac{\sqrt{\tau}-\sqrt{\bar\tau}}{\sqrt{\tau-\bar\tau}}\right)+\varepsilon\lambda_1\frac{\tau\sqrt{\tau}-\bar\tau\sqrt{\bar\tau}}{\sqrt{\tau-\bar\tau}}\mathcal{H}''\left(\lambda_0\frac{\sqrt{\tau}-\sqrt{\bar\tau}}{\sqrt{\tau-\bar\tau}}\right)+\mathcal{O}(\varepsilon^2) \tag{2.7.63}$$

$$\mathcal{H}'\left(\frac{|\lambda_c(\tau)+\lambda_c(\bar\tau)|}{\sqrt{\tau-\bar\tau}}\right) = \mathcal{H}'\left(\lambda_0\frac{\sqrt{\tau}+\sqrt{\bar\tau}}{\sqrt{\tau-\bar\tau}}\right)+\varepsilon\lambda_1\frac{\tau\sqrt{\tau}+\bar\tau\sqrt{\bar\tau}}{\sqrt{\tau-\bar\tau}}\mathcal{H}''\left(\lambda_0\frac{\sqrt{\tau}+\sqrt{\bar\tau}}{\sqrt{\tau-\bar\tau}}\right)+\mathcal{O}(\varepsilon^2) \tag{2.7.64}$$

Injecting the Taylor developments in the Euler response equation, we obtain

$$\begin{aligned}\partial_\xi\eta(\lambda_c(\tau),\tau) = \frac{r_0}{\pi}\int_0^\tau \frac{1}{\sqrt{\bar\tau}}\Big[\mathcal{H}'\Big(\lambda_0\frac{\sqrt{\tau}-\sqrt{\bar\tau}}{\sqrt{\tau-\bar\tau}}\Big)+\mathcal{H}'\Big(\lambda_0\frac{\sqrt{\tau}+\sqrt{\bar\tau}}{\sqrt{\tau-\bar\tau}}\Big)\Big]d\bar\tau\\ + \frac{\varepsilon r_1}{\pi}\int_0^\tau \sqrt{\bar\tau}\Big[\mathcal{H}'\Big(\lambda_0\frac{\sqrt{\tau}-\sqrt{\bar\tau}}{\sqrt{\tau-\bar\tau}}\Big)+\mathcal{H}'\Big(\lambda_0\frac{\sqrt{\tau}+\sqrt{\bar\tau}}{\sqrt{\tau-\bar\tau}}\Big)\Big]d\bar\tau\\ + \frac{\varepsilon r_0\lambda_1}{\pi}\int_0^\tau \frac{1}{\sqrt{\bar\tau}}\Big[\frac{\tau\sqrt{\tau}-\bar\tau\sqrt{\bar\tau}}{\sqrt{\bar\tau}}\mathcal{H}''\Big(\lambda_0\frac{\sqrt{\tau}-\sqrt{\bar\tau}}{\sqrt{\tau-\bar\tau}}\Big)+\frac{\tau\sqrt{\tau}+\bar\tau\sqrt{\bar\tau}}{\sqrt{\bar\tau}}\mathcal{H}''\Big(\lambda_0\frac{\sqrt{\tau}+\sqrt{\bar\tau}}{\sqrt{\tau-\bar\tau}}\Big)\Big]d\bar\tau\end{aligned} \tag{2.7.65}$$

Then, the double change of variable β_- and β_+ (Equation (2.7.49)) will be applied

$$\begin{aligned}\partial_\xi\eta(\lambda_c(\tau),\tau) = -r_0\sqrt{\tau}\lambda_0\Big[\frac{-4}{\pi}\int_0^{\lambda_0}\frac{2\lambda_0\beta_-}{(\beta_-^2+\lambda_0^2)^2}\mathcal{H}'(\beta_-)d\beta_- + \frac{-4}{\pi}\int_{\lambda_0}^{+\infty}\frac{2\lambda_0\beta_+}{(\beta_+^2+\lambda_0^2)^2}\mathcal{H}'(\beta_+)d\beta_+\Big]\\ - \varepsilon r_1\tau\sqrt{\tau}\Big[\int_0^{\lambda_0}\frac{-8\lambda_0^2\beta_-(\beta_-^2-\lambda_0^2)^2}{\pi(\beta_-^2+\lambda_0^2)^4}\mathcal{H}'(\beta_-)d\beta_- + \int_{\lambda_0}^{+\infty}\frac{-8\lambda_0^2\beta_+(\beta_+^2-\lambda_0^2)^2}{\pi(\beta_+^2+\lambda_0^2)^4}\mathcal{H}'(\beta_+)d\beta_+\Big]\\ - \varepsilon r_0\lambda_1\tau\sqrt{\tau}\Big[\int_0^{\lambda_0}\frac{-8\lambda_0\beta_-^2(\beta_-^4+3\lambda_0^4)}{\pi(\beta_-^2+\lambda_0^2)^4}\mathcal{H}''(\beta_-)d\beta_- + \int_{\lambda_0}^{+\infty}\frac{-8\lambda_0\beta_+^2(\beta_+^4+3\lambda_0^4)}{\pi(\beta_+^2+\lambda_0^2)^4}\mathcal{H}''(\beta_+)d\beta_+\Big]\end{aligned} \tag{2.7.66}$$

Again, the parameter β can be introduced with the total domain which is $[0;+\infty]$

$$\begin{aligned}\partial_\xi\eta(\lambda_c(\tau),\tau) &= -r_0\sqrt{\tau}\lambda_0\frac{-4}{\pi}\int_0^{+\infty}\frac{2\lambda_0\beta}{(\beta^2+\lambda_0^2)^2}\mathcal{H}'(\beta)d\beta\\ &\quad - \varepsilon r_1\tau\sqrt{\tau}\int_0^{+\infty}\frac{-8\lambda_0^2\beta(\beta^2-\lambda_0^2)^2}{\pi(\beta^2+\lambda_0^2)^4}\mathcal{H}'(\beta)d\beta\\ &\quad - \varepsilon r_0\lambda_1\tau\sqrt{\tau}\int_0^{+\infty}\frac{-8\lambda_0\beta^2(\beta^4+3\lambda_0^4)}{\pi(\beta^2+\lambda_0^2)^4}\mathcal{H}''(\beta)d\beta\\ &= -r_0\lambda_0\varphi_\kappa(\lambda_0)\sqrt{\tau}+\varepsilon\big(-r_0\lambda_1\varphi_s(\lambda_0)-r_1\varphi_t(\lambda_0)\big)\tau\sqrt{\tau}\end{aligned} \tag{2.7.67}$$

where the functions $\varphi_s(\lambda)$ and $\varphi_t(\lambda)$ are defined as following

$$\varphi_s(\lambda) = \frac{-8}{\pi}\int_0^{+\infty}\frac{\beta^2\lambda(\beta^4+3\lambda^4)}{(\beta^2+\lambda^2)^4}\mathcal{H}''(\beta)d\beta \quad\text{and}\quad \varphi_t(\lambda) = \frac{-8}{\pi}\int_0^{+\infty}\frac{\beta\lambda^2(\beta^2-\lambda^2)^2}{(\beta^2+\lambda^2)^4}\mathcal{H}'(\beta)d\beta \tag{2.7.68}$$

In Figure 2.15, the functions φ_r, φ_q, φ_s and φ_t are represented.

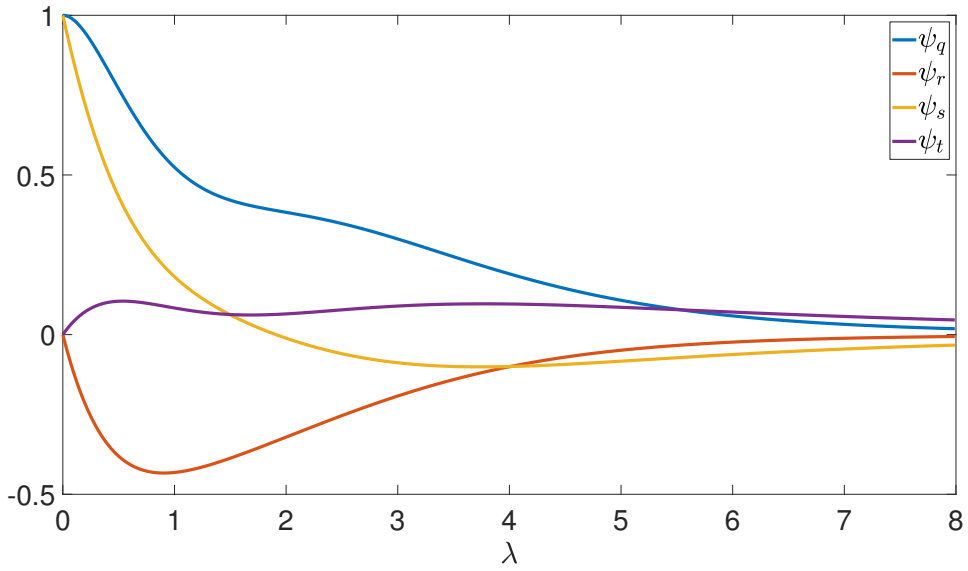

Figure 2.15: Functions φ_r, φ_q, φ_s and φ_t.

Comparing the fast and slow solutions in terms of power ε

$$(\varepsilon^0): \quad r_0\varphi_\kappa(\lambda_0) = \kappa \tag{2.7.69}$$

$$(\varepsilon^1): \quad -\varphi_s(\lambda_0)r_0\lambda_1 - \varphi_t(\lambda_0)r_1 = -\kappa\lambda_1 + \frac{\psi\lambda_0^3}{6} + \chi\lambda_0 \tag{2.7.70}$$

At leading order, the solution is totally equivalent to the solution Equation (2.6.19). Taking into account the contribution at leading order on the position and the slope, the system for the high order to solve is

$$\begin{pmatrix} \frac{1}{4}\varphi_q(\lambda_0) & r_0\varphi_r(\lambda_0) + \kappa\lambda_0 \\ -\varphi_t(\lambda_0) & \kappa - r_0\varphi_s(\lambda_0) \end{pmatrix} \begin{pmatrix} r_1 \\ \lambda_1 \end{pmatrix} = \begin{pmatrix} \frac{\psi\lambda_0^4}{24} + \frac{\chi\lambda_0^2}{2} + \frac{\alpha}{2} \\ \frac{\psi\lambda_0^3}{6} + \chi\lambda_0 \end{pmatrix} \tag{2.7.71}$$

In Figure 2.16b, The solutions λ_1 and r_1 are represented for different sets of α, χ and ψ values. Like in the case $(\alpha + \psi) > 0$, when $\kappa/\nu \geq 1$, the contact is discrete meaning that $\lambda_c = 0$ involving $\lambda_1 = \lambda_0 = 0$. For the reaction, by continuity, the reaction is extrapolated in the discrete case to satisfy at $\pm\lambda_c$ the contact between the wall and the beam. In general, the reaction is negative to avoid a complete detachment of the beam against the wall. Moreover, with the high order, the contact length is reduced due to the negative value λ_1. Some exception can be observed for example $\kappa/\nu = 0.3$ with $\alpha = \psi = -1$ and $\chi = 1$. Indeed, λ_1 is positive meaning that the high order accelerates the speed of propagation of the contact $\pm\lambda_c(\tau)$ and the reaction r_1 is positive avoid the penetration in the wall at these positions.

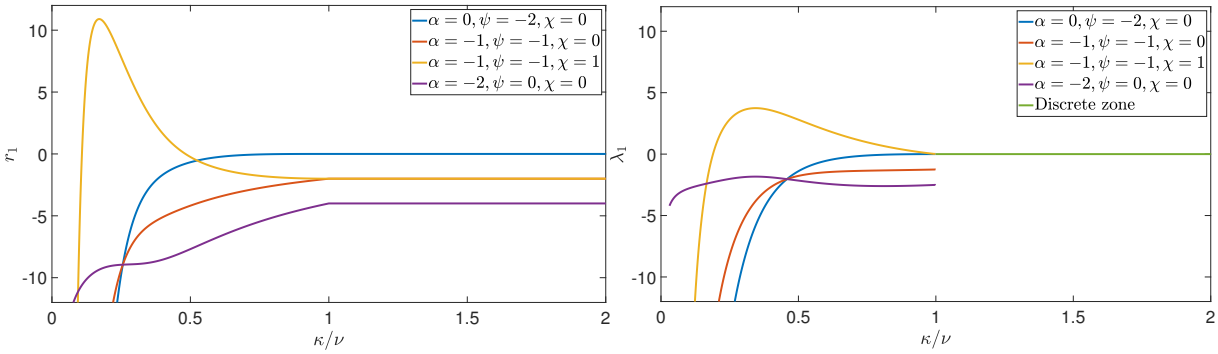

(a) Solution r_1 as function of α, ψ and χ. **(b)** Solution λ_1 as function of α, ψ and χ.

Figure 2.16: Solutions r_1 and λ_1 at high order for $\alpha + \psi < 0$.

In Figure 2.17, the beam impacts the wall with the following parameter: $\nu = 1$, $\kappa = 2$, $\alpha = -1$, $\psi = -1$ and $\chi = 0$ for $\tau = 0.1$, 0.25 and 0.5. Because to $\kappa/\nu \geq 1$, the type of contact is a discrete contact as shown on the Figure.

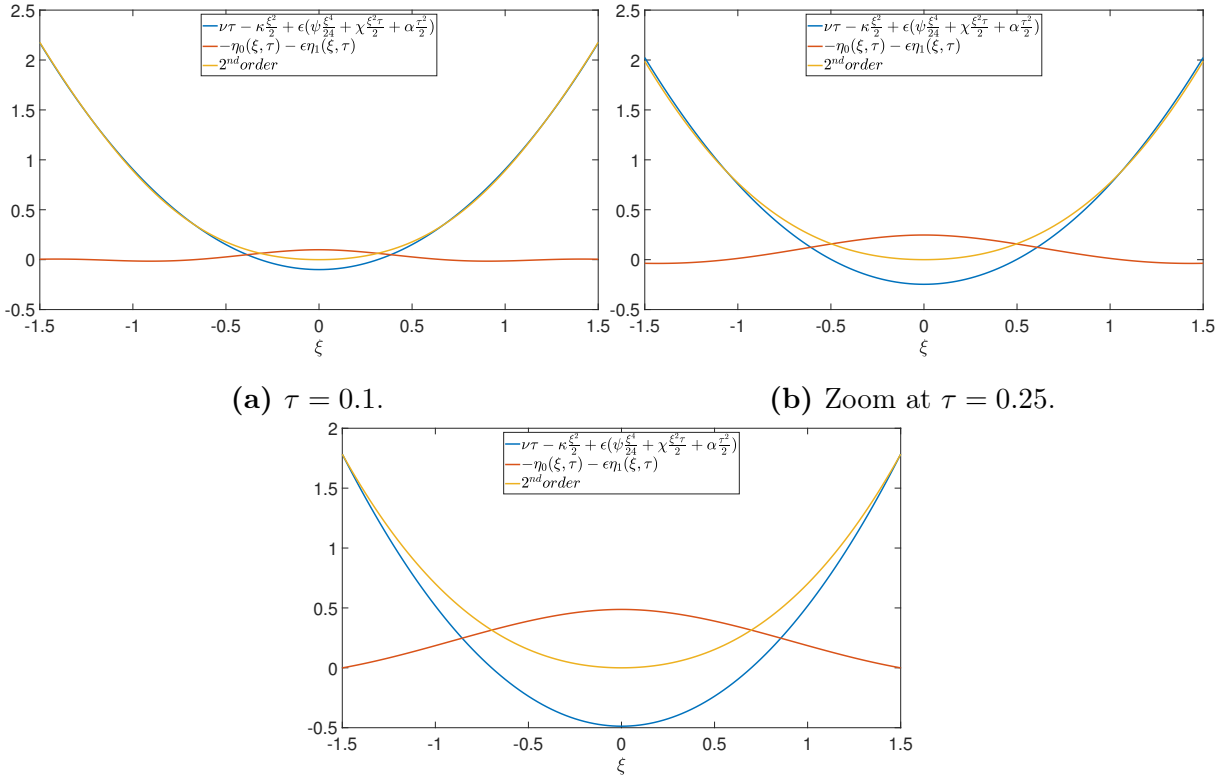

(a) $\tau = 0.1$. **(b)** Zoom at $\tau = 0.25$.

(c) $\tau = 0.5$.

Figure 2.17: Beam impacting an rigid surface for $\nu = 1, \kappa = 2$, $\alpha = -1$, $\psi = -1$, $\chi = 0$ at different time τ.

In Figure 2.18, the analytic solution is represented at different time τ. On the zoom part, the detachment increases with time. However, a small penetration in the wall can also be observed at the contact $\xi = \pm\lambda_c(\tau)$. This problem can be explained by the no-validity of the assumption to make the Taylor series when the time becomes important. Indeed, with $\kappa/\nu = 0.5$, the parameter λ_0 is 1.1089. The parameter λ_1 is -1.7729. Consequently, we have at $\tau = 0.5$: $|-1.7729 \cdot 0.5\sqrt{0.5}| = 0.6268 < 0.7205 = 1.0189\sqrt{0.5}$. There

is not one order of magnitude of difference, the value is almost the same provoking the non validity of the assumption.

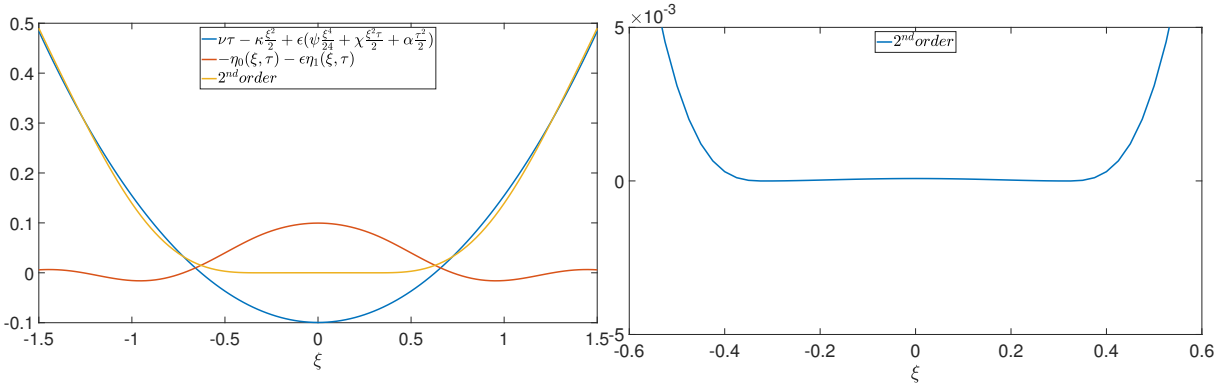

(a) $\tau = 0.1$. **(b)** Zoom at $\tau = 0.1$.

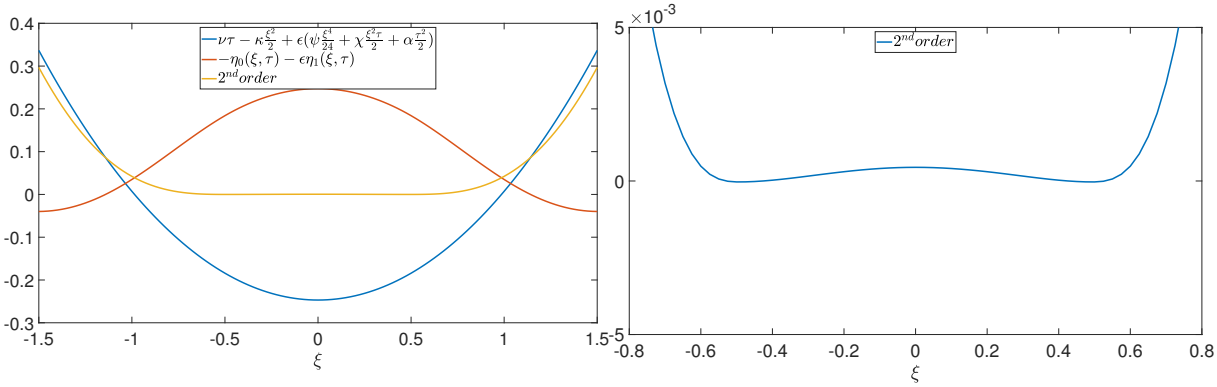

(c) $\tau = 0.25$. **(d)** Zoom at $\tau = 0.25$.

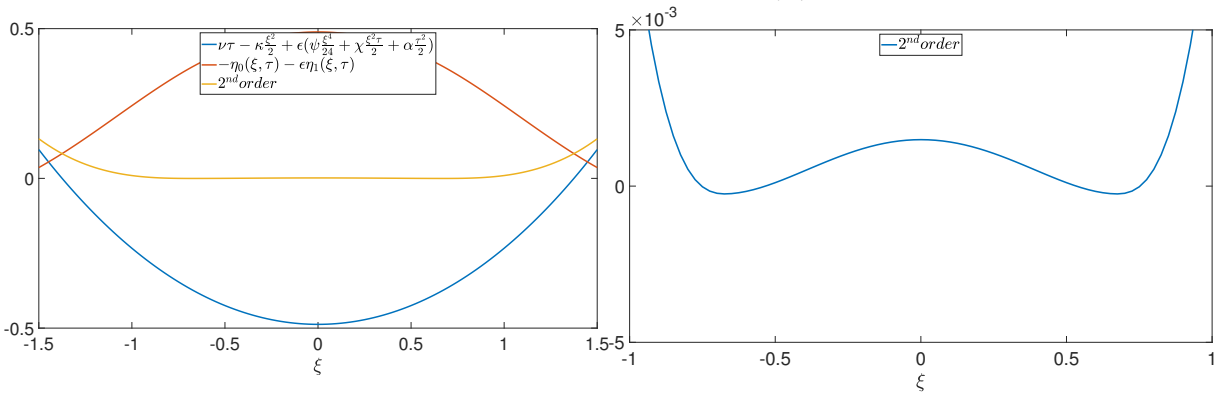

(e) $\tau = 0.5$ **(f)** Zoom at $\tau = 0.5$.

Figure 2.18: Beam impacting a rigid surface for $\nu = 1, \kappa = 0.5$, $\alpha = -1$, $\psi = -1$, $\chi = 0$ at different time τ.

3 Numerical Part

The semi-analytic approach on the beam which impacts the wall is now done. The calculations have been effectuated by distinguishing the different types of contact reaction which are generated to satisfy the complementary condition. Now, the new objective is to confirm all these results obtained using a numerical software. We will have to keep a critical mind on the numerical results and see the limitations of the solver. Before going deeper into the numerical simulations of the problem, a description of the numerical model is presented with the beam discretization and the way to take into account the unilateral contact. Moreover, the time integration method will be discussed. Two small examples to validate the Euler beam model (which are static problems) are applied to validate the model comparing to the analytic solution. Then, a full analysis is performed on all the numerical parameters (h, Δx, ρ_∞,...) to optimise them. Finally, the matching between the analytic and numerical parts is effectuated at leading order and high order with the difficulties encountered to make the complete analysis.

3.1 Discretization

To be coherent with the analytic part, the beam is modelized with Euler-Bernoulli theory like in [6], [7], [8], [9] and [10]. In this model, some assumptions are made

- Small deflections of the beam;
- Horizontal displacement not taken into account in the model;
- No transverse shear strain;
- Cross section orientation θ matches with the gradient displacement dw/dx ($\theta \approx dw/dx$);
- The dimension lengths of the section are smaller compared to the length of the beam.

Taking one element beam discretized with a length l_e (Figure 3.1), the set of DOF's is (w_1, θ_1, w_2, θ_2) where w corresponds to the vertical displacement and the slope $\theta \approx dw/dx$ for each node (which is correct due the assumption of the Euler-Bernoulli beam). The dimensionless number ξ equals to the ratio x/l_e is introduced. It varies in the range $[0; 1]$.

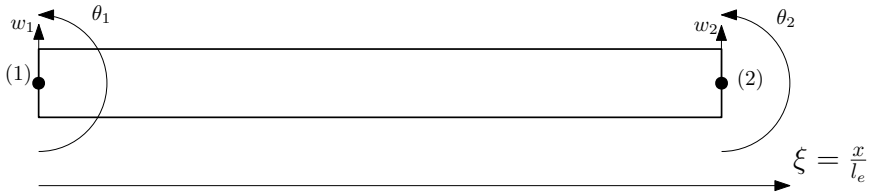

Figure 3.1: Degree of freedom of an Euler beam.

With the shape functions, the vertical displacement at position ξ can be determined

$$w(\xi) = N_1(\xi) \cdot w_1 + N_2(\xi) \cdot \theta_1 + N_3(\xi) \cdot w_2 + N_4(\xi) \cdot \theta_2 \tag{3.1.1}$$

In Appendix A.6, the shape functions are defined and shown for the variable ξ varying in the interval $[0; 1]$.

The strain energy of deformation for one element is

$$\mathcal{V}_e = \frac{1}{2}\int_0^{l_e} EI\left(\frac{\partial^2 w}{\partial x^2}\right)^2 dx \tag{3.1.2}$$

By discretization, the strain energy for one element of the beam is

$$\mathcal{V}_e = \frac{1}{2}(\mathbf{q}_e - \mathbf{q}_{0,e})^T \mathbf{K}_e (\mathbf{q}_e - \mathbf{q}_{0,e}) \tag{3.1.3}$$

where the vector $\mathbf{q}_{0,e}$ is the initial configuration of the degree of freedom and the matrix $\mathbf{K}_e$ is defined as follows

$$\mathbf{K}_e = \int_0^1 EI\left(\frac{d^2\mathbf{N}_e}{d\xi^2}\right)^T \left(\frac{d^2\mathbf{N}_e}{d\xi^2}\right)^T \frac{d\xi}{l^3} \tag{3.1.4}$$

In the matrix form, the stiffness matrix $\mathbf{K}_e$ can be written as

$$\mathbf{K}_e = \frac{EI}{l_e^3}\begin{bmatrix} 12 & 6l_e & -12 & 6l_e \\ 6l_e & 4l_e^2 & -6l_e & 2l_e^2 \\ -12 & -6l_e & 12 & -6l_e \\ 6l_e & 2l_e^2 & -6l_e & 4l_e^2 \end{bmatrix} \tag{3.1.5}$$

The kinetic energy of one element beam is

$$\mathcal{K}_e = \frac{1}{2}\dot{\mathbf{q}}_e \mathbf{M}_e \dot{\mathbf{q}}_e \tag{3.1.6}$$

where the matrix $\mathbf{M}_e$ is defined as follows:

$$\mathbf{M}_e = \int_0^1 m\mathbf{N}_e^T \mathbf{N}_e l d\xi \tag{3.1.7}$$

In matrix form, the mass matrix $\mathbf{M}_e$

$$\mathbf{M} = \frac{\mu l_e}{420}\begin{bmatrix} 156 & 22l_e & 54 & -13l_e \\ 22l_e & 4l_e^2 & 13l_e & -3l_e^2 \\ 54 & 13l_e & 156 & -22l_e \\ -13l_e & -3l_e^2 & -22l_e & 4l_e^2 \end{bmatrix} \tag{3.1.8}$$

At high order, an acceleration a_0 will be applied on the system through a conservative force (which is independent of the taken path). The conservative energy of one element beam is

$$E_a = \frac{m_e w_1 a_0}{2} + \frac{m_e w_2 a_0}{2} \tag{3.1.9}$$

For the beam section, in order to satisfy the assumption, a square section ($b = d$) is selected with a length of $b = d = 0.01$ $[m]$ and the quadratic moment which is $I = bd^3/12 = 8.33 \cdot 10^{-10}$ $[m^4]$. For the density ρ, having the mass per unit length μ and the cross section A, we have $\rho = \mu/A$.

To confirm the discretization, two examples with static solver will be performed and compared to the analytic solution: beam fixed at both ends and cantilever beam.

The first example studied is the beam fixed at both ends as shown in Figure 3.2.

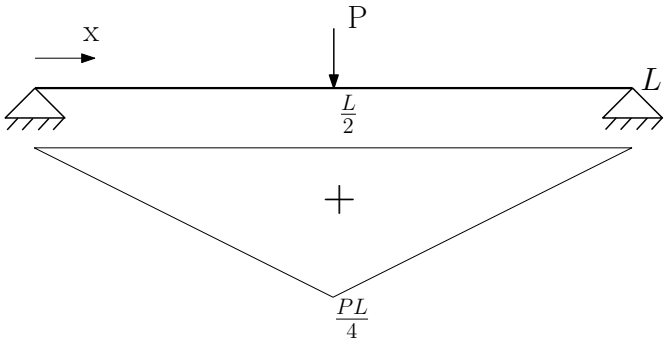

Figure 3.2: Fixed beam at both ends submitted to a concentrated force P at the middle of the beam with bending moment diagram.

At $x = 0$ and $x = L$, the vertical displacement of the beam is blocked ($w(0) = 0$ and $w(L) = 0$). Moreover, at the middle of the beam by symmetry, the slope of the beam is zero ($dw/dx(0) = 0$). A concentric force P is applied at the middle of the beam. Using the fundamental elastic equation

$$\frac{d^2w}{dx^2} = -\frac{M}{EI} \tag{3.1.10}$$

The analytic solution will be performed on the first part $[0; L/2]$ and by symmetry the solution can be extrapolated in $[L/2; L]$. By integrated two times the transverse displacement, the analytic solution can be written as

$$w(x) = -\frac{Px^3}{12EI} + C_1x + C_2 \tag{3.1.11}$$

$$= -\frac{Px^3}{12EI} + \frac{PL^2x}{16EI} \tag{3.1.12}$$

using the two boundaries conditions $C_2 = 0$ and $C_1 = PL^2/16EI$.
In Figure 3.3, the numerical and analytical solution are superimposed.

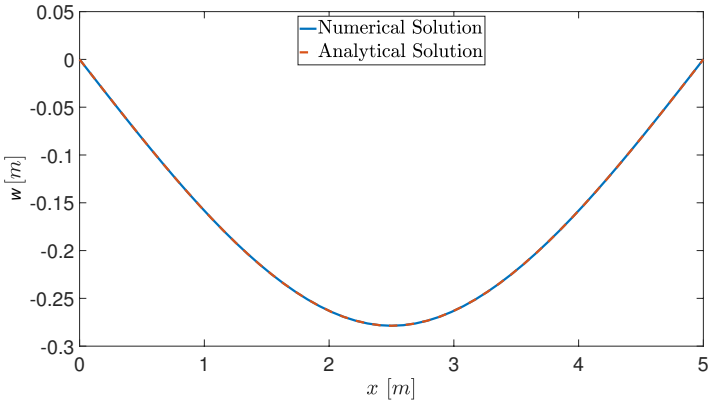

Figure 3.3: Encastre beam at $x = 0$ and $x = L$ where $L = 5$ $[m]$, $EI = 9.345 \cdot 10^3$ $[N \cdot m^2]$, $P = 5 \cdot 10^5$ $[N]$ and 52 elements.

An another example is the cantilever beam where a force P is applied on the extremity of the beam at $x = L$ and the beam is completely fixed at $x = 0$ as shown in Figure 3.4.

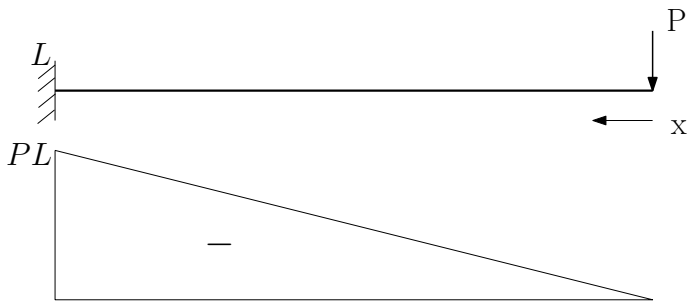

Figure 3.4: Cantilever beam submitted to a concentrated force P on the extremity of the beam with bending moment diagram.

With the bending moment $M(x) = -Px$, the elastic equation to solve becomes

$$\frac{d^2w}{dx^2} = \frac{Px}{EI} \tag{3.1.13}$$

As previously, by integrating two times, we obtain

$$w(x) = \frac{Px^3}{6EI} + C_1x + C_2 \tag{3.1.14}$$

Using the boundary conditions at $x = 0$ ($w(0) = 0$ and $dw/dx(0) = 0$), $C_1 = -PL^2/2EI$ and $C_2 = PL^3/3EI$, the final solution can be written as

$$w(x) = \frac{Px^3}{6EI} - \frac{PL^2x}{2EI} + \frac{PL^3}{3EI} \tag{3.1.15}$$

In Figure 3.5, again, there is correspondence between the numerical and analytical solution.

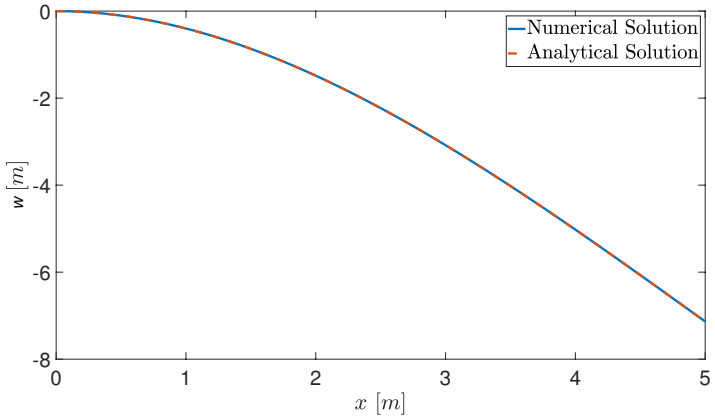

Figure 3.5: Cantilever beam completely fixed at $x = L$ and a concentric force is applied at $x = 0$ where $L = 5$ $[m]$, $EI = 9.345 \cdot 10^3$ $[N \cdot m^2]$, $P = 8 \cdot 10^5$ $[N]$ and 52 elements.

With these 2 examples, the discretization of the Euler beam is correctly implemented and will be applied for the impact beam.

3.2 Nonsmooth Generalized-α Method

During an impact between two rigid bodies, the dynamics, which is a smooth response, becomes non-smooth due to the apparition of impulsive reactions and velocity jumps.

Two principal types of constraint exist:

- Bilateral constraints which are linked to kinematic joints. These joints impose relative motions of bodies.
- Unilateral constraints which characterize the non-penetration condition at the contact point.

Thus, for the beam impacting on the surface, the constraints are only unilateral constraints. One simple method to solve unilateral constraint is called Moreau-Jean method where the constraint is applied at the velocity level but with a constraint drift at the position level. A simple example is the bouncing ball having only one degree of freedom with the dynamic equations

$$\dot{q} = v \tag{3.2.1}$$

$$M\dot{v} - g_q^T \lambda = -mg \tag{3.2.2}$$

$$0 \leq g(q) \perp \lambda \geq 0 \tag{3.2.3}$$

To take into account the non-smooth dynamic response at the contact time, an impact law is introduced

$$g_q(q(t^+))v(t^+) = -eg_q(q(t^-))v(t^-) \tag{3.2.4}$$

where e is the coefficient of restitution $\in [0; 1]$, t^- the time just before the impact and t^+ the time just after the impact. For a rigid body, this coefficient defines the amount of energy dissipated by the body during the impact. Thus, after the impact of the ball on the wall, the ball velocity changes by taking the opposite direction with an amplitude $e \cdot v$. In Figure 3.6, the bouncing ball is dropped with a height of 0.5 $[m]$ at rest with a coefficient of restitution e equals to 0.9. The time integration method is the Euler implicit method with a time step $h = 0.001$ $[s]$. We can observe logically that at each impact the new maximal height is smaller. Indeed, with $e = 0.9$, there is some energy dissipation at each impact. In this case with the Moreau-Jean method, the potential new position q is evaluated and if this value is negative, the unilateral constraint is activated with the impact law. Thus, the true new position is evaluated using the impact law by applying the change of direction of the velocity. Consequently, in the zoom, we can observe that the position of the bouncing ball does not reach the wall meaning that the constraint drifts at the position level. This phenomenon of gap between the wall and the ball can be controlled by the time step by reducing its value.

As it was previously explained, in our impact problem, only unilateral contact occurs, the dynamic system to solve can be written in matrix form as

$$\dot{\mathbf{q}} = \mathbf{v} \tag{3.2.5}$$

$$\mathbf{M}(\mathbf{q})\dot{\mathbf{v}} - \mathbf{g}_\mathbf{q}^T(\mathbf{q})\boldsymbol{\lambda} = \mathbf{f}(\mathbf{q}, \mathbf{v}, t) \tag{3.2.6}$$

$$\mathbf{0} \leq \mathbf{g}(\mathbf{q}) \perp \boldsymbol{\lambda} \geq 0 \tag{3.2.7}$$

where t is the time, $\mathbf{q}$ and $\mathbf{v}$ represent respectively the vector position and speed of degree of freedom of the system. $\mathbf{M}(\mathbf{q})$ is the mass matrix. $\mathbf{f}$ is the forces vector containing

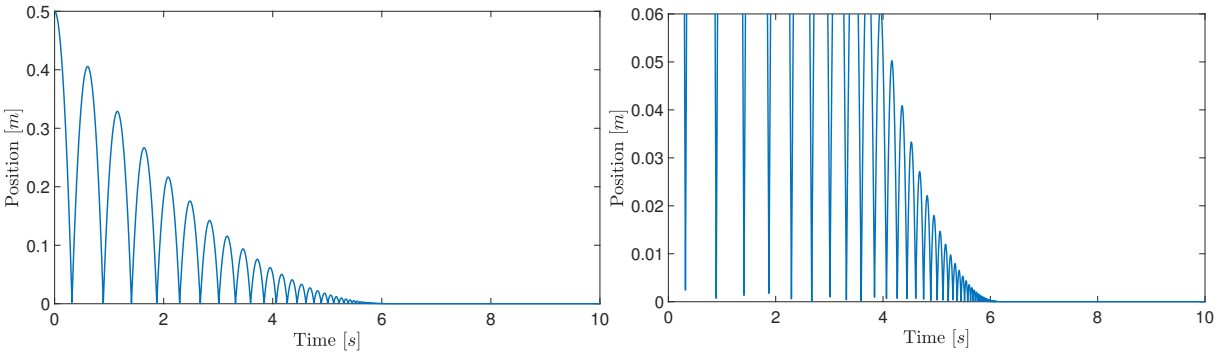

Figure 3.6: Bouncing ball with $q_0 = 0.5[m]$, $v_0 = 0[m/s]$, $h = 0.001$ $[s]$ and $e = 0.9[-]$. Zoom at the level contact on the right figure.

internal, external and damping forces. $\mathbf{g}$ is the set of unilateral constraints and $\mathbf{g_q}$ is the matrix of constraint gradients. $\boldsymbol{\lambda}$ is the vector containing the Lagrange multiplier representing the reaction forces of the unilateral contacts.

At the position level, the unilateral contact k is active at time t_i if the constraint $g^k(\mathbf{q}(t_i))$ is equal to 0. Consequently, either the reaction at the contact k is just zero or positive meaning ($\lambda_k \geq 0$). This condition of active unilateral constraint at the position level can be written as

$$\lambda^k(t_i) - r g^k(\mathbf{q}(t_i)) \geq 0 \tag{3.2.8}$$

where r is a strictly positive real number. Moreover, to avoid penetration at the next iteration, the unilateral contact must be also applied at the velocity level by imposing the gap velocity $g^k_{\mathbf{q}}(\mathbf{q}(t_i))\mathbf{v}(t_i)$ positive. The unilateral contact can be written as

$$0 \leq g^k_{\mathbf{q}}(\mathbf{q}(t_i))\mathbf{v}(t_i) \perp \lambda^k \geq 0 \tag{3.2.9}$$

The contact is active at time t_i for the unilateral constraint k if $g^k_{\mathbf{q}}(\mathbf{q}(t_i))\mathbf{v}(t_i) = 0$ (velocity level) and $g^k(\mathbf{q}(t_i)) = 0$ (position level). In the same way that at the position level, the Lagrange multiplier must be non-negative giving the active unilateral constraint at the velocity level

$$\lambda^k(t_i) - r g^k_{\mathbf{q}}(\mathbf{q}(t_i))\mathbf{v}(t_i) \geq 0 \tag{3.2.10}$$

The same operation can be applied at acceleration level where the gap acceleration is $g^k_{\mathbf{q}}(\mathbf{q}(t_i))\dot{\mathbf{v}}(t_i) + h^k(\mathbf{q}(t_i), \mathbf{v}(t_i))$.The term $\mathbf{h}(\mathbf{q}, \mathbf{v})$ is a quadratic operator with respect to its second argument defined as

$$\mathbf{h}(\mathbf{q}, \mathbf{v}) = \frac{\partial\big(\mathbf{g_q}(\mathbf{q})\mathbf{v}, \mathbf{v}\big)}{\partial \mathbf{q}}\mathbf{v} \tag{3.2.11}$$

The constraint is active if $g^k_{\mathbf{q}}(\mathbf{q}(t_i))\mathbf{v}(t_i) = 0$ (velocity level), $g^k_{\mathbf{q}}(\mathbf{q}(t_i)) = 0$ (position level) and $g^k_{\mathbf{q}}(\mathbf{q}(t_i))\dot{\mathbf{v}}(t_i) + h^k(\mathbf{q}(t_i), \mathbf{v}(t_i)) = 0$ (acceleration level). The active unilateral constraint at the acceleration level is

$$\lambda^k - r\big(g^k_{\mathbf{q}}(\mathbf{q}(t_i))\dot{\mathbf{v}}(t_i) + h^k(\mathbf{q}(t_i), \mathbf{v}(t_i))\big) \geq 0 \tag{3.2.12}$$

In the solver used, the unilateral constraint is verified at the three levels at the same time to offer a better accuracy on the solution.

For an impact phenomenon, there are impulsive reaction forces and jumps in the velocity field which must be characterized. Because a jump of velocity occurs, the acceleration is not well defined in the usual sense. The velocity will be represented in terms of the measure associated

$$d\mathbf{v} = \dot{\mathbf{v}}dt + \sum_i (\mathbf{v}^+(t_i) - \mathbf{v}^-(t_i))\delta_{t_i} \tag{3.2.13}$$

Similarly, for the impulse of the reaction forces, we have

$$d\mathbf{i} = \boldsymbol{\lambda}dt + \sum_i \mathbf{p}_i \delta_{t_i} \tag{3.2.14}$$

where $\boldsymbol{\lambda}$ is the vector of nonimpulsive Lagrange multipliers associated and $\mathbf{p}_i$ is the impulse producing the jump at time t_i. The dynamics system can be rewritten in matrix form as

$$\dot{\mathbf{q}} = \mathbf{v} \tag{3.2.15}$$

$$\mathbf{M}(\mathbf{q})d\mathbf{v} - \mathbf{g}_\mathbf{q}^T d\mathbf{i} = \mathbf{f}(\mathbf{q}, \mathbf{v}, t)dt \tag{3.2.16}$$

$$\mathbf{0} \leq \mathbf{g}(\mathbf{q}) \perp d\mathbf{i} \geq \mathbf{0} \tag{3.2.17}$$

When an impact occurs at the time t_i, the constraint condition for the unilateral is written as

$$\mathbf{0} \leq \mathbf{g}(\mathbf{q}) \perp \mathbf{p}_i \geq 0 \tag{3.2.18}$$

Consequently, the condition of active unilateral constraint at the position level at contact k is

$$p_i^k - r g^k(\mathbf{q}(t_i)) \geq 0 \tag{3.2.19}$$

Using the impact law (3.2.4), the unilateral contact at the velocity level is

$$p_i^k - r\left(g_\mathbf{q}^k(\mathbf{q}(t_i))\mathbf{v}(t_i) + e^k g_\mathbf{q}^k(\mathbf{q}(t_i))\mathbf{v}^-(t_i)\right) \geq 0 \tag{3.2.20}$$

The nonsmooth generalized-α method will split the motion into two parts. The smooth contribution with a trajectory having a continuous displacement and velocity. The nonsmooth contribution takes into account the velocity jumps, impulsive reactions and the correction on the positions. For the smoother part, a second order time discretization is applied which is the second-order generalized-α method and for nonsmooth part a first order time discretization is implemented (first-order backward Euler scheme). The explanation comes from [11], [12] and [13] where more details can be found. One point to know is that the solver does not modelize frictional contact conditions.

3.3 Numerical Analysis

During the numerical analysis, a lot of parameters must be taken into account. They are either numerical parameters (coefficient of restitution, numerical damping,...) or physical parameters (EI, μ, V_0, ...). Some of them will be restricted to satisfy the different assumptions on the problem statement.

For the numerical parameters, their influence will be studied to optimise the solver to obtain the best solution which represents and validates the analytic solution. In the next part, two important parameters for the solution accuracy will be examined: the time step h and the mesh of the beam. Then, the coefficient of restitution and the numerical damping will also be explored to see their impact on the solution. Finally, the two models investigated to represent the constraints of no penetration in the wall will be simulated. Once all these numerical parameters are correctly chosen, the analysis to rediscover the analytic solution will be performed at leading order and high order.

3.3.1 Time step

Two important parameters which must be studied are the mesh discretization (see Section 3.3.2) of the beam and the time step which both have a direct impact on the quality of the results. The beam impact on the wall problem generates quick wave propagation into the beam. Two discontinuities must be caught to represent correctly the evolution of the beam during the impact.

- The first discontinuity is the temporal one, which happens when the contact occurs on one constraint to satisfy the no-penetration.
- The second discontinuity is the spatial discontinuity on the beam. Indeed, at the level of the contact length $\pm\lambda_c$, the beam curvature changes brutally from K to 0 in order to satisfy the curvature of the wall which is zero.

Firstly, the time step h is investigated to see the influence on the accuracy of the solution. To select the time step, it is interesting to have an order of magnitude of the impact duration. For example with $V_0 = 20\ [m/s]$, $EI = 1\ [N \cdot m^2]$, $\mu = 1\ [kg/m]$ and $\tau = 0.01\ [-]$, the impact time is $2.5 \cdot 10^{-5}\ [s]$. Consequently, the time step must be at least $10^{-5} - 10^{-6}$. To make the analysis, a test case is selected with the following set of parameters: the middle method ($\xi = 0.5$) for constraints, $L = 50\ [m]$, $EI = 1\ [N \cdot m^2]$, $\mu = 1\ [kg/m]$, $V_0 = 20\ [m/s]$, $K = 1\ [m^{-1}]$, uniform mesh on the contact domain with $\Delta x = 2.5 \cdot 10^{-3}\ [m]$ and $e = 1.25\ [-]$.

In Table 3.1, 5 simulations are effectuated with different time steps h for this parameter set. With $h = 10^{-6} - 10^{-7}$, the maximal number of iterations and mean number of iterations for the Newton-Raphson correction are higher than the other time steps. If the time step is too high for the mesh, during one time iteration, the contact length can travel several elements of beam. Thus, the correct behavior can not be correctly caught with this time step. Thus, we will compare with smaller time steps $h = 5 \cdot 10^{-8}$, $2.5 \cdot 10^{-8}$ and $10^{-8}\ [s]$. As expected in Table 3.1, the CPU time increases when the time step decreases because the number of time iterations increases.

To select a correct range for the time step h, the beam geometry at the end of the impact, the reaction force and the contact length will be investigated. Firstly, in Figure 3.7, the geometry of the beam is shown. Whatever the time step h, a detachment of the beam can be observed in the middle in order $2 \cdot 10^{-4}\ [m]$ which is due to numerical

h $[s]$	time $[s]$	Maximum number of iterations	Mean number of iterations
10^{-6}	90	18	5.233
10^{-7}	235	5	1.2767
$5 \cdot 10^{-8}$	381.83	5	1.0933
$2.5 \cdot 10^{-8}$	715.86	4	1.035
10^{-8}	1753.98	4	1.011

Table 3.1: CPU time, maximal number of iterations and mean number of iteration for different time step h.

errors. Ideally, with the analytic solution, we know that the contact zone must be flat and glued on the wall located at $y = 0$. These numerical errors will be discussed later and will be a major problem to be able to catch the solution at high order.

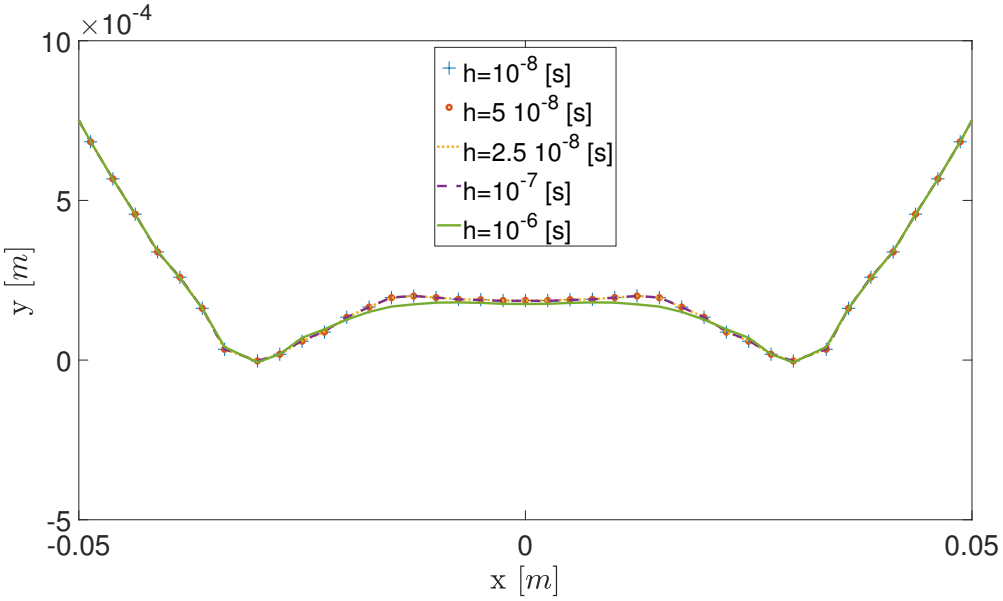

Figure 3.7: Zoom on the impact zone for different time step h at $t_f = 2.5 \cdot 10^{-5}[s]$.

In Figure 3.8, for the contact length, we can observe that for $h = 10^{-6}$ $[s]$, the solver have more difficulties to catch the curve. For the smaller time steps, the analytic curve is found with steps which are bigger and bigger. It can be easily explained by the fact that in the contact zone the mesh is uniform. Knowing that the contact zone is in the form

$$\lambda_c(t) = \lambda_0 \sqrt{t} \tag{3.3.1}$$

Thus, by derivation, the velocity of the propagation of the impact is

$$\dot{\lambda}_c(t) = \frac{\lambda_0}{2} \frac{1}{\sqrt{t}} \tag{3.3.2}$$

At the beginning of the impact, the propagation of the first element is effectuated in few time iterations. Then, to travel the second element of the beam, because the velocity is $\propto 1/\sqrt{t}$, the necessary time to travel it is consequently bigger than the first one. For the next elements, the time increases and increases provoking in Figure 3.8 steps which are longer and longer. To avoid this problem, an idea is to create a non-uniform mesh in the contact zone which is investigated later.

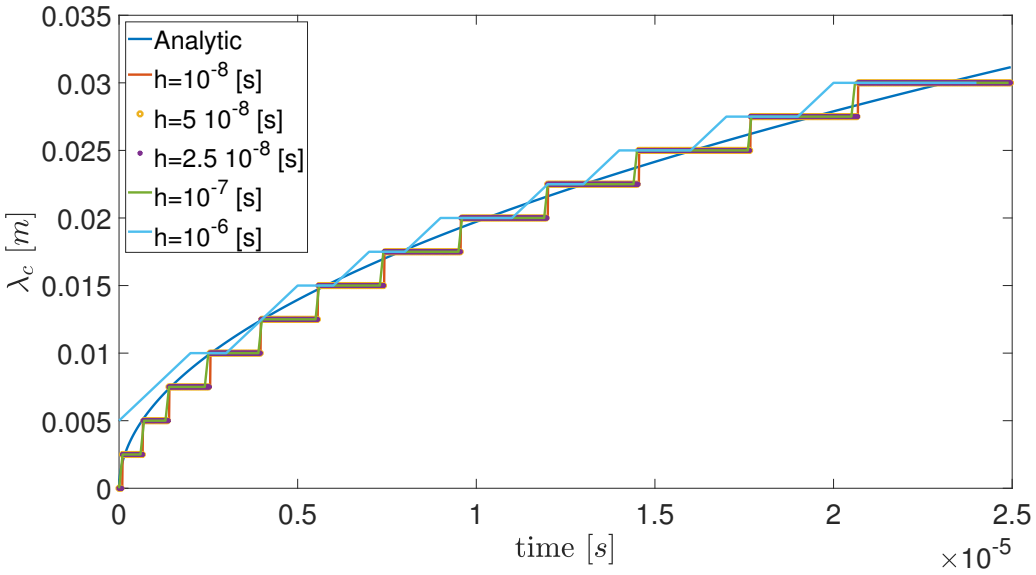

Figure 3.8: Contact zone λ_c for different time step h.

With the geometry and the contact length, the time step must be small and do not influence a lot the solution. For the contact reaction, we will see that the time step plays a role on the solution. In Figure 3.9, the time steps $h = 10^{-6}$ and 10^{-7} can be excluded because the solution can not catch the behavior in $\propto 1/\sqrt{t}$ of the analytic solution at the very beginning of the impact. For $h = 5 \cdot 10^{-8}$, the time step seems again to be too big to catch the solution. For $h = 10^{-8}$ and $h = 2.5 \cdot 10^{8}$, the behavior seems to be caught. In this example, in *Matlab*, a filter of order 1 is applied with the function $filtfilt$ with 0.04 for the cut of frequency. One important fact is that for the reaction the time step influences a lot the solution, which is very sensitive and being in the same order of magnitude. Consequently, because the CPU cost is less expensive with $h = 2.5 \cdot 10^{-8}$ $[s]$, this time step is chosen for the following.

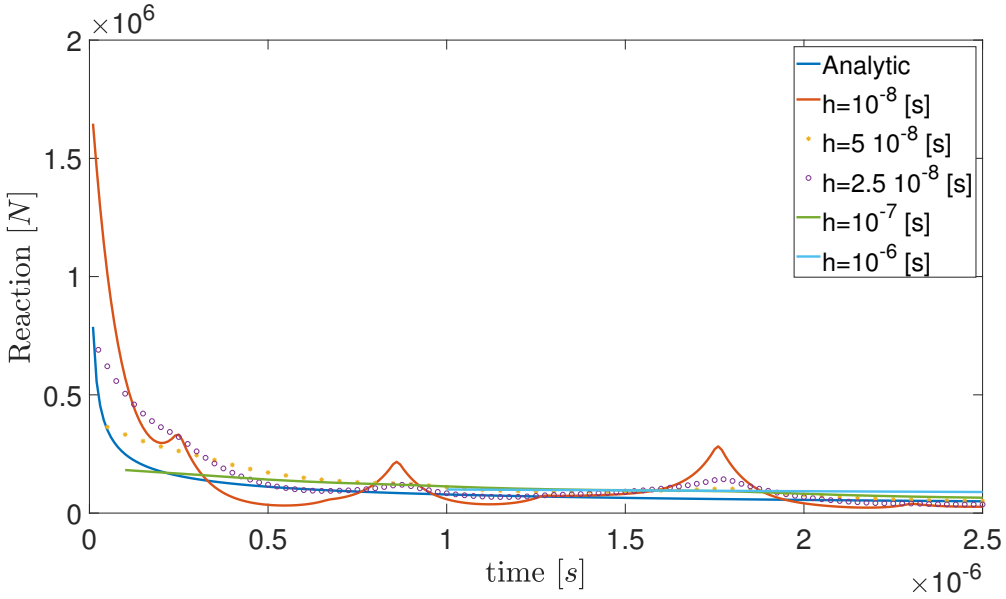

Figure 3.9: Reaction contact R for different time step h.

3.3.2 Mesh

Having chosen the time step $h = 2.5 \cdot 10^{-8}$ $[s]$, the mesh will be studied to see the advantages and disadvantages of the different types of mesh. Three types of mesh will be tested. The first approach is the classical uniform mesh on all the beam by fixing the spatial step Δx between each node. One example is effectuated with this mesh, to have a spatial step $\Delta x = 2.5 \cdot 10^{-3}$ $[m]$ on a length $L = 5$ $[m]$, the number of elements is 2000. Consequently, for a length $L = 50$ $[m]$, a problem of memory occurs due to the big number of elements. The software is not able to run the code. For $L = 5$ $[m]$, $\tau = 0.01$ and $h = 2.5 \cdot 10^{-8}$ $[s]$, the CPU time for the simulation is 8513.72 $[s]$ which is expensive. To go at time $\tau = 0.1$, the waiting time exceeds one and a half day while running on my personal computer. It would be impossible to make all the next test cases. The number of elements must be reduced by modifying the mesh to reduce these problems of CPU time and memory.

The second type of mesh is to keep this uniformity in the contact zone and in the area near the contact zone (security zone) with the same spatial step Δx. Away from the contact zone and the security zone, the mesh becomes irregular by increasing gradually moving away from this zone. The goal of this mesh is to save memory by reducing the number of elements outside the interesting zone and save CPU time. In the outside domain, the spatial step Δx evolves like

$$\Delta x_i = e \cdot \Delta x_{i-1} \tag{3.3.3}$$

where the parameter e characterizes the increase of the spatial step and the element i is more fairway of the contact zone of one element compared to the element $i - 1$. If the parameter $e = 1$, this situation corresponds to a uniform mesh. Thus, to reduce the number of elements, the parameter must be greater than 1 ($e > 1$). With this irregular mesh, the spatial step Δx in the contact zone and the parameter e can be tuned to optimize the results and save CPU time and memory.

Firstly, the mesh density in the contact zone is studied. In Figure 3.10, by refining the mesh, the numerical errors stay in the same order for the geometry of the beam. The mesh does not play a significant role on the accuracy of the transverse displacement of the beam.

In Figure 3.11, the evolution of the contact zone is shown. For $\Delta x = 5 \cdot 10^{-3}$ $[m]$, the solution obtained is quite a staircase. The bigger the element length, the longer the time spent in it. For $\Delta x = 1.5 \cdot 10^{-3}$ $[m]$, at the end of impact, a deviation on the curve is found with oscillations. Consequently, with this analysis case, the spatial step $\Delta x = 2.5 \cdot 10^{-3}$ $[m]$ is the better.

In Figure 3.12, as with the time step, the spatial step is very sensitive on the results obtained for the contact reaction R. Indeed, for $\Delta x = 1.5 \cdot 10^{-3}$ $[m]$, the reaction at the beginning is not caught with $\propto 1/\sqrt{t}$ and for $\Delta x = 5 \cdot 10^{-3}$ $[m]$, the solution is overestimated. Thus, for this test case with $V_0 = 20$ $[m/s]$ and $K = 1$ $[m^{-1}]$, the optimal parameters are $\Delta x = 2.5 \cdot 10^{-3}$ $[m]$ and $h = 2.5 \cdot 10^{-8}$ $[s]$ for $K = 1/80$. In Section 3.4, the spatial dependancy on the contact reaction is investigated with the discrete contact. This analysis shows clearly that the mesh density plays an important role on the solution.

For the parameter e, because the mesh stays uniform in the contact zone, no difference appears on the geometry contact, the contact length evolution and the reaction contact. In Table 3.2, for the uniform mesh ($e = 1$), as expected, the number of elements is too expensive. To be able to run a simulation on the computer, the limit of number elements

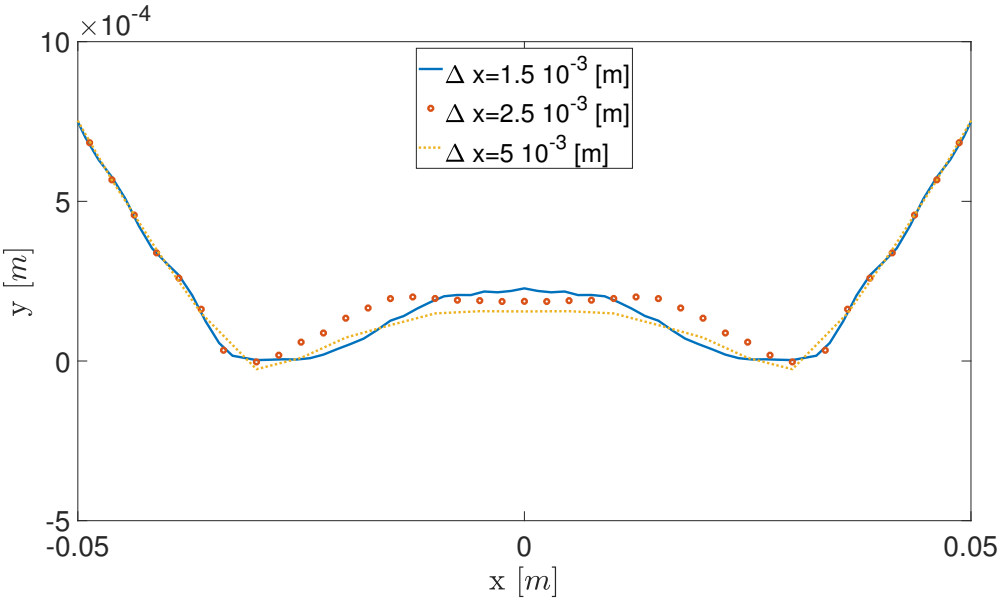

Figure 3.10: Zoom on the impact zone for different spatial step Δx at $t_f = 2.5 \cdot 10^{-5}[s]$.

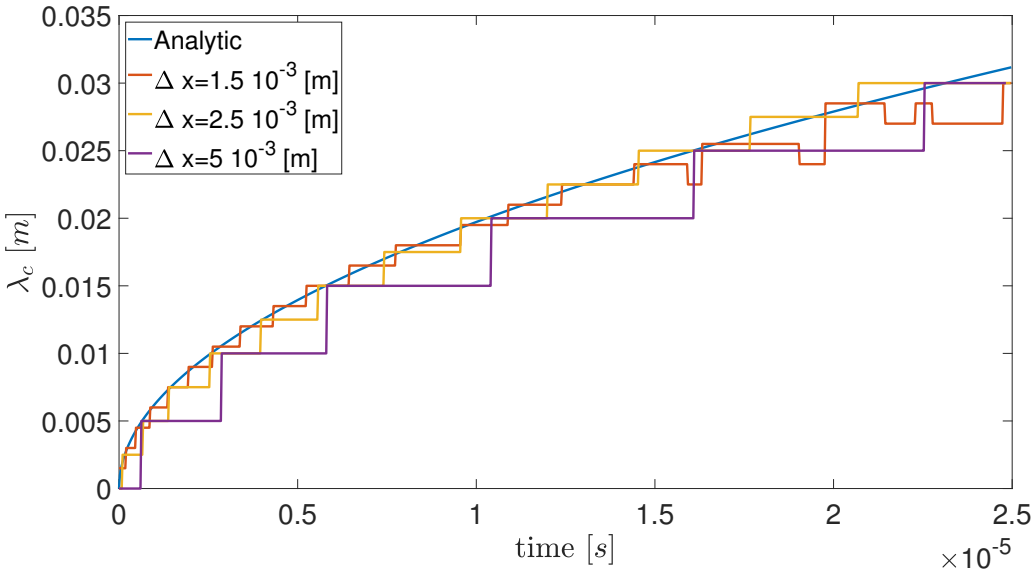

Figure 3.11: Contact zone λ_c for different spatial step Δx.

is in the order of 1500-2000 elements. Thus, by applying this no-uniform mesh in the outside domain, this number decreases strongly reducing the CPU cost. In Table 3.2, taking $e = 1.25$, the length of the smaller element is $\Delta x = 2.5 \cdot 10^{-3}$ $[m]$ (which is independent of e) and the larger element is 0.2994 $[m]$. For correct calculations, a not too big difference must appear between these sizes (see next paragraph).

For cases where the time of impact is longer or the speed of propagation is faster due to the parameter λ_0, the contact zone where the uniform mesh is applied becomes very important giving an important number of elements. Thus, the parameter must be not too small to have a correct number of elements. For example with $e = 1.25$, $\kappa/\nu = 6.25 \cdot 10^{-4}$, $L = 50$ $[m]$, $\tau = 0.1$ $[-]$, $\Delta x = 2.5 \cdot 10^{-3}$ $[m]$ which is one the cases that needs the most elements, this number is 1496 being reasonable. Consequently, for the next analysis, this parameter is selected to 1.25.

By refining too much the elements in the contact mesh, some errors occur. To explain

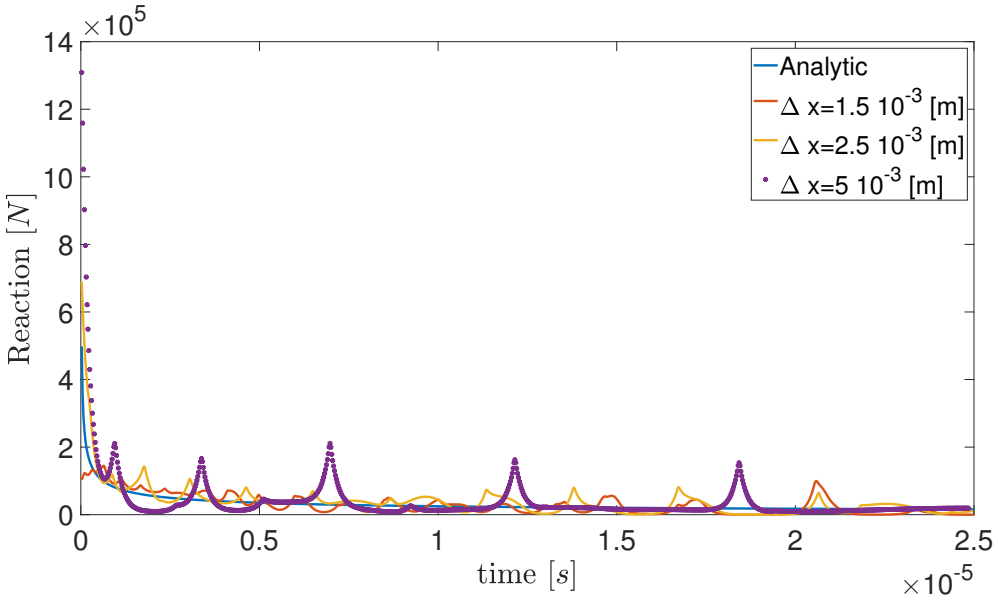

Figure 3.12: Reaction contact R for different spatial step Δx.

e	number of elements
1	20 000
1.05	302
1.1	192
1.25	120
1.5	92

Table 3.2: Number of elements as function of the parameter e for $L = 50$ $[m]$ at $\tau = 0.01$ $[-]$, $\Delta x = 2.5 \cdot 10^{-3}$ $[m]$ with $\kappa/\nu = 0.05$.

it, a reminder is effectuated on the matrix $\mathbf{S}_T$. This matrix $\mathbf{S}_T$ which allows to obtain the correction for the position, velocity and Lagrange multiplier is defined as

$$\mathbf{S}_T = \begin{pmatrix} c_r(c_a\mathbf{M} + c_g(c_v\mathbf{C}_t + c_q\mathbf{K}_t)) & c_r c_\lambda \mathbf{g}_\mathbf{q}^T \\ (c_{phipos}c_q + c_{phivel}c_v + c_{phiacc}c_a)\mathbf{g}_\mathbf{q} & \mathbf{0} \end{pmatrix} \tag{3.3.4}$$

where c_r, c_a, c_g, c_v, c_q, ... are the coefficients for the solver, $\mathbf{M}$ is the mass matrix, $\mathbf{C}_t = \partial\mathbf{f}/\partial\dot{\mathbf{q}}$ is the tangent damping matrix and $\mathbf{K}_t = \partial(\mathbf{f} + \mathbf{g}_\mathbf{q}^T\boldsymbol{\lambda})/\partial\mathbf{q}$ the tangent stiffness matrix. For example, with $\Delta x = 10^{-4}$ $[m]$, a problem occurs which is "Matrix is close to singular or badly scaled" for the matrix $\mathbf{S}_T$. This problem can be explained by the fact that, in the contact zone, the mass of the beam is very small compared the mass of the beam at its extremities due to the size of the length. Moreover, the stiffness matrix depends also on the element length. Thus, for small size, these elements become hyper-rigid compared to the others. Consequently, the matrix $\mathbf{M}$ and $\mathbf{K}_t$ are ill-conditionning and a problem occurs for the inversion of the matrix $\mathbf{S}_T$.

In order to avoid the ill conditionning, a limitation ratio of the length on the biggest elements which are located in the extremities of the domain is introduced. The idea is to add a condition to avoid that the length of the largest element is not bigger than ratio_mesh $\cdot\, \Delta x$. By choice, this ratio is selected to 10^3. In this example, with $e = 1.25$, no problem of matrix occurs. The second point, a limitation on the size of the smaller element (which corresponds to the spatial step Δx) is selected. Thus, the spatial step is

not smaller than 10^{-3} $[m]$ to avoid hyper-rigidity for the stiffness matrix.

The third method to mesh the beam is based on the fact we want to satisfy the similarity of time needed to travel one element in the contact domain. Indeed, it is the same time for the first element or the last element in the contact zone. Thus, the mesh is adaptive due to the evolution of the contact length. Taking the analytic solution, we know that the contact length at time τ is $\lambda_c(\tau) = \lambda_0\sqrt{\tau}$. By symmetry of the problem, the mesh is identical on each side of the first point of impact which is exactly the middle of the beam (positive and negative x).

When the impact occurs at the middle of the beam, the time spent into the first elements (in the positive and negative directions) for the contact length can be expressed as the time step h

$$t_{el} \sim a \cdot h \tag{3.3.5}$$

where the parameter a must be optimized, this number must be larger than 1 to have at least one iteration where the contact length is located in the element. Knowing that the velocity of the contact zone is in the form

$$\dot{\lambda}_c(t) = \frac{\lambda_0}{2}\frac{1}{\sqrt{t}} \tag{3.3.6}$$

Using this velocity, the length of the first element can be obtained by integration between 0 and ah to find the length element L_0

$$L_0 = \int_0^{ah} \frac{\lambda_0}{2}\frac{1}{\sqrt{t}}dt = \lambda_0\sqrt{ah} \tag{3.3.7}$$

Having the first element length, the second element is characterized by a length which implies the contact length to stay in the element between the times ah and $2ah$

$$L_1 = \int_{ah}^{2ah} \frac{\lambda_0}{2}\frac{1}{\sqrt{t}}dt = \lambda_0(\sqrt{2ah} - \sqrt{ah}) = \lambda_0(\sqrt{2ah} - L_0) \tag{3.3.8}$$

This length L_1 is expressed in terms of the length L_0. The expression can be generalized for the length of the element i to catch the contact zone evolution, we have

$$L_i = \int_{iah}^{(i+1)ah} \frac{\lambda_0}{2}\frac{1}{\sqrt{t}}dt = \lambda_0\sqrt{(i+1)ah} - \sum_{j=0}^{i-1} L_j \tag{3.3.9}$$

Outside the contact zone, the mesh increases gradually with the parameter e previously selected at 1.25 to reduce the number of elements. Consequently the CPU time is decreased and memory is saved. In Figure 3.13, the mesh with the positions of the nodes is represented for a length beam of $L = 50$ $[m]$, $\kappa/\nu = 6.25 \cdot 10^{-4}$, duration of the impact $\tau = 0.01$ $[-]$, $e = 1.25$ $[-]$ and $a = 5$ $[-]$. Starting at the middle, the first elements are big due to the quick velocity of the propagation contact. Then, because the velocity slows down gradually, in order to have the same time of the contact zone in one element, the element size decreases. Arriving at the element where the contact occurs at time $\tau = 0.01$, the mesh density increases with the factor $e = 1.25$. In the same way than the

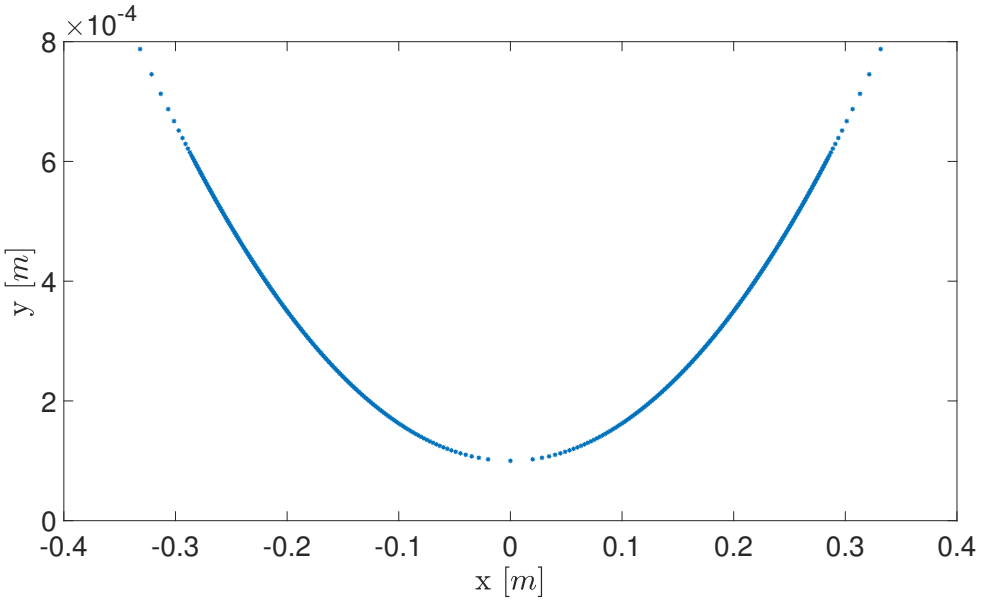

Figure 3.13: Zoom mesh representation with the nodes before the impact for a length beam $L = 50$ $[m]$, $\kappa/\nu = 6.25 \cdot 10^{-4}$, duration of the impact $\tau = 0.01$, $e = 1.25$ and $a = 5$.

non-uniform mesh with a regular mesh at the contact zone, a ratio coefficient ratio_mesh is applied to avoid problem on the matrix $\mathbf{M}$ and $\mathbf{K}_t$.

One simulation is effectuated with this mesh for the following parameters: $\kappa/\nu = 6.25 \cdot 10^{-4}$, $h = 2.5 \cdot 10^{-8}$ $[s]$, $\tau = 0.01$ $[-]$, $EI = 1$ $[N \cdot m^2]$, $\mu = 1$ $[kg/m]$, $e = 1.25$ $[-]$ and $a = 5$ $[-]$. In Figure 3.14, at $\tau = 0.01$ $[-]$, the geometry at the contact level is shown to compare the uniform mesh and the "square" mesh in the contact zone. We can observe that, at the node located at the middle of the beam, a penetration occurs in order of $1.8 \cdot 10^{-4}$ $[m]$ for the third method mesh called mesh "square". Moreover, more oscillations appear compared to the uniform mesh and the amplitude is also greater compared to the middle method.

In Figure 3.15, for the contact zone, the solution is correctly caught without steps compared the solution obtained with the uniform mesh. It can be explained by the fact the time spent in all elements is the same. For the reaction contact (Figure 3.16), the reaction contact is also caught at the beginning with a slight overestimation. This problem can provide from the time step, the mesh density or the filter. Thus, the reaction contact is very sensitive.

To summarise, the "square" mesh provides a better solution on the contact length by the fact that there is no steps. For the reaction contact, the general behavior is caught. One disadvantage of this type of mesh is that the geometric point of view is less physical because of the penetration at the center. Moreover, another disadvantage is the number of elements created with this type of mesh. For example, for $\kappa/\nu = 0.5$ and $\tau = 0.1$, the number of elements is 96 for the uniform mesh compared to 4210 elements for "square" mesh. Consequently, some limitations of memory occur. Thus, for the next of the report, the uniform mesh will be selected with a progressive increasing of the length outside the domain.

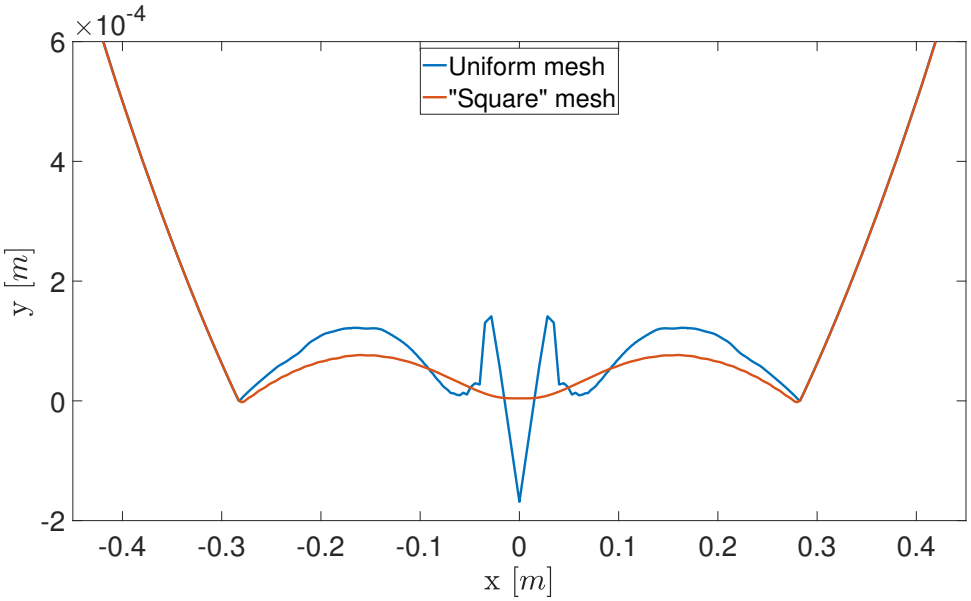

Figure 3.14: Geometry of the beam at $\tau = 0.01$ $[-]$. Comparison between the two types of mesh for $\kappa/\nu = 6.25 \cdot 10^{-4}$, $h = 2.5 \cdot 10^{-8}$ $[s]$, $EI = 1$ $[N \cdot m^2]$, $\mu = 1$ $[kg/m]$, $e = 1.25$ $[-]$ and $a = 5$ $[-]$.

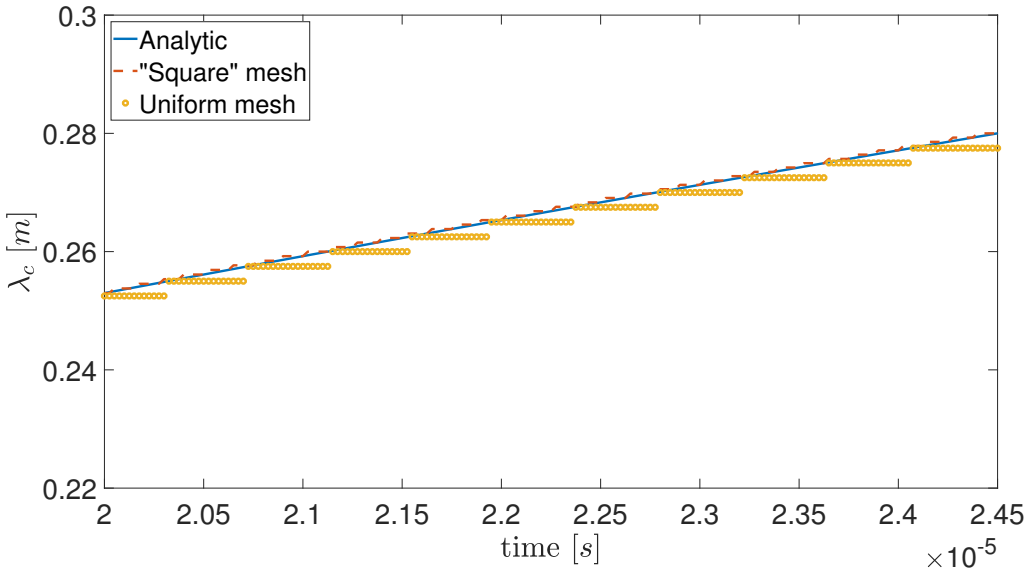

Figure 3.15: Contact length until $\tau = 0.01$ $[-]$ for $\kappa/\nu = 6.25 \cdot 10^{-4}$, $h = 2.5 \cdot 10^{-8}$ $[s]$, $EI = 1$ $[N \cdot m^2]$, $\mu = 1$ $[kg/m]$, $e = 1.25$ $[-]$ and $a = 5$ $[-]$ ("square mesh").

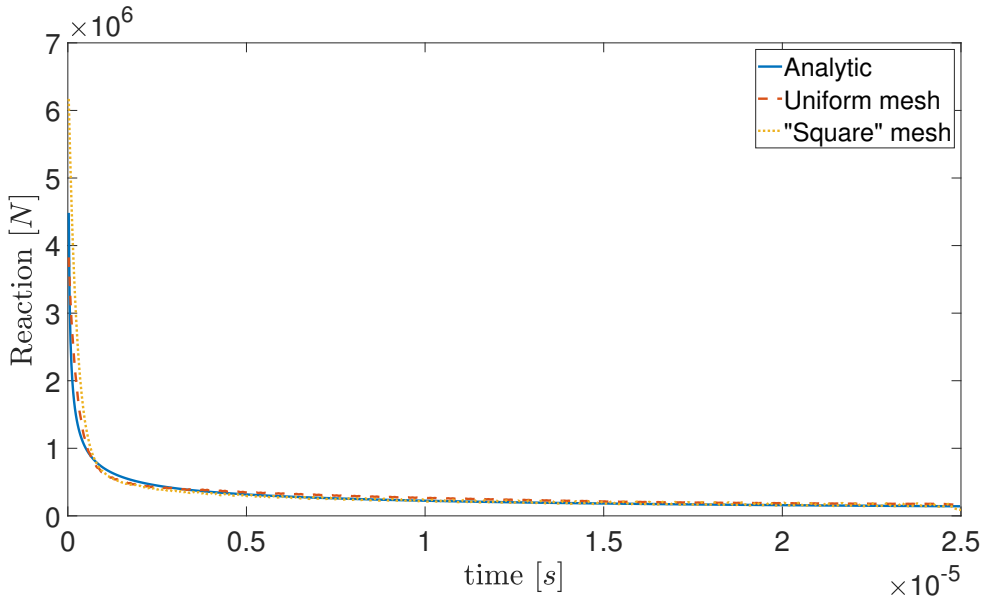

Figure 3.16: Reaction contact until $\tau = 0.01$ $[-]$ for $\kappa/\nu = 6.25 \cdot 10^{-4}$, $h = 2.5 \cdot 10^{-8}$ $[s]$, $EI = 1$ $[N \cdot m^2]$, $\mu = 1$ $[kg/m]$, $e = 1.25$ $[-]$ and $a = 5$ $[-]$ ("square mesh").

3.3.3 Numerical Damping

In the numerical model, for the smoother part, the time integration solver is an explicit solver, more precisely the Chung-Hulbert method which is a second-order scheme. The modeling problem is an impact between two bodies. The outbreak of the contact needs to have a large range of modes (so needs to have high frequencies). Thus, the time step selected must be small to offer a large range of modes to be able to represent the double problem of discontinuity (spatial and temporal). For the mesh, by refining the mesh to catch the behavior of the solution like the contact length, some higher modes are created. They are artefacts. These modes do not represent the real physics. At high frequency, the complexity of this problem is that the artefacts modes are mixed with the mode introduced due to the time step. Without numerical damping, the instabilities can arise. Thus, the artefact modes must be attenuated with numerical damping using the spectral radius at infinite frequencies ρ_∞ including in the range $[0; 1]$. If $\rho_\infty = 1$, the numerical errors due to the high frequencies are absolutely not dissipated. With the nonsmooth generalized-α method, the time integration which is the generalized-α method is applied on the system. The set of equations for the position $\mathbf{q}$, the velocity $\mathbf{v}$ and the acceleration $\mathbf{a}$ are

$$\mathbf{q}_{n+1} - \mathbf{q}_n = h\mathbf{v}_n + h^2(0.5 - \beta)\mathbf{a}_n + h^2\beta\mathbf{a}_{n+1} + \mathbf{U}_{n+1} \tag{3.3.10}$$

$$\mathbf{v}_{n+1} - \mathbf{v}_n = h(1 - \gamma)\mathbf{a}_n + h\gamma\mathbf{a}_{n+1} + \mathbf{W}_{n+1} \tag{3.3.11}$$

$$(1 - \alpha_m)\mathbf{a}_{n+1} + \alpha_m\mathbf{a}_n = (1 - \alpha_f)\dot{\tilde{\mathbf{v}}}_{n+1} + \alpha_f\dot{\tilde{\mathbf{v}}}_n \tag{3.3.12}$$

where h is the time step, $\mathbf{U}$ is the vector containing the position correction, $\mathbf{W}$ is the velocity jump and $\dot{\tilde{\mathbf{v}}}$ is the smooth acceleration. The coefficients α_M, α_F, γ and β are linked to the numerical damping ρ_∞ as follows

$$\alpha_M = \frac{2\rho_\infty - 1}{\rho_\infty + 1} \tag{3.3.13}$$

$$\alpha_F = \frac{\rho_\infty}{\rho_\infty + 1} \tag{3.3.14}$$

$$\gamma = 0.5 + \alpha_F - \alpha_M \tag{3.3.15}$$

$$\beta = 0.25 \cdot (\gamma + 0.5)^2 \tag{3.3.16}$$

One possible major impact on the solution due to the numerical damping is the evolution of the energy for the beam. Indeed, during the impact, the energy is dissipated due the impact of the two bodies. When a node or a middle point enters into contact, the kinetic energy of the beam at this location is pushed to zero with the coefficient of restitution which is fixed to $g = 0$. This energy is either absorbed by the wall or transformed into heat and friction. However, due to the numerical parameter ρ_∞, some numerical dissipation happens for the system. For the energy evolution during the impact (Figure 3.18), the observation is the numerical dissipation decreases very slowly the energy of the system compared to the enery lost due to the impact. In Figure 3.17, several simulations are effectuated by varying the numerical damping to see the influence on the geometry of the beam in order to reduce the numerical errors. We can observe that there is no major change. Consequently, during all the numerical part, the parameter ρ_∞ is fixed to 0.8 to have small numerical dissipation.

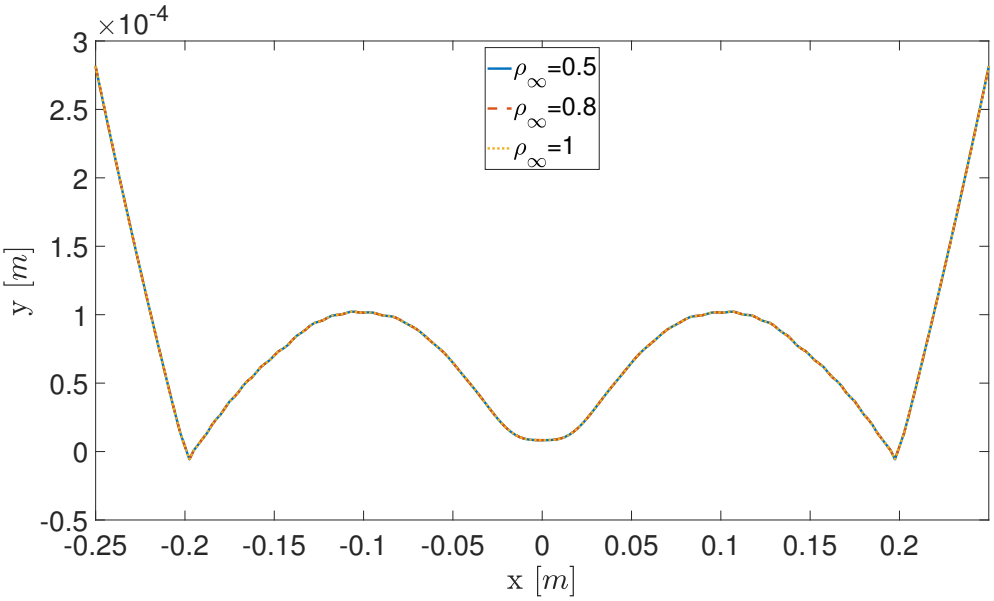

Figure 3.17: Geometry of the beam at $\tau = 0.01$ $[-]$. Uniform mesh at the contact zone for $\kappa/\nu = 1.3 \cdot 10^{-3}$, $h = 2.5 \cdot 10^{-8}$ $[s]$, $EI = 1$ $[N \cdot m^2]$, $\mu = 1$ $[kg/m]$, $\Delta x = 2.5 \cdot 10^{-3}$ $[m]$ and $e = 1.25$ $[-]$.

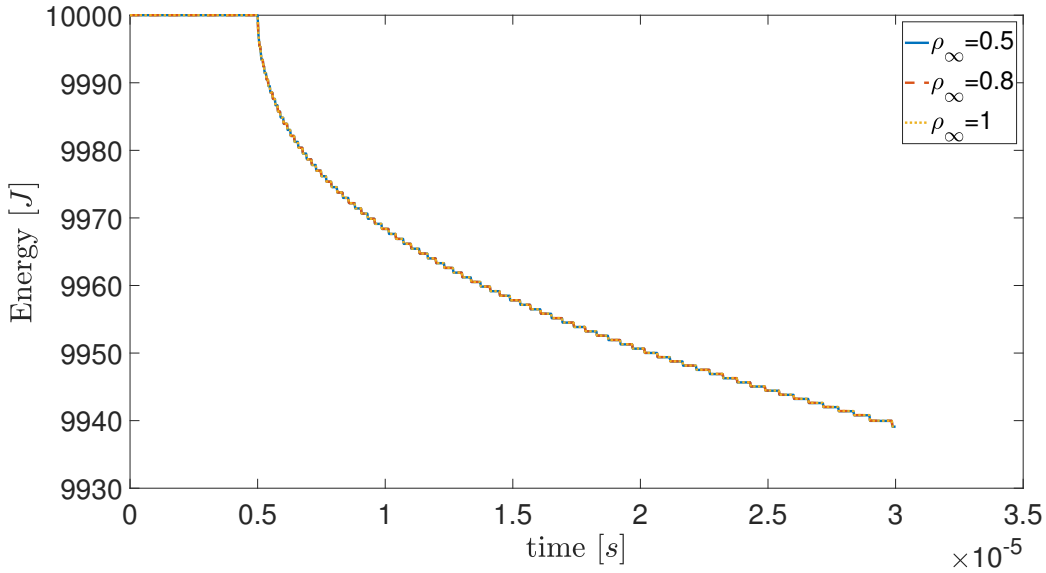

Figure 3.18: Energy of the beam at $\tau = 0.01$ $[-]$. Uniform mesh at the contact zone for $\kappa/\nu = 1.3 \cdot 10^{-3}$, $h = 2.5 \cdot 10^{-8}$ $[s]$, $EI = 1$ $[N \cdot m^2]$, $\mu = 1$ $[kg/m]$, $\Delta x = 2.5 \cdot 10^{-3}$ $[m]$ and $e = 1.25$ $[-]$.

3.3.4 Coefficient of restitution

As explained previously in Section 3.2, the coefficient of restitution characterizes the unilateral contact by an impact law between two bodies. Due to the discretization of the beam, a unilateral contact occurs either at the node or at the middle of each element of the beam. Two numerical simulations will be applied with $g = 0$ and $g = 1$ to observe the effect that this parameter provokes in the results. In the analytic part, in the general way, during the impact, the beam remains glued to the surface. One set of parameters is selected and the coefficient of restitution is changed either 0 or 1. To study the coefficient of restitution g, the set of parameters is: $\tau = 0.1$ $[-]$, uniform mesh at the contact zone for $\kappa/\nu = 1.3 \cdot 10^{-3}$, $h = 2.5 \cdot 10^{-8}$ $[s]$, $EI = 1$ $[N \cdot m^2]$, $\mu = 1$ $[kg/m]$, $\Delta x = 2.5 \cdot 10^{-3}$ $[m]$ and $e = 1.25$ $[-]$. In Figure 3.19, the geometry of the beam at $\tau = 0.1$ $[-]$ is shown. Due to the coefficient of restitution, for $g = 1$, the beam has more complex geometry which is less smooth at the contact level. The general detachment is greater due to the velocity that these nodes obtained. Indeed, after the impact, the velocity of these nodes is V_0 in the opposite direction (up direction). Consequently, for the geometry aspect, the coefficient of restitution must be equal to zero to represent the fact that the beam stays glued when the contact occurs on the beam. For the reaction contact, some quick oscillations appear and at the beginning the value is overestimated for $g = 1$ (Figure 3.20). In Figure 3.21, the evolution energy is represented for $g = 0$ and $g = 1$. For both cases, at the beginning, a step is present which characterizes the time before that the first contact between the beam and the wall occurs. For g=0, when the contact occurs, the kinetic energy of the node is put from $0.5mV^2$ to 0. Thus, the energy decreases proportionally to the contact area which evolves $\propto \sqrt{t}$. For $g = 1$, the behavior is totally different. With time, a slight increase is observed. Indeed, the kinetic energy is conserved during the impact and the strain energy increases with time in square root. Consequently, the situation which represents the best the analytic behavior is to take $g = 0$.

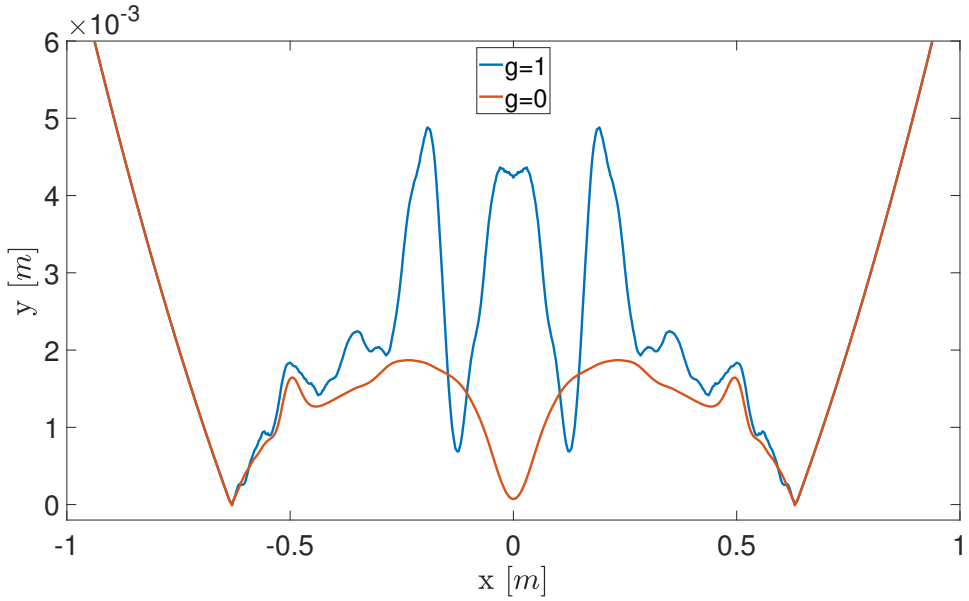

Figure 3.19: Comparison of the beam geometry at $\tau = 0.1$ $[-]$. Uniform mesh at the contact zone for $\kappa/\nu = 1.3 \cdot 10^{-3}$, $h = 2.5 \cdot 10^{-8}$ $[s]$, $EI = 1$ $[N \cdot m^2]$, $\mu = 1$ $[kg/m]$, $\Delta x = 2.5 \cdot 10^{-3}$ $[m]$ and $e = 1.25$ $[-]$.

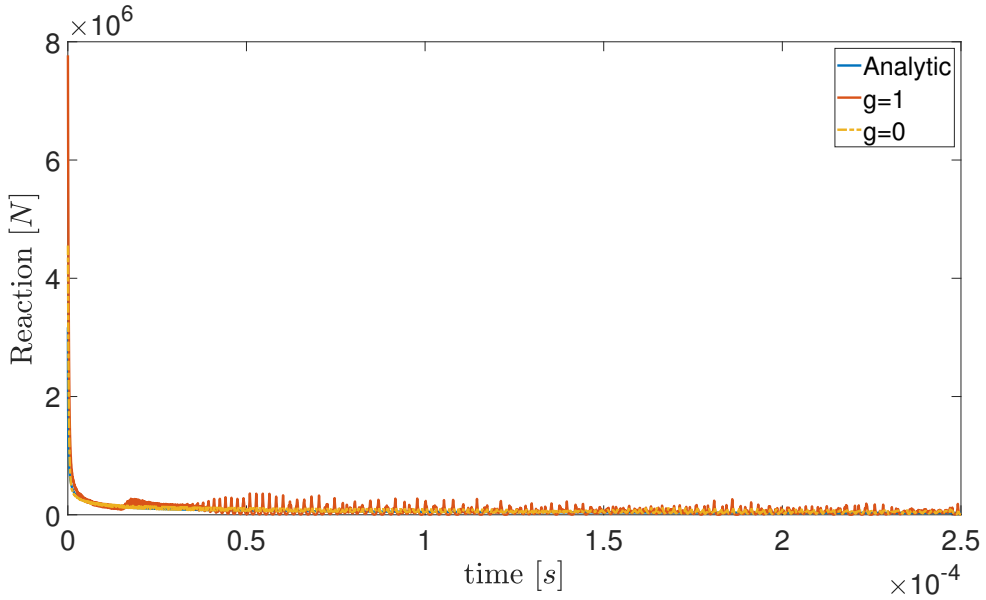

Figure 3.20: Comparison of the reaction contact until $\tau = 0.1$ $[-]$. Uniform mesh at the contact zone for $\kappa/\nu = 1.3 \cdot 10^{-3}$, $h = 2.5 \cdot 10^{-8}$ $[s]$, $EI = 1$ $[N \cdot m^2]$, $\mu = 1$ $[kg/m]$, $\Delta x = 2.5 \cdot 10^{-3}$ $[m]$ and $e = 1.25$ $[-]$.

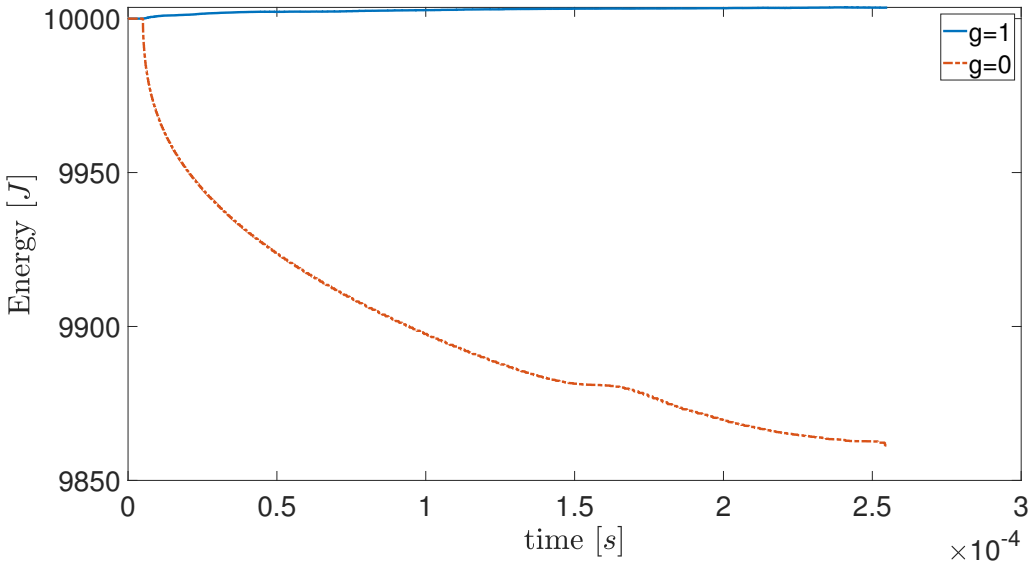

Figure 3.21: Comparison of the energy until $\tau = 0.1$ $[-]$. Uniform mesh at the contact zone for $\kappa/\nu = 1.3 \cdot 10^{-3}$, $h = 2.5 \cdot 10^{-8}$ $[s]$, $EI = 1$ $[N \cdot m^2]$, $\mu = 1$ $[kg/m]$, $\Delta x = 2.5 \cdot 10^{-3}$ $[m]$ and $e = 1.25$ $[-]$.

3.3.5 Contact node VS Contact middle

To take into account the unilateral contact between the discretized beam and the wall, two different methods of constraint will be applied. As a reminder, in Section 3.2, the constraints are simultaneously verified at the position, velocity and acceleration level. The first method consists in directly applying on the nodes the constraint of unilateral contact. For the second method, the constraint on each element is applied on the position located at the middle of the beam. The transverse displacement at this point $\xi = 0.5$ is defined using the shape function defined in Appendix A.6. Thus, a linear interpolation is applied using the four DOF's at the nodes of the beam. Unfortunately, the curvature of the beam is not taken into account for the correct transverse displacement. However, because in the contact length the spatial step Δx is small, this interpolation is not a too big error. In the software, the threshold to activate the contact is selected to 0 (by default the wall is horizontal in the plane xy with $y = 0$).

To start, a schematic representation shows the configuration of the discretization in Figure 3.22. During all the report, the mesh contains an odd number of nodes and so an even number of elements. Thus, the first contact is activated directly with the method node. For the middle method, the node at the middle of the beam will penetrate in the wall until the transverse displacement at $\xi = 0.5$ for the first elements reaching the wall ($y = 0$). In Section 3.4, this explanation is developed with the discrete contact. For the analysis with the continuous reaction, for $K = 1/80$ $[m^{-1}]$ and $\Delta x = 2.5 \cdot 10^{-3}$ $[m]$, for the middle method, the penetration of the node at the middle must travel to activate the contact of the order $1.45 \cdot 10^{-8}$ $[m]$. Thus, with a velocity speed $V_0 = 20$ $[m/s]$, the time needed is $7 \cdot 10^{-10}$ $[s]$ which is less than the time step $h = 2.5 \cdot 10^{-8}$ $[s]$. In Appendix A.7, the same analysis is realized for $K = 1$ $[m^{-1}]$ where this offset can be visualized at the beginning of the evolution on the curve $\lambda_c(t)$.

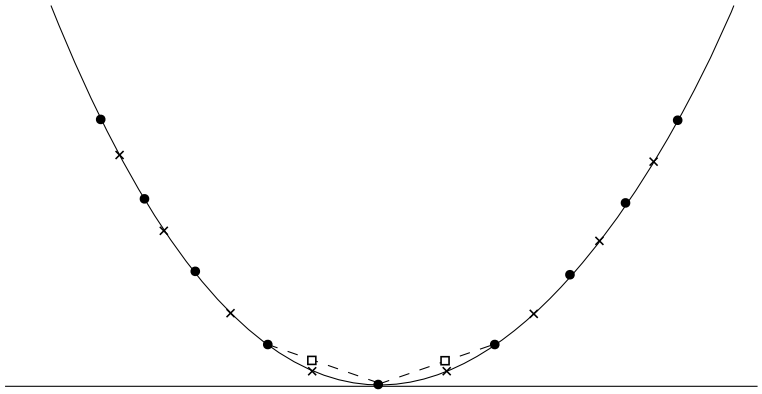

Figure 3.22: Beam discretization with nodes (•) and middle nodes (×) with the interpolation of the transverse displacement (□) at the middle position.

In Figure 3.23 and Figure 3.24, the geometry at the contact level is shown at different times t. As expected, the point of contact $\pm\lambda_c$ increases with time on the wall. However, for both methods, a double detachment appears with time: the first detachment between $-\lambda_c$ and 0 and the second detachment between 0 and λ_c. This evolution is in contraction with the semi-analytic solution expected (flat solution). At $t = 2.5 \cdot 10^{-4}$ $[s]$, for the middle method, the peak for the transverse displacement is of the order $1.7 \cdot 10^{-3}$ $[m]$ compared to $1.7 \cdot 10^{-4}$ $[m]$ for the node method. Thus, one order of accuracy is won with the node method. This accuracy on the geometry will be important to catch the solution at the

second order (high order) later in this work. In both cases, this detachment (numerical errors) increases with time.

In Figure 3.25, for the contact length, no significant difference is found between the 2 models with the analytic solution as explained previously. The contact length evolves in square root with time. The methodology to detect the position of λ_c is to start on one extremity of the beam and go to the center of the beam. When the first minimum is found or when the value at this position is less than 10^{-6}, this position corresponds to $\pm\lambda_c$. We can observe that the assumption of symmetry is always valid for both methods.

For the reaction, the non smooth solver returns the matrix λ_{tot} which contains the impulsive and non impulsive contributions as defined in (3.2.14). This matrix contains the reaction applied to satisfy the no-penetration in the wall during the time step interval h. Thus, to obtain the total reaction at the time t, the sum is applied on all nodes and divided by this interval of reaction (the time step h). In Appendix A.7, the evolution of the contact reaction on one side of the beam, for example in positive x, is detailed. The reaction is very noisy and must be filtered. The function $filtfilt$ in $Matlab$ is applied to filter the signal. In Figure 3.26 with filtering, the two methods are in the same order of magnitude than the analytic curve having the general behavior in $1/\sqrt{t}$.

In Figure 3.27 and Figure 3.28, the energy and the strain energy are represented. At the beginning during few iterations, the beam is free and moves in the direction of the wall. During this time, no modification occurs for the energy and the strain energy. The energy is mainly due to the kinetic energy of the beam ($0.5MV_0^2$). The strain energy is equal to zero because the beam is naturally bent. When the first contact occurs, the strain energy starts to increase which represents the change of geometry at the contact. As the contact length evolves in square root, the geometry changes, and thus the strain energy increases in this way. At $t = 10^{-4}[s]$, due to numerical errors and the geometry complexity, noise appear on the strain energy but the general behavior is conserved. For the energy, a decreasing is observed with time. When a node is in a contact, due to the coefficient of restitution, as it has been explained previously, the velocity speed goes from V_0 to 0, theoretically. Consequently, the nodes near $\pm\lambda$ have suddenly no kinetic energy. Thus, the kinetic energy reduction evolves also proportionally in square root like the contact length. For the energy, because the glueing is more respected with the node method with one more order of accuracy on the geometry, it means the velocity after the impact is near of 0 compared to the middle method. Thus, the energy dissipated is larger than the one of middle method. Less strain energy is also generated due to the lower deformation of opposite curvature of the element beam in the contact domain. Indeed, at $t = 2.5 \cdot 10^{-4}$ $[s]$, the strain energy is 38 $[J]$ and 3.8 $[J]$, for middle method and node method, respectively. This difference of order can be linked to the order of difference on the geometry. Indeed, the strain energy is proportional to the deformation.

To summarise, for $K = 1/80$ $[m^{-1}]$, at the contact length, the 2 methods are able to catch the behavior correctly. For the geometry, the node method is one order better on the accuracy compared to the middle method. For the reaction contact, less noise is present for the middle contact. Thus, for the high order, to catch the behavior, the method of nodes will be applied. At leading order, to catch in the best way the reaction, the middle method is applied.

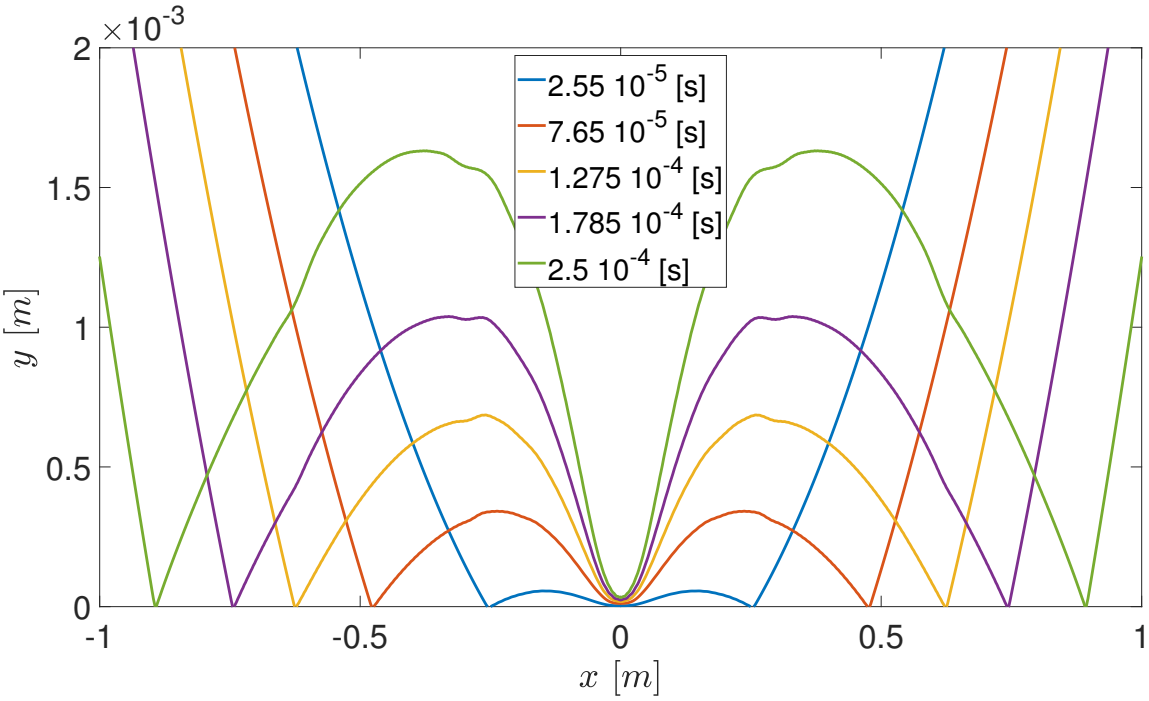

Figure 3.23: Geometry of the beam at the contact level for different time t with middle method.

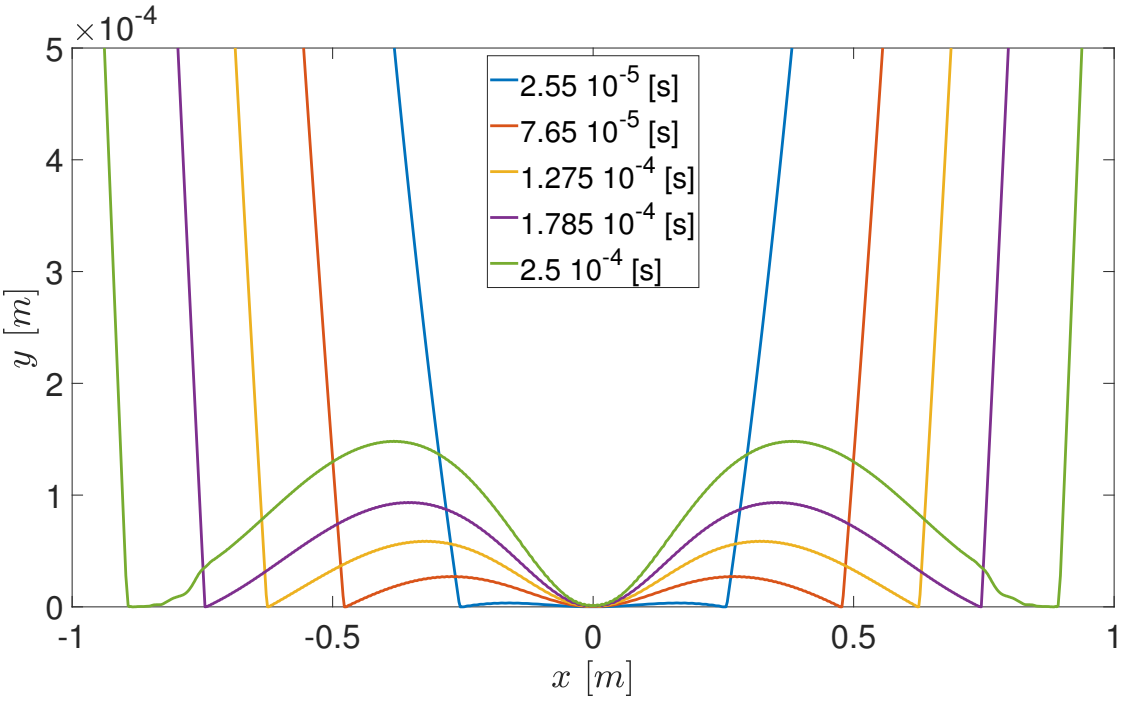

Figure 3.24: Geometry of the beam at the contact level for different time t with node method.

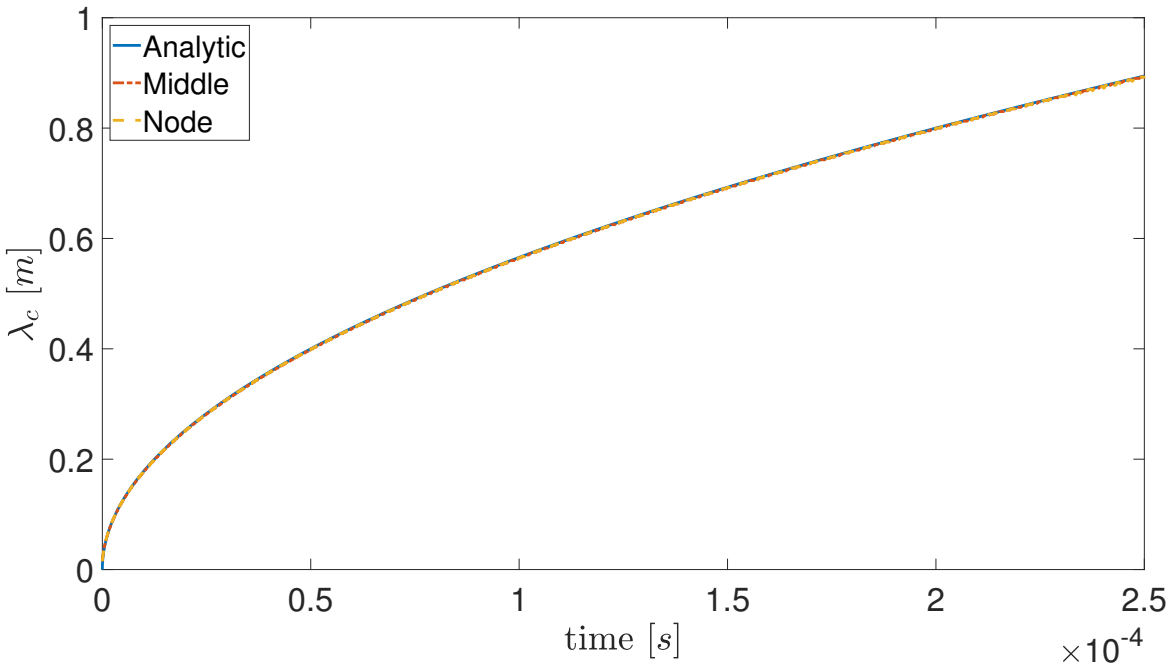

Figure 3.25: Comparison between the node and middle method for the contact length.

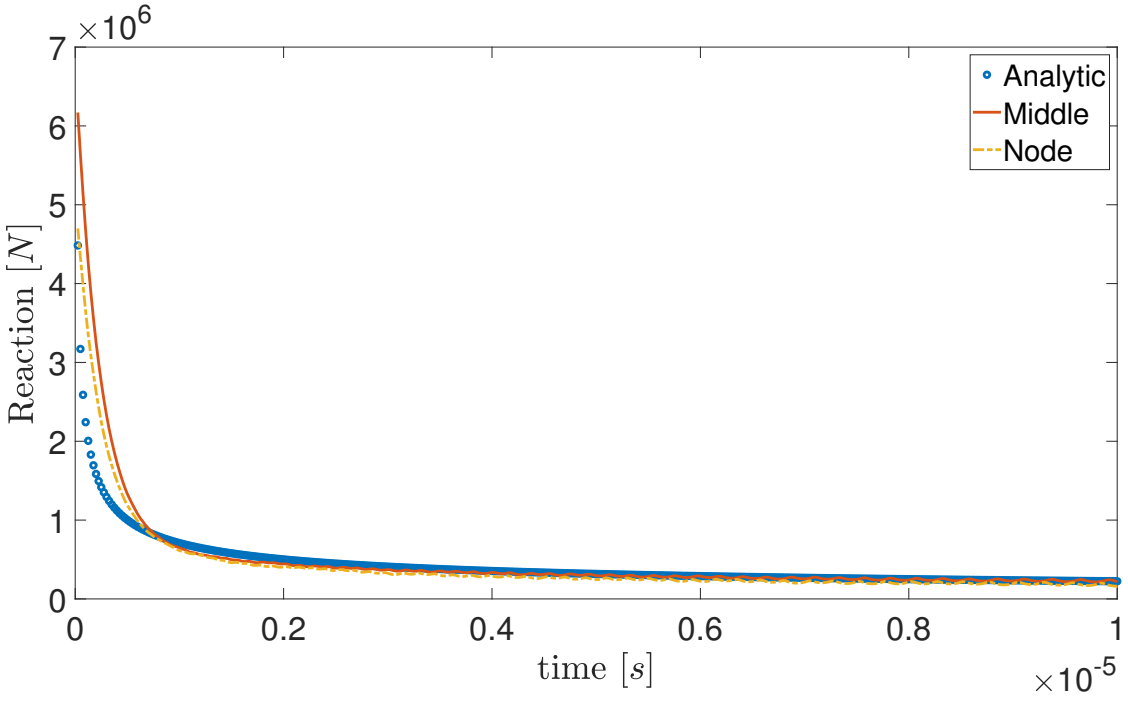

Figure 3.26: Comparison between the node and middle method for the contact reaction on one side.

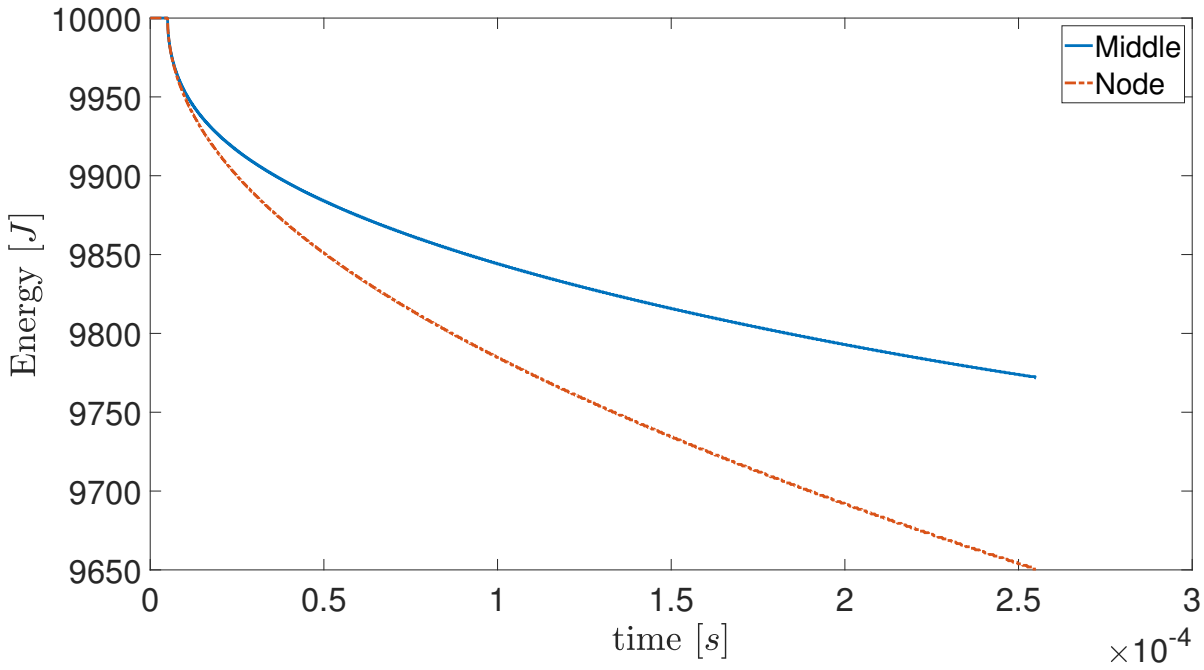

Figure 3.27: Comparison between the node and middle method for the energy.

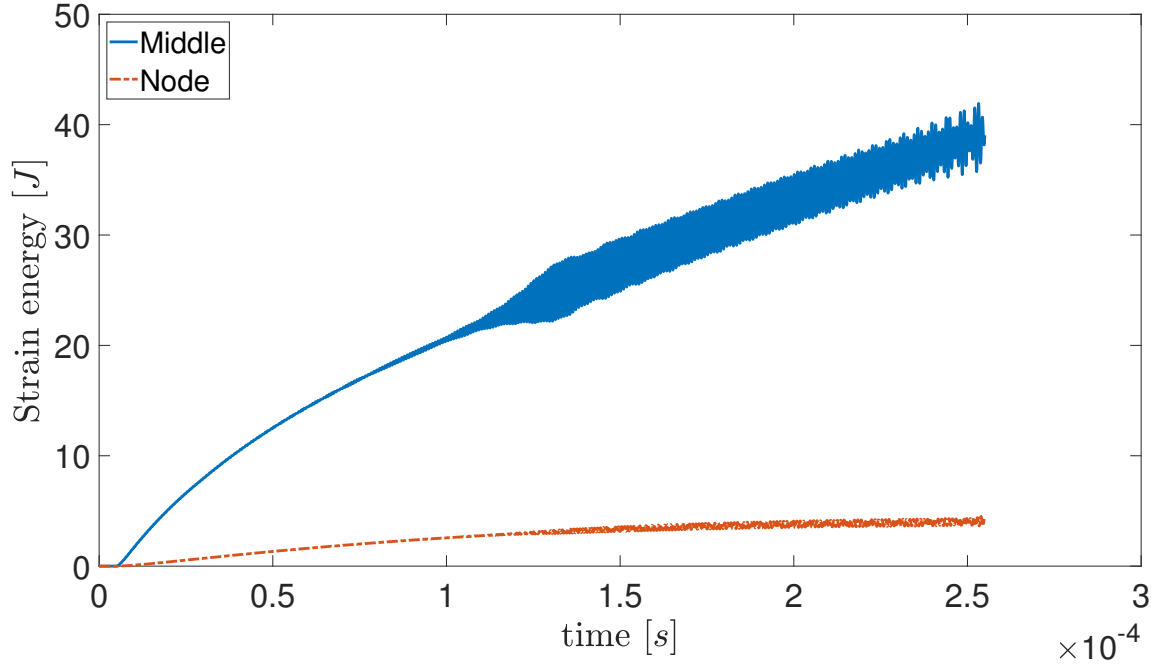

Figure 3.28: Comparison between the node and middle method for the strain energy.

3.4 Leading order

To summarise, the numerical analysis on the solver have been performed to select the better parameters to make the matching between the numerical and analytic solutions. In Table 3.3, the numerical parameters selected are presented. For the contact method, because of the output which is less noisy, the middle method is selected to determine λ_0 and r_0 .

Middle contact	-
h	$2.5 \cdot 10^{-8}$ $[s]$
ρ_∞	0.8 $[-]$
g	1 $[-]$
Mesh uniform in the contact zone	-
Δx	$2.5 \cdot 10^{-3}$ $[m]$
e	1.25 $[-]$

Table 3.3: Numerical parameters selected.

Having the numerical parameters, some assumptions must be verified to guarantee the matching qualitatively and quantitatively with the analytic results.

- For the development of the fast dynamics, the beam is assumed to be infinitely long. To satisfy that, numerically, the length of the beam is chosen to 50 $[m]$ which is big compared to the contact length. To have an idea, the contact length is in the order $0.1 - 1$ $[m]$. Due to the limitation of memory linked to the number of elements, the beam can not be longer.

- In the problem statement, two different time scales are separated by a dimensionless parameter ε which is defined as

$$\varepsilon = \left(\sqrt{\frac{EI}{\mu}}\frac{1}{V_0 L^*}\right)^2 \tag{3.4.1}$$

  This parameter must be small ($0 < \varepsilon \ll 1$). To satisfy that, during the impact, the velocity is high in order of 20 $[m/s]$. Moreover, the parameter L^* is half the length of the beam ($L^* = 25[m]$). For the bending stiffness EI and the mass per unit length μ, these parameters are fixed to 1 $[N \cdot m^2]$ and 1 $[kg/m]$, respectively. Thus, the criterion is satisfied with this set of parameter giving $\varepsilon = 2 \cdot 10^{-3}$.

As explained previously, the parameters EI and μ are chosen to $1\,[Nm^2]$ and $1[kg/m]$, respectively. With this choice, for the velocity and the curvature between the dimensional and dimensionless, we have the following relation

$$\frac{K}{V_0} = \frac{\kappa y^*/L^{*2}}{\nu y^*/T^*} = \frac{\kappa}{\nu}\sqrt{\frac{\mu}{EI}} = \frac{\kappa}{\nu} \tag{3.4.2}$$

which allows to link directly the dimensionless and dimension curvature and speed. For a dimensionless time of impact τ, the real time of the impact is

$$t = t^*\tau = \varepsilon T^*\tau = \left(\sqrt{\frac{EI}{\mu}}\frac{1}{V_0 L^*}\right)^2 \sqrt{\frac{\mu L^{*4}}{EI}}\tau = \sqrt{\frac{EI}{\mu}}\frac{\tau}{V_0^2} \tag{3.4.3}$$

Knowing that $EI = 1\,[N \cdot m^2]$, $\mu = 1[kg/m]$, $V_0 = 20\,[m/s]$ to have a small parameter ε, the time of impact is $2.5 \cdot 10^{-4}\,[s]$ for $\tau = 0.1\,[-]$.

The objective is now to rediscover the analytic solution with the curve λ_0 and r_0 as a function of the ratio κ/ν. To obtain these two curves, the velocity V_0 is fixed to 20 $[m/s]$ to satisfy the parameter ε. Thus, to change the ratio κ/ν, the curvature of the beam K will be changed by taking different values (Table 3.4).

$K\ [m^{-1}]$	1/80	1/40	1/20	1/10	1/5	1/2	1	5	10

Table 3.4: Set of the curvature K to browse the range for the ratio κ/ν.

In Figure 3.29 and Figure 3.30, the curves of λ_0 and r_0 are shown. In the dimensionless analysis, the parameters λ_0 and r_0 are parameters without units. In the dimensional analysis, for λ_0 to be consistent, we have

$$\lambda_c(t) = \lambda_0\sqrt{t} \tag{3.4.4}$$

where λ_0 have the unit $[m^2/s]$. The reaction R which takes into account only the reaction at one side of the beam is in the form

$$R_0 = r_0/\sqrt{t} \tag{3.4.5}$$

where the unit of the parameter r_0 is $[N \cdot \sqrt{s}]$.

A good accuracy is found for λ_0 despite it was more difficult to catch the solution for large value κ/ν on the curve. For the reaction r_0, due the sensitivity on the solution with the mesh and the time step, some differences appear which overestimate or underestimate the value but the general behavior of the curve is found. On the right part on the Figures, so for larger value κ/ν, the contact evolution is slower. Thus, for $K \in [1/10; 1/2]$, the mesh is refined in the contact domain with $\Delta x = 1.5 \cdot 10^{-3}\,[m]$ and for $K = 5, 10\,[m^{-1}]$ the spatial step is readjusted to $10^{-3}\,[m]$. Indeed, if the curvature K increases, the parameter λ_0 is smaller provoking a slower evolution of the contact length. This evolution needs to refine the mesh to be caught correctly and not have a staircase solution. Thus, by refining the mesh, the number of points in the contact domain stays about the same to obtain correctly the contact reaction. As explained in Section 3.3.1, some limitations will occur if the mesh is to refine. Indeed, For the stiffness matrix, the elements in the contact domain will become hyper-rigid and the matrix $\mathbf{S}_T$ is ill-conditionning preventing the guaranty of the accuracy of the solution.

In Section 3.3.5 with Figure 3.23 and Figure 3.24, the geometry was investigated. We can observe a progressive detachment which comes from numerical errors. These numerical errors may come from the vibration modes at high frequencies. At time $\tau = 0.1\,[-]$, these numerical errors are in order $1.5 \cdot 10^{-3}$ (middle method) and $1.5 \cdot 10^{-4}$ (node method). Indeed, the analytic solution is that the beam stays gluing on the wall in the complete domain $\mathcal{D}$ without detachment. Thus, it would be a major problem for the high order. In the conclusion, some tracks will proposed to improve the solver. The goal will be to obtain at leading order the flat solution in the contact domain with an accuracy 10^{-6}.

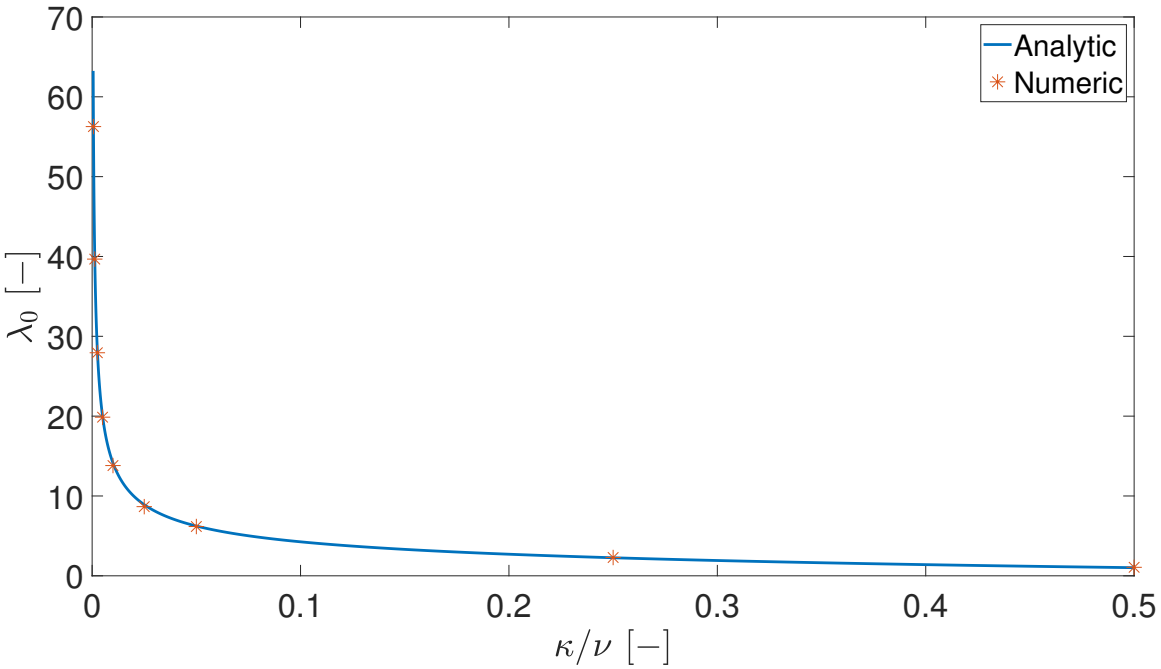

Figure 3.29: Curve λ_0 as function the ratio κ/ν with numerical and analytic results.

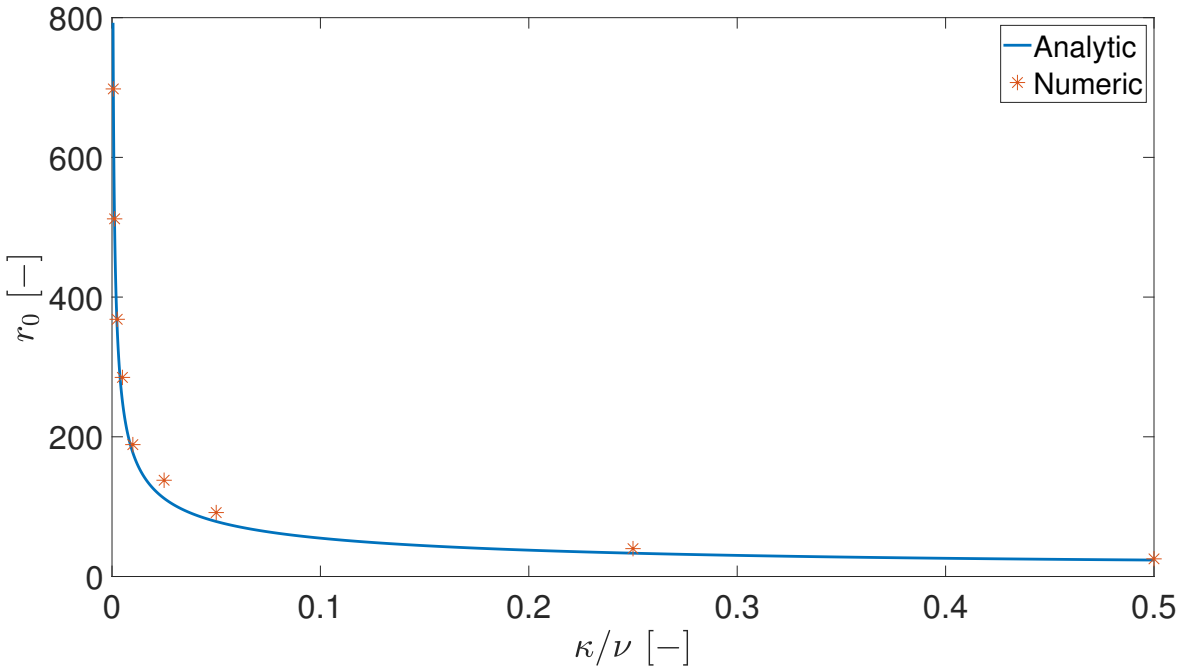

Figure 3.30: Curve R_0 as function the ratio κ/ν with numerical and analytic results.

In the analytic analysis, three types of contact reactions have been noticed: the discrete contact reaction, the double contact reaction and the continuous contact reaction. At leading order, as a function of the value of the ratio κ/ν, the contact reaction is either discrete contact reaction ($\kappa/\nu \geq 1$) or double contact reaction ($\kappa/\nu < 1$).

For $K = 1/80$ $[m^{-1}]$ and $V = 20$ $[m/s]$, the situation corresponds to a continuous contact of the beam on the wall. In Figure 3.31, the reaction between the wall and the beam is shown in space-time. We can observe that the reaction contact occurs initially at the middle and then splits into 2 parts which follow the evolution of the contact length at position $\pm\lambda_c(t)$. Thus, the contact reaction is a double contact reaction.

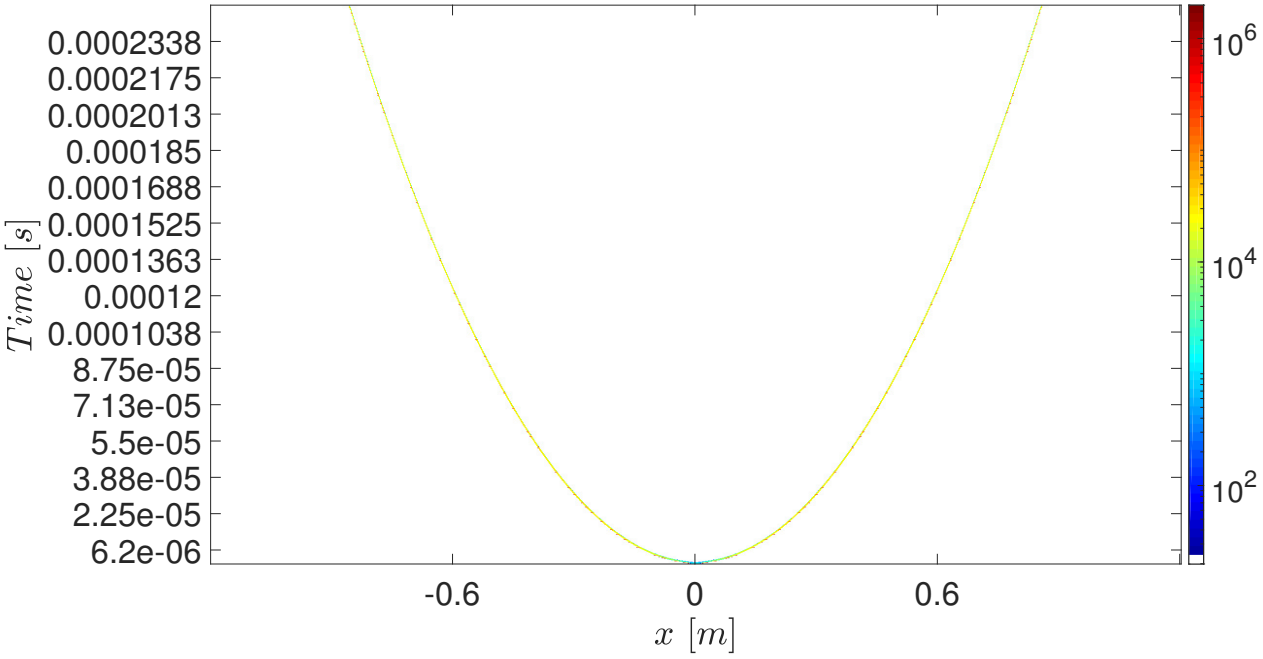

Figure 3.31: Evolution of the reaction contact expressed in $[N]$.

The second type of contact at leading order is the discrete contact reaction which occurs for $\kappa/\nu \geq 1$. Thus, the simulation is effectuated for $V_0 = 20$ $[m/s]$ and $K = 25$ $[m^{-1}]$ giving $\kappa/\nu = 1.25$. This case is analyzed with the 2 methods. The goal is to check if the contact reaction is a discrete contact reaction with no contact length propagation.

In Figure 3.32, simulations are effectuated with the following set of parameters: complete uniform mesh with $\Delta x = 5 \cdot 10^{-2}[m]$, $L = 50[m]$, $EI = 1$ $[N \cdot m^2]$, $\mu = 1$ $[kg/m]$, $\tau = 0.01$ $[-]$, $V_0 = 20$ $[m/s]$ and $K = 25$ $[m^{-1}]$.

In part (a) of the Figure, the evolution of the geometry is shown at the beginning and the end of the impact for the contact node. We can observe that the contact stays discrete at the middle of the beam and the curvature is conserved.

In part (b), as explained previously, with the middle method the condition of no-penetration is applied at the center of each element and not on the nodes of the beam. Thus, a penetration is observed with this method for the node located at $x = 0$ (center of the beam). Knowing that initially the node at the middle is located at $(0, 0 + \varepsilon)$ and the neighbor node at $(0.05, 0.0312 + \varepsilon)$ where ε is a small offset. Thus, some iterations occur before the contact between the 2 bodies. Using trigonometry, the transverse displacement of the center node in the wall goes with a penetration of $1.57 \cdot 10^{-2}$ before activating the unilateral contact. Thus, the time activation needed is very important around $7.85 \cdot 10^{-4}$ $[s]$ ($\sim \tau = 0.3$ $[-]$). Consequently, the activation of the unilateral contact can not be observed for a duration $\tau = 0.01$ $[-]$.

In Figure (c), with the node method, at $t = 5 \cdot 10^{-5}$ $[s]$, a sudden decrease is observed corresponding to the activation of the constraint at the node $x = 0$. This lost of energy is linked to the element beam of length $l_e = \Delta x$ (in the interval $[-\Delta x/2; \Delta x/2]$) due to the node at $x = 0$. Thus, the value of this lost can be determined with the kinematic energy $1/2 m V_0^2$ where $m = \mu \cdot l_e$. After calculation, the energy lost is 10 $[J]$ as shown in the Figure. For the node method with $\Delta x = 5 \cdot 10^{-2}$, at impact instant located at the node $(x = 0)$, the value λ_{tot} is 1. Thus, when the contact occurs an impulse effect happens. By refining the time step until $h = 10^{-10}$ $[s]$, this effect stays identical at this impact instant.

In Figure (d), the mesh density influence is investigated with a total length $L = 1$ $[m]$ in order to be able to use more refined mesh such as $\Delta x = 5 \cdot 10^{-4}$ $[m]$. At the iteration containing the impact, the dynamic equation is

$$m\Delta v - \lambda = 0 \tag{3.4.6}$$

where the jump velocity is $\Delta v = 0 - V_0 = -V_0$ due to the coefficient of restitution $g = 0$ and m is the mass linked to the node which is $\mu \Delta x$. For example, for $\Delta x = 5 \cdot 10^{-2}$ and $\Delta x = 10^{-2}$, the theoretical value λ obtained is 1 and 0.2, respectively. These results can be observed in the numerical simulations in the Figure. After, this impulsive effect of unilateral contact disappears for the next iterations and the dependance on the time step appears and so the force becomes finite. We can observe that the mesh density influences again the reaction contact. However, a general tendance can be observed when the time increases: for all density a convergence seems to appear. Thus, the mesh density influences a lot the reaction contact and shows the difficulty to catch the correct physical behavior at the beginning of the impact.

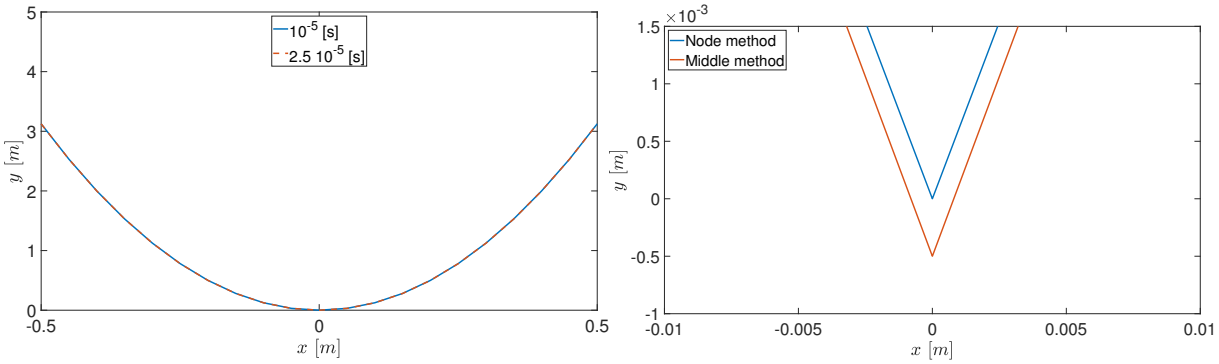

(a) Geometry of the beam for the node method. **(b)** Zoom on the geometry of the beam at $x = 0$.

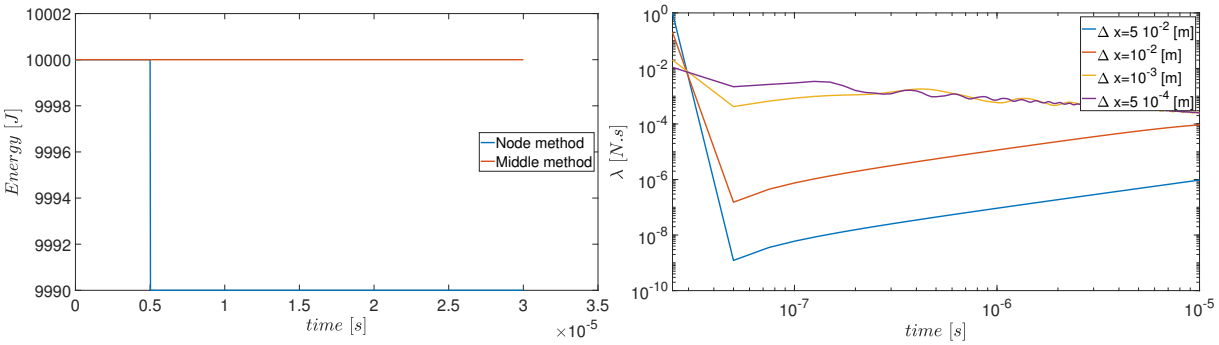

(c) Energy for both methods. **(d)** Constraint λ for different spatial step.

Figure 3.32: Discrete case at leading order

3.5 High order

Having investigated the leading order, the new objective is to link again the numerical solution with the analytic solution at high order. However, some limitations on the results would appear due to the numerical errors and CPU cost. In the analytic part, two dimensionless parameters are used to represent the leading order with κ and ν. These dimensionless parameters are directly linked to the velocity of the impact V_0 and the curvature of the beam K.

At high order, three new dimensionless parameters have been used to characterize the evolution of the beam. As a reminder, the parameter α corresponds to the dimensionless acceleration, the parameter χ is the dimensionless rate of the curvature change and the parameter ψ is the fourth derivative with respect to dimensionless abscissa ξ.

In the numerical model, the two last parameters (χ and ψ) are more difficult to implement. Thus, by simplicity, only the acceleration parameter a_0 will be applied in the solver through a force which is also proportional to the mass matrix of the beam.

As a reminder, the semi-analytic solution solution for the fast dynamic is written as

$$\eta(\xi,\tau) = \eta_0(\xi,\tau) + \varepsilon\eta_1(\xi,\tau) \tag{3.5.1}$$

where $0 < \varepsilon \ll 1$. However, if the parameter ε is too small, the contribution of the second order is completely negligible and so difficult to observe. The idea is to satisfy this criterion while being as large as possible: the parameter ε must tend to 0.1 where the definition ε is recalled

$$\varepsilon = \left(\sqrt{\frac{EI}{\mu}}\frac{1}{V_0 L^*}\right)^2 \tag{3.5.2}$$

To be able to link the dimensionless and dimensional for the velocity and the curvature, the bending stiffness is $EI = 1\ [N \cdot m^2]$ and the mass per unit length $\mu = 1\ [kg/m]$. Moreover, the dimensionless length is $L^* = 1$ consequently the total length of the beam L is 2 $[m]$ which will not completely satisfy the assumption of an infinite beam (discussed later). Thus, the ε value is only influenced directly by the velocity V_0. For $V_0 = 3.5\ [m/s]$, we find $\varepsilon = 0.0816$ which is very close to 0.1. To link the dimensionless and dimensional, the acceleration and velocity dimensionless definitions are used

$$a_0 = \alpha y^*/T^{*2} \tag{3.5.3}$$

$$V_0 = \nu y^*/T^* \tag{3.5.4}$$

By taking the ratio of these two equations to eliminate y^* and using the slow dynamics time definition

$$\frac{a_0}{V_0} = \frac{\alpha}{\nu}\frac{1}{T^*} = \frac{\alpha}{\nu}\sqrt{\frac{EI}{\mu L^{*4}}} \tag{3.5.5}$$

The major problem would be to catch the effect of the acceleration. For example, in the case with the detachment $\alpha + \psi < 0$, the first contact occurs on the node at the middle of the beam. Then this node is accelerated in the opposite direction of the general movement of the beam. It creates a progressive detachment. Using the uniformly accelerated linear motion principle, starting at rest with an acceleration a_0, the displacement can be calculated as follows

$$y = \frac{1}{2}a_0 t^2 \tag{3.5.6}$$

The time of impact t_f can deduced by $t_f = \tau/V_0^2$. For $\tau = 0.1$ $[-]$ and $V_0 = 3.5$ $[m/s]$, the impact time t_f is $8 \cdot 10^{-3}$ $[s]$. With $EI = 1$ $[N \cdot m^2]$, $\mu = 1$ $[kg/m]$ and $L^* = 1$, the acceleration a_0 can be written as

$$a_0 = \frac{\alpha V_0}{\nu} \tag{3.5.7}$$

where the parameter ν is selected here to have the same order between the leading order and high order, to see the influence of the high order because the numerical errors are not negligible. Using the fact that $\varepsilon \sim 0.1$ and $\tau \sim 0.1$, we have $\nu \sim 5 \cdot 10^{-3}\alpha$ which can be injected in (3.5.7)

$$a_0 = \frac{V_0}{5 \cdot 10^{-3}} \tag{3.5.8}$$

Thus, for $V_0 = 3.5$ $[m/s]$, we obtain an acceleration of 700 $[m/s^2]$. With this scale relation, the dimensional acceleration a_0 is linked to the dimensional velocity V_0 and unfortunately a direct link is not found between the dimensionless and dimensional accelerations(see later to obtain the link).

With this acceleration, at $\tau = 0.05$, the transverse displacement is in the order of $5.8 \cdot 10^{-3}$ $[m]$ which can be caught because the numerical errors is in the order of $4 \cdot 10^{-4}$ without acceleration. For limitations of CPU, the dimensionless $\tau = 0.05$ $[-]$ is selected with a duration around one day because the real time is around $4 \cdot 10^{-3}$ $[s]$ with a time step $h = 2.5 \cdot 10^{-8}$ $[s]$.

To summarize, for the two simulations ($a_0 = 700$ and -700 $[m/s^2]$), the parameter set is: $V_0 = 3.5$ $[m/s]$, $K = 0.35$ $[m^{-1}]$, $L = 2$ $[m]$, $\Delta x = 2.5 \cdot 10^{-3}$ $[m]$, $h = 2.5 \cdot 10^{-8}$ $[s]$, $e = 1.25$, $\rho_\infty = 0.8$, node method, $EI = 1$ $[N \cdot m^2]$ and $\mu = 1$ $[kg/m]$.

In Figure 3.33, the geometry is shown at the end of the impact ($t = 4 \cdot 10^{-3}$ $[s]$). Without acceleration ($a_0 = 0$ $[m/s^2]$), the solution corresponds at leading order. For $a = 700$ $[m/s^2]$ which corresponds to the case $\alpha + \psi > 0$ in the dimensionless analysis, the geometry stays gluing on the wall with an accuracy of $3.2 \cdot 10^{-4}$ which is in the same magnitude than at leading order ($4.1 \cdot 10^{-4}$). Due to the acceleration in the direction of the movement of the beam, the contact domain is larger than at leading order. For $a = -700$ $[m/s^2]$ which corresponds to the case $\alpha + \psi < 0$ in the dimensionless analysis, the detachment in the centre of the beam is observed due to the acceleration generated in the opposite direction of the movement. The position of the contact length is smaller than at leading order.

In Figure 3.34 on the first line (a) and (b), the evolution of the geometry is shown for the two cases ($a_0 = 700$ $[m/s^2]$ and $a_0 = -700$ $[m/s^2]$). For $a = 700$ $[m/s^2]$, the contact between the beam and the wall occurs with an accuracy in the order 10^{-4}. With time, the numerical errors increase and the geometry is more and more complex instead of staying completely flat like in the analytic solution. For $a = -700$ $[m/s^2]$, we can easily observe a detachment of the beam which is one-two order bigger than the geometry at leading order. At time $t = 3.7 \cdot 10^{-3}$ $[s]$, the limit of the problem starts to be reached. Indeed, the beam starts to be completely detached from the wall because the impact time becomes important. In the analytic part, the concept of perturbation method is verified meaning that the high order is a correction on the leading order. However, here to observe the effect of the high order, the acceleration was selected as such manner that the contribution of the leading order and high order are in the same order at $\tau = 0.1$. Thus, at the end

of the impact ($\tau = 0.05$), this complete detachment of the beam can be explained by the fact that the assumption of perturbation is not valid.

With these two simulations, we can validate the fact that an acceleration in the opposite direction of the general movement generates the detachment at the middle of the beam. For an acceleration which accentuates the general movement of the beam downwards. It proves that the beam stays gluing on the wall.

For the contact length (Figure 3.34 second line (c) and (d)), the analytic solution which is represented is the solution at leading order $\lambda_c(t) = \lambda_0 t$. Also, the numerical solution at leading order is shown for $a_0 = 0$ $[m/s^2]$. To remember, in the analytic analysis, the contact length is written as

$$\lambda_c(\tau) = \lambda_0 \tau + \lambda_1 \tau \sqrt{\tau} \tag{3.5.9}$$

where λ_0 is obtained with the leading order and λ_1 with the high order. Without acceleration, the parameter λ_0 at leading order is correctly caught. For $a_0 = 700$ $[m/s^2]$, the contact length increases more quickly than the leading order meaning that the term λ_1 must be positive. For $a = -700$ $[m/s^2]$, the opposite effect is found with a slower evolution of the contact length compared to the leading order. Using the function $cftool$ in $Matlab$, the parameter λ_1 can be found by using the λ_0 value and the expression (3.5.9): for $a_0 = 700$ $[m/s^2]$ $\lambda_1 \approx 227$ and for $a_0 = -700$ $[m/s^2]$ $\lambda_1 = -270.8$. As expected, in the general way, in the analytic analysis, we have obtained for $\alpha + \psi > 0$ that the parameter λ_1 is positive and for $\alpha + \psi < 0$ the parameter λ_1 is negative. However, it is impossible to quantify with the analytic solution because no direct link was effectuated between the dimensional and dimensionless acceleration (a_0 and α). Indeed, the idea was to be able to catch the influence of the high order by applying a significant acceleration a_0 in order to see the detachment. In both cases, with the evolution of the contact length, the contact length position oscillates more and more with time. One explanation is that the geometry is more and more complex with time. This problem can be caused by the reflexion of the waves at both ends of the domain of the beam. Indeed, in these simulations, the assumption of an infinite beam is not respected when we have a beam of length $L = 2$ $[m]$ with a total domain of contact of order 0.6 $[m]$ at $\tau = 0.05$. Thus, with time, the reflexion plays a bad role which is more and more important.

Starting from Equation (3.5.7), to compare the value for λ_1 with a dimensionless acceleration $\alpha = 4$ with $V_0 = 3.5$ $[m/s]$ and $\nu = 0.1$, the acceleration a_0 must be 17 $[m/s^2]$, which is very smaller compared to the previous acceleration ($a = 700$ $[m/s^2]$). At $\tau = 0.05$, the detachment is only $1.42 \cdot 10^{-4}$ $[m]$ and for $\tau = 0.5$ is $1.42 \cdot 10^{-2}$ $[m]$. At $\tau = 0.05$ $[-]$, the amplitude of detachment is in the same order of magnitude than the numerical errors. For $\tau = 0.5$, the CPU cost is too expensive (around 10-12 days) to be run on my personal computer. Actually, some limitations are present to make a complete analysis at high order. In the conclusion, some tracks will be discussed in order to increase the accuracy.

In Figure 3.34 (third lined (e) and (f)), the reaction contact is shown. No difference happens at the beginning of the impact with or without acceleration. During the impact, for $a = 700[m/s^2]$, in general, a slight increase is observed due to the acceleration contribution on the contact. However, in Figure 3.35, the contact reaction occurs at the contact length and also at localized points in the domain contact during a short interval. These results are in contradiction with the analytic solution. Unfortunately, due to the complexity of the geometry, this contact is not uniform in the domain contact during all the time to represent the uniform contact reaction. For $a = -700$ $[m/s^2]$, at the end of

the impact, no reaction happens due to the complete detachment of the beam as shown in Figure 3.36. One positive point is that the contact reaction is a double contact reaction (Figure 3.36).

Moreover, for the reaction contact at the contact length, according to analytic analysis, the reaction behavior must be in the form

$$R = r_0/\sqrt{t} + r_1\sqrt{t} \tag{3.5.10}$$

where r_0 and r_1 are the contribution at leading and high order, respectively. In Figure 3.34 (third lines (e) and (f)), at the beginning of the impact, the behavior in $1/\sqrt{t}$, corresponding at leading order, is caught. However, finding r_1 which evolves in $\sqrt{t}$ is difficult due to the numerical errors. Moreover, because the time impact is in order $10^{-3} - 10^{-4}$, the contribution r_1 is very difficult to catch. We will assume that r_0 and r_1 are in the same order of magnitude, which is acceptable by examining in Figure 2.7b, Figure 2.12a and Figure 2.16a the semi-analytic analysis. Thus, for a simulation going until $t_f = 10^{-4}$ $[s]$, at this instant, the contribution at leading order is in the magnitude of 100 compared to 10^{-2} for the high order which proves the difference of magnitude to catch it.

To summarise, despite the impossibility to compare directly with the semi-analytic results due to the numerical errors and the CPU cost, some general trends can be observed. For $\alpha + \psi > 0$, the beam stays gluing on the wall with numerical errors no-negligible. The contact length evolves more quickly than at leading order ($\lambda_1 > 0$) and some contact reaction occurs in contact domain of the beam due to the acceleration contribution but not uniformly as expected. For $\alpha + \psi < 0$, the double contact reaction is obtained with a detachment of the beam at the center. Moreover, the contact length propagates slower than at leading order ($\lambda_1 < 0$). In both cases, due to the order of the time impact, the contribution r_1 at the contact reaction is difficult to observe. Thus, some improvements are necessary on the software to catch the high order contribution (see Conclusion).

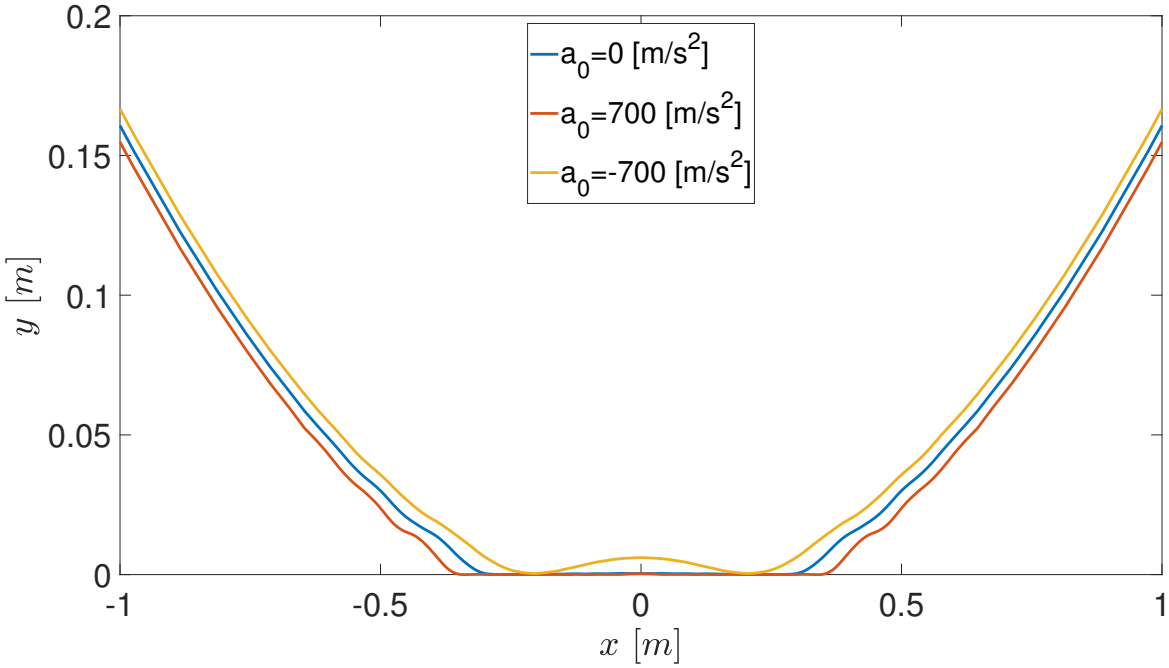

Figure 3.33: Geometry at $\tau = 0.05$ with/without acceleration.

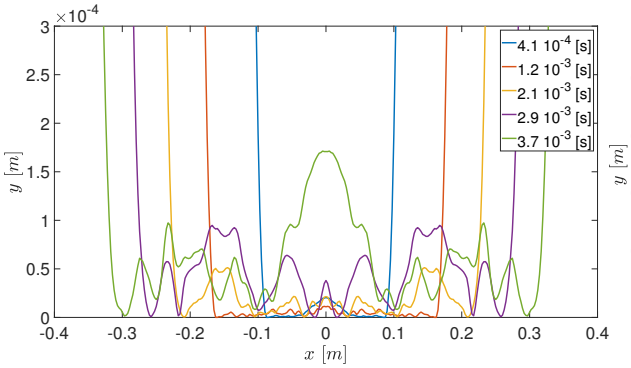

(a) Beam geometry at different times for $a_0 = 700\ [m/s^2]$.

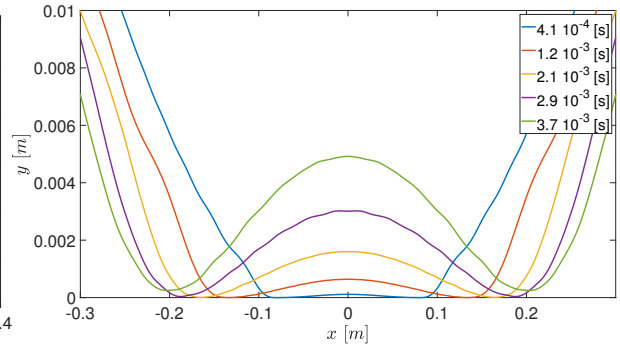

(b) Beam geometry at different times for $a_0 = -700\ [m/s^2]$.

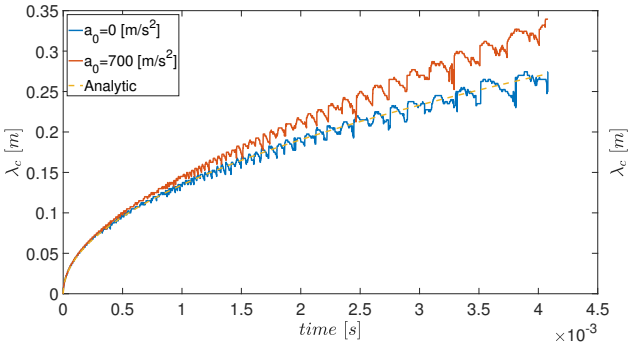

(c) Contact length by comparing with the leading order for $a_0 = 700\ [m/s^2]$.

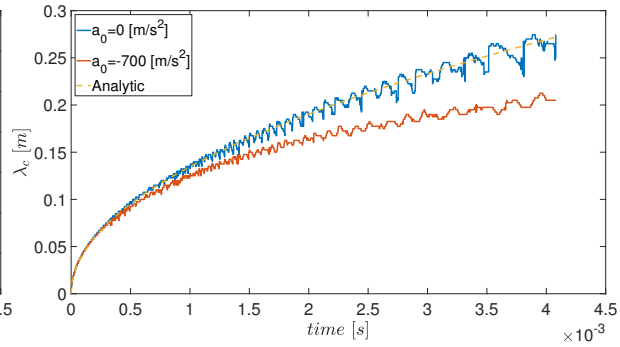

(d) Contact length by comparing with the leading order for $a_0 = -700\ [m/s^2]$.

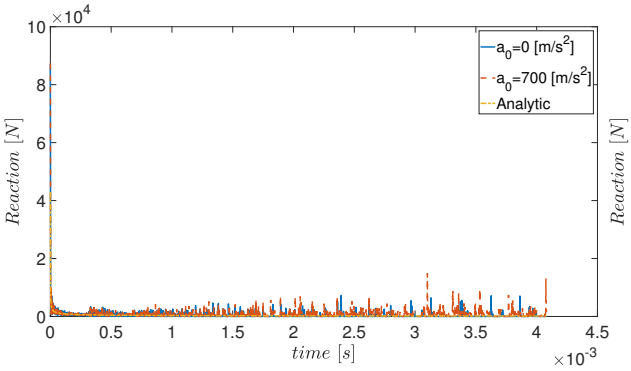

(e) Contact reaction by comparing with the leading order for $a_0 = 700\ [m/s^2]$.

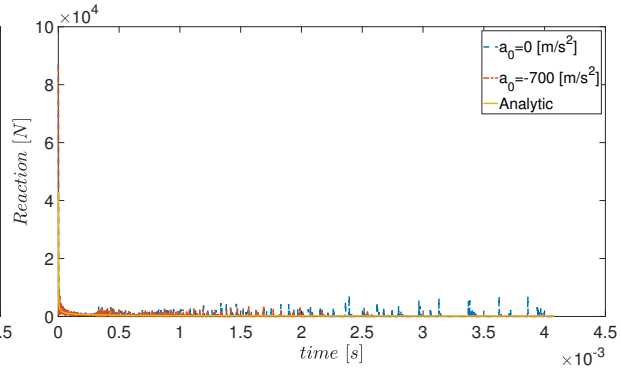

(f) Contact reaction by comparing with the leading order for $a_0 = -700\ [m/s^2]$.

Figure 3.34: Results at high order for $a = 700\ [m/s^2]$ and $a = -700\ [m/s^2]$ on the geometry, contact length and contact reaction.

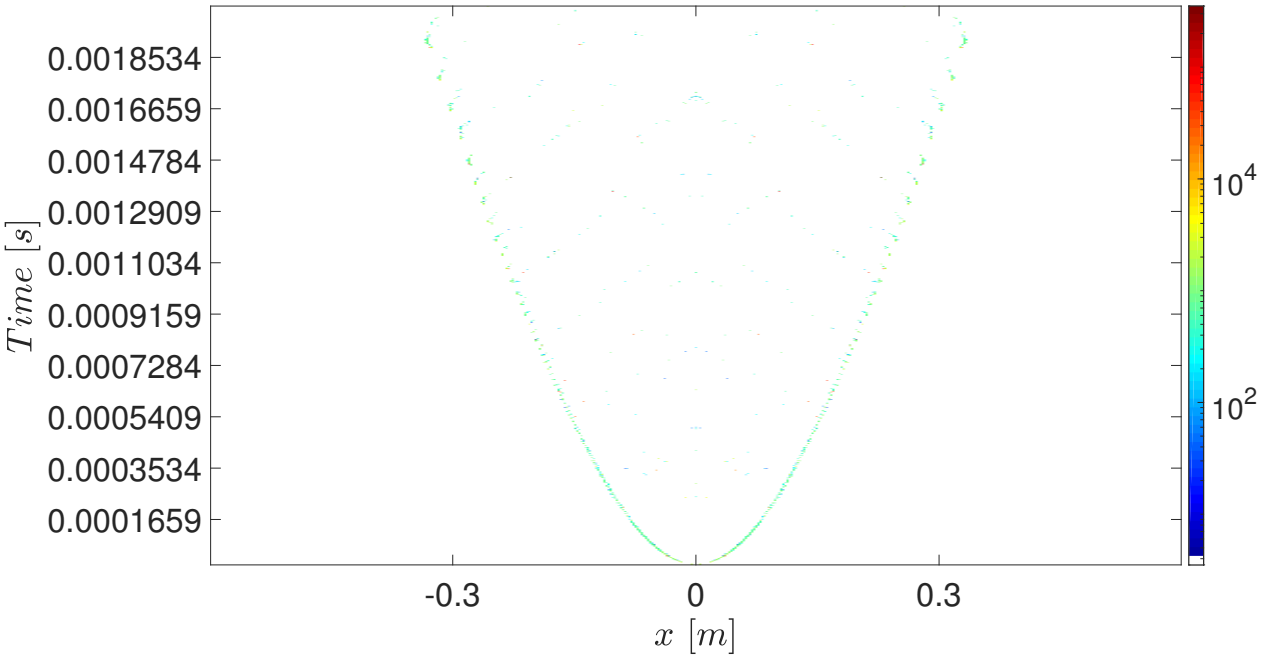

Figure 3.35: Evolution of the reaction contact expressed in $[N]$ for $a = 700\ [m/s^2]$.

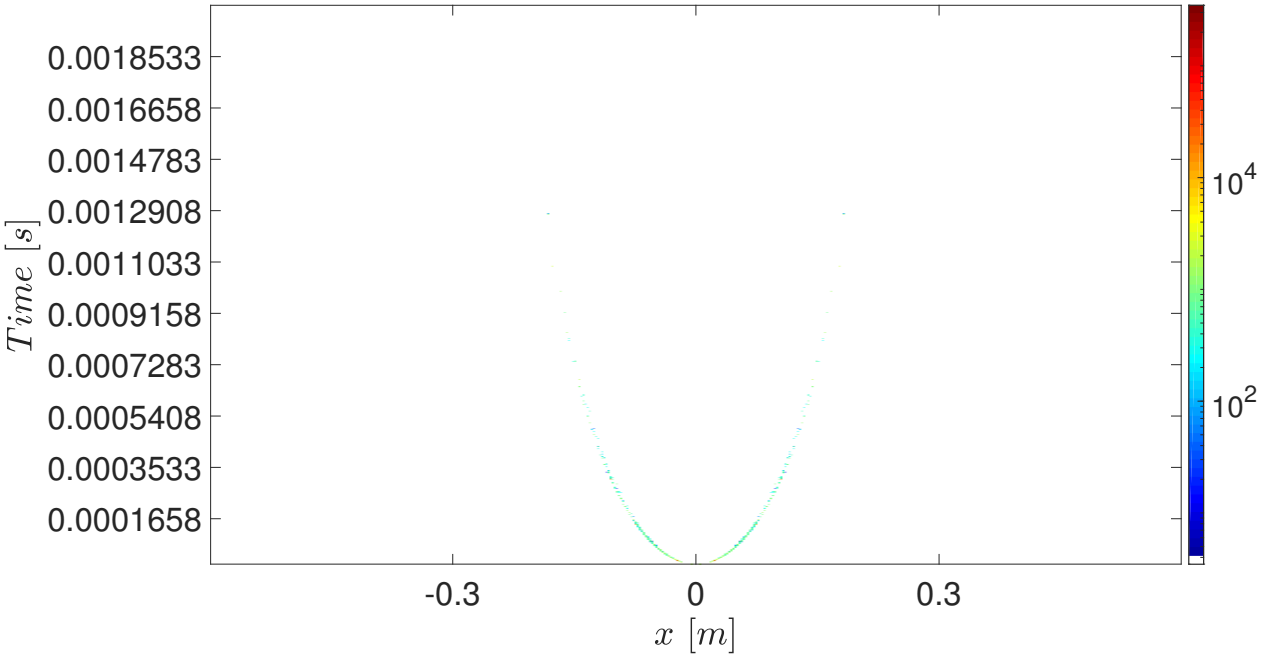

Figure 3.36: Evolution of the reaction contact expressed in $[N]$ for $a = -700\ [m/s^2]$.

4 Conclusion

The impact of a natural bent beam on a wall has been studied by two approaches in order to see if the results obtained are coherent: the semi-analytic and numerical. In both cases, the beam is represented by Euler-Bernoulli theory. Some assumptions are made to be able to develop a complete analysis:

- Symmetric problem where the impact occurs firstly at the middle of the beam.
- The fast dynamic (due to the impact) is solved for an infinitely long beam in semi-analytic approach.
- Separation of time scales between the slow dynamic (representing the natural vibration modes) T^* and the fast dynamic (propagation wave due to the impact of the beam on the rigid wall) t^* by introducing the parameter $\varepsilon = t^*/T^*$

For the analytic analysis, at leading order, two possible behaviors are determined: the discrete contact ($\kappa/\nu \geq 1$) described by a discrete contact reaction at the middle of the beam or the continuous contact ($\kappa/\nu < 1$) with the double contact reaction occurs at $\pm\lambda_c$. The contact length λ_c evolves

$$\lambda_c(\tau) = \lambda_0 \tau \tag{4.0.1}$$

and the reaction contact is

$$R = 2\sqrt{\frac{2}{\pi}}\frac{r_0}{\sqrt{\tau}} \tag{4.0.2}$$

where the two parameters λ_0 and r_0 are directly linked to the values κ and ν in order to satisfy the complementary condition.

Then, the contribution at high order is injected in the problem. The solution of the fast dynamic, in order to assure the complementary condition, is

$$\eta(\xi, \tau) = \eta_0(\xi, \tau) + \varepsilon\eta_1(\xi, \tau) \tag{4.0.3}$$

where η_0 is the leading solution and η_1 is the high solution which is a perturbation due to the presence of ε ($0 < \varepsilon \ll 1$). At high order, the solution is characterized by three dimensionless parameters: ψ, χ and α. Whatever the values α, ψ and χ, if $\kappa/\nu \geq 1$, a discrete contact (with a discrete contact reaction) occurs. If the ratio is $\kappa/\nu < 1$, two cases are possible as function of the sign of $\alpha + \psi$. A distributed uniform reaction appears in the contact domain which is $\varepsilon(\alpha + \psi)$. For $\alpha + \psi > 0$, this uniform reaction occurs on the beam to avoid penetration in the wall. A continuous contact domain is still observed. For $\alpha + \psi < 0$, another dynamics is encountered. It consists of a detachment of the beam at the middle without this uniform reaction. Thus, at high order, the complete contact length becomes

$$\lambda_c(\tau) = \lambda_0\tau + \varepsilon\lambda_1\sqrt{\tau}\tau \tag{4.0.4}$$

where the first term is due to the leading order and the second term due to the high order. The contact reaction at $\pm\lambda_c$ for $\kappa/\nu < 1$ or at the middle of the beam for $\kappa/\nu \geq 1$ is

$$R = 2\sqrt{\frac{2}{\pi}}\frac{r_0}{\sqrt{\tau}} + 2\varepsilon\sqrt{\frac{2}{\pi}}r_1\sqrt{\tau} \tag{4.0.5}$$

where the two new parameters λ_1 and r_1 characterize the high order contribution. In the development at high order, the assumption that the contact length is dominated by the leading order compared to the high order, which is a perturbation, is effectuated. This assumption allows to apply Taylor development.

The second part of the analysis of the problem is the numerical part. A nonsmooth generalized-α solver has been used. The unilateral contact have been characterized between the beam and the wall using an impact law. A numerical analysis has been performed to select the numerical parameters such as the mesh, time step, method. The impact of the beam is characterized by the temporal discontinuity (activation of the constraint) and the spatial discontinuity (change of curvature at $\pm\lambda_c$).

At leading order, in the continuous contact $\kappa/\nu < 1$, the λ_0 curve is recovered. For the parameter r_0, the tendency in $r_0/\sqrt{t}$ is also found. However, in the analytic solution, in the contact domain, the beam is completely flat to match with the wall. For the numerical solution, the accuracy of the solution is in the order 10^{-4} with the contact node. At this level, the behavior of the shape is double bell shaped. For the high order, a great accuracy is needed to catch the perturbation such the detachment when $\alpha + \psi > 0$.

Numerically, only the parameter α is represented by the dimensional acceleration a_0 for the high order. One improvement could be to represent the two others parameters ψ and χ in dimensional form in the software.

Due to the numerical errors, a great acceleration is applied to visualize the behavior of the beam. The acceleration is selected such that the leading and high order are in the same magnitude ($\nu\tau \sim \varepsilon\tau^2\alpha/2$). For $\alpha + \psi > 0$, we can observe that the beam stays gluing on the wall with an accuracy order 10^{-4}. The contact length evolves more quickly due to the contribution at high order ($\lambda_1 > 0$). For $\alpha+\psi < 0$, the detachment is observed at the center of the beam and the contact length evolves slower than at the leading order ($\lambda_1 < 0$). In both cases, the contribution at the contact reaction can not be caught at high order with r_1 which evolves in $\sqrt{t}$ compared to $1/\sqrt{t}$ for the leading order. Moreover, for $\alpha + \psi > 0$, the uniform reaction $\varepsilon(\alpha + \psi)$ is felt at some points in the contact domain at particular instant. Consequently, the reaction on the wall is very difficult to catch.

Thus, some restrictions are present on the numerical model to catch correctly the high order solution. One track to reduce the numerical errors which generate the complex geometry is to work on the constraints. Actually, the constraints are activated either on the nodes or at the middle of the elements. The idea is to verify on all the domain of contact if the Signorini condition is satisfied

$$0 \leq \int_{-\lambda_c}^{\lambda_c} ||y(x)||^2 dx \perp \int_{-\lambda_c}^{\lambda_c} \lambda_{tot}(x) dx \leq 0 \tag{4.0.6}$$

If the contact has not yet occurred, we have $\lambda_c = -\lambda_c = 0$ and $\lambda_{tot}(x) = 0$ so the second integral is null. When the contact occurs, in the domain, to satisfy the condition that the beam is flat on the wall meaning that the first element must be null. This criterion can be applied at leading order and at high order with $\alpha + \psi > 0$; not for $\alpha + \psi < 0$ to represent the detachment.

In further works, during the impact, to avoid complex geometry, a frictional contact could be introduced. Thus, the curvature of the beam which suddenly becomes flat in order to keep the same length of the element should be better observed.

By applying greater acceleration to satisfy that the leading order and high order are the same magnitude, the general behavior can be observed. Indeed, for $\alpha + \psi > 0$, the

gluing with an accuracy of order 10^{-4} is observed with a faster propagation of the contact length due to $\lambda_1 > 0$. For $\alpha + \psi < 0$, a detachment of the beam can be observed with a slower propagation.

To conclude, analytical and numerical study of bent beam impact on a rigid surface have been carried on in this master thesis. For the majority of the results at leading order, the results obtained with both approaches are consistent. The high order have also been introduced. However, we met troubles because of numerical errors and thus the only the tendencies could be observed. The tracks given in the end of this document may be investigated to get the matching.

A Appendix

A.1 Abel integral equation

To obtain the general form for $\tilde{R}_0$ and $\tilde{R}_1$ in the semi-analytic calculations, Abel integral equation must be solved which is in the form

$$\int_0^x (x-t)^\beta \varphi(t) dt = x^\lambda \tag{A.1.1}$$

where $\lambda \geq 0$ and $\beta > -1$. According to [14], the solution $\varphi(t)$ is

$$\varphi(t) = \frac{\Gamma(\lambda+1)}{\Gamma(\beta+1)\Gamma(\lambda-\beta)} t^{\lambda-\beta-1} \tag{A.1.2}$$

where $\Gamma(x)$ is the Euler integral defined as follows

$$\Gamma(x) = \int_0^{+\infty} e^{-t} \cdot t^{x-1} dt \tag{A.1.3}$$

At leading order, the equation to solve for the discrete contact at the position level is

$$\int_0^\tau \frac{1}{\sqrt{2\pi}} \tilde{R}_0(\bar{\tau}) \sqrt{\tau - \bar{\tau}} d\bar{\tau} = \nu\tau \tag{A.1.4}$$

where $\lambda = 1$ and $\beta = 1/2$ giving the solution

$$\tilde{R}_0(\bar{\tau}) = \sqrt{2\pi} \frac{\Gamma(2)}{\Gamma(3/2)\Gamma(1/2)} \frac{\nu}{\sqrt{\bar{\tau}}} = 2\sqrt{\frac{2}{\pi}} \frac{\nu}{\sqrt{\bar{\tau}}} \tag{A.1.5}$$

where $\Gamma(2) = 1$, $\Gamma(1/2) = \sqrt{\pi}$ and $\Gamma(3/2) = \sqrt{\pi}/2$.
For the double contact reaction, the generalization can be effectuated by replacing ν by r_0 which depends on ν and κ

$$\tilde{R}_0(\bar{\tau}) = 2\sqrt{\frac{2}{\pi}} \frac{r_0}{\sqrt{\bar{\tau}}} \tag{A.1.6}$$

At high order for the discrete contact reaction, the equation to solve is

$$\int_0^\tau \tilde{R}_1(\bar{\tau}) \sqrt{\frac{\tau - \bar{\tau}}{2\pi}} d\bar{\tau} = \frac{\alpha\tau^2}{2} \tag{A.1.7}$$

where $\beta = 1/2$ and $\lambda = 2$. The solution can be easily determined

$$\tilde{R}_1(\bar{\tau}) = \frac{\sqrt{2\pi}\alpha}{2} \frac{\Gamma(3)}{\Gamma(3/2)\Gamma(3/2)} \sqrt{\bar{\tau}} = 4\alpha\sqrt{\frac{2}{\pi}} \sqrt{\bar{\tau}} \tag{A.1.8}$$

For $\kappa/\nu < 1$, the same generalization is applied by replacing 2α by r_1 which depends on ν, κ, ψ, α and chi

$$\tilde{R}_1(\bar{\tau}) = 2r_1\sqrt{\frac{2}{\pi}} \sqrt{\bar{\tau}} \tag{A.1.9}$$

A.2 φ_κ definition

For the demonstration of the complementary at $\pm\lambda_c$ at leading order, the function φ_κ must be expressed directly in terms of the function $\mathcal{H}$ and not the second derivative $\mathcal{H}$. The part integration will be effectuated twice as follows

$$\varphi_\kappa(\lambda) = \frac{-4}{\pi}\left[\frac{\lambda}{\beta^2+\lambda^2}\mathcal{H}'(\beta)\Big|_0^{+\infty} + \int_0^{+\infty}\frac{2\lambda\beta}{(\beta^2+\lambda^2)^2}d\beta\right] \tag{A.2.1}$$

$$= \frac{-4}{\pi}\int_0^{+\infty}\frac{2\lambda\beta}{(\beta^2+\lambda^2)^2}d\beta \tag{A.2.2}$$

$$= \frac{-4}{\pi}\left[\frac{2\lambda\beta\mathcal{H}(\beta)}{(\beta^2+\lambda^2)^2}\Big|_0^{+\infty} - \int_0^{+\infty}\frac{2\lambda(\beta^2+\lambda^2)^2-8\lambda\beta^2(\beta^2+\lambda^2)}{(\beta^2+\lambda^2)^4}\mathcal{H}(\beta)d\beta\right] \tag{A.2.3}$$

$$= \frac{4}{\pi}\int_0^{+\infty}\frac{2\lambda(\beta^2+\lambda^2)^2-8\lambda\beta^2(\beta^2+\lambda^2)}{(\beta^2+\lambda^2)^4}\mathcal{H}(\beta)d\beta \tag{A.2.4}$$

$$= \frac{4}{\pi}\int_0^{+\infty}\frac{2\lambda(\lambda^2-3\beta^2)\mathcal{H}(\beta)}{(\beta^2+\lambda^2)^3}d\beta \tag{A.2.5}$$

A.3 Prove of the complementary at first order

The change of variable is $\beta_\pm = \lambda_0 \frac{\sqrt{\tau}\pm\sqrt{\bar{\tau}}}{\sqrt{\tau-\bar{\tau}}}$, the goal is to demonstrate these two following relations

$$\int_0^\tau \sqrt{\frac{\tau-\bar{\tau}}{\bar{\tau}}}\mathcal{H}\left(\lambda_0\frac{\sqrt{\tau}+\sqrt{\bar{\tau}}}{r\sqrt{\tau-\bar{\tau}}}\right)d\bar{\tau} = 16\lambda_0^3\tau\int_{\lambda_0}^{+\infty}\frac{\beta_+^2\mathcal{H}(\beta_+)}{(\beta_+^2+\lambda_0^2)^3}d\beta_+ \tag{A.3.1}$$

$$\int_0^\tau \sqrt{\frac{\tau-\bar{\tau}}{\bar{\tau}}}\mathcal{H}\left(\lambda_0\frac{\sqrt{\tau}-\sqrt{\bar{\tau}}}{r\sqrt{\tau-\bar{\tau}}}\right)d\bar{\tau} = 16\lambda_0^3\tau\int_{0}^{\lambda_0}\frac{\beta_-^2\mathcal{H}(\beta_-)}{(\beta_-^2+\lambda_0^2)^3}d\beta_- \tag{A.3.2}$$

Starting with β_+, the demonstration will be made in the opposite way

$$16\lambda_0^3\tau\int_{\lambda_0}^{+\infty}\frac{\beta_+^2\mathcal{H}(\beta_+)}{(\beta_+^2+\lambda_0^2)^3}d\beta_+ = 16\lambda_0^3\tau\int_{\lambda_0}^{+\infty}\frac{\lambda_0^2\frac{(\sqrt{\tau}+\sqrt{\bar{\tau}})^2}{\tau-\bar{\tau}}\mathcal{H}\left(\lambda_0\frac{\sqrt{\tau}+\sqrt{\bar{\tau}}}{\sqrt{\tau-\bar{\tau}}}\right)}{\left(\lambda_0^2\frac{(\sqrt{\tau}+\sqrt{\bar{\tau}})^2}{\tau-\bar{\tau}}+\lambda_0^2\right)^3}d\beta_+ \tag{A.3.3}$$

$$= \frac{16\tau}{\lambda_0}\int_{\lambda_0}^{+\infty}\frac{\frac{(\sqrt{\tau}+\sqrt{\bar{\tau}})^2}{\tau-\bar{\tau}}}{\left(\frac{(\sqrt{\tau}+\sqrt{\bar{\tau}})^2}{\tau-\bar{\tau}}+1\right)^3}\mathcal{H}\left(\lambda_0\frac{\sqrt{\tau}+\sqrt{\bar{\tau}}}{\sqrt{\tau-\bar{\tau}}}\right)d\beta_+ \tag{A.3.4}$$

$$= 8\tau\int_0^\tau\frac{\frac{(\sqrt{\tau}+\sqrt{\bar{\tau}})^2}{\tau-\bar{\tau}}}{\left(\frac{(\sqrt{\tau}+\sqrt{\bar{\tau}})^2}{\tau-\bar{\tau}}+1\right)^3}\mathcal{H}\left(\lambda_0\frac{\sqrt{\tau}+\sqrt{\bar{\tau}}}{\sqrt{\tau-\bar{\tau}}}\right)\frac{\sqrt{\tau}\sqrt{\bar{\tau}}+\tau}{\sqrt{(\tau-\bar{\tau})^3}\sqrt{\bar{\tau}}}d\bar{\tau} \tag{A.3.5}$$

$$= \tau\int_0^\tau\frac{(\tau-\bar{\tau})^2(\sqrt{\tau}+\sqrt{\bar{\tau}})^2}{(\tau+\sqrt{\tau}\sqrt{\bar{\tau}})^3}\frac{\sqrt{\tau}\sqrt{\bar{\tau}}+\tau}{\sqrt{(\tau-\bar{\tau})^3}\sqrt{\bar{\tau}}}\mathcal{H}\left(\lambda_0\frac{\sqrt{\tau}+\sqrt{\bar{\tau}}}{\sqrt{\tau-\bar{\tau}}}\right)d\bar{\tau} \tag{A.3.6}$$

$$= \int_0^\tau\sqrt{\frac{\tau-\bar{\tau}}{\bar{\tau}}}\mathcal{H}\left(\lambda_0\frac{\sqrt{\tau}+\sqrt{\bar{\tau}}}{\sqrt{\tau-\bar{\tau}}}\right)d\bar{\tau} \tag{A.3.7}$$

where $d\beta_+ = \frac{\lambda_0}{2}\frac{\sqrt{\tau}\sqrt{\bar{\tau}}+\tau}{\sqrt{(\tau-\bar{\tau})^3}\sqrt{\bar{\tau}}}d\bar{\tau}$, $\bar{\tau}=0\rightarrow\beta_+=\lambda_0$ and $\bar{\tau}=\tau\rightarrow\beta_+=+\infty$. The same procedure can be applied for β_-

$$16\lambda_0^3\tau\int_0^{\lambda_0}\frac{\beta_-^2\mathcal{H}(\beta_-)}{(\beta_-^2+\lambda_0^2)^3}d\beta_- = -\tau\int_\tau^0\frac{(\tau-\bar{\tau})^2(\sqrt{\tau}-\sqrt{\bar{\tau}})^2}{(\tau-\sqrt{\tau}\sqrt{\bar{\tau}})^3}\frac{(\sqrt{\bar{\tau}}\sqrt{\tau}+\tau)}{\sqrt{(\tau-\bar{\tau})^3}\sqrt{\bar{\tau}}}\mathcal{H}\left(\lambda_0\frac{\sqrt{\tau}-\sqrt{\bar{\tau}}}{\sqrt{\tau-\bar{\tau}}}\right)d\bar{\tau} \tag{A.3.8}$$

$$= \int_0^\tau\sqrt{\frac{\tau-\bar{\tau}}{\bar{\tau}}}\mathcal{H}\left(\lambda_0\frac{\sqrt{\tau}-\sqrt{\bar{\tau}}}{\sqrt{\tau-\bar{\tau}}}\right)d\bar{\tau} \tag{A.3.9}$$

where $d\beta_- = \dfrac{\sqrt{\bar{\tau}}\sqrt{\tau}-\tau}{\sqrt{(\tau-\bar{\tau})^3}\sqrt{\bar{\tau}}}$, $\bar{\tau}=0\rightarrow\beta_-=\lambda_0$ and $\bar{\tau}=\tau\rightarrow\beta_-=0$.

A.4 Continuous reaction: Simplification of the solution

With the continuous reaction, the fast solution reads as

$$\eta(\xi,\tau) = \tilde{r}\int_0^{\tau}\sqrt{\frac{\tau-\bar{\tau}}{2\pi}}\int_{-\lambda_c(\bar{\tau})}^{\lambda_c(\bar{\tau})}\mathcal{H}\left(\frac{|\xi-\bar{\xi}|}{\sqrt{\tau-\bar{\tau}}}\right)d\bar{\xi}d\bar{\tau} \tag{A.4.1}$$

where the domain $\mathcal{D}$ is $[-\lambda_c(\tau);\lambda_c(\tau)]$ at time τ. The idea to simplify the solution is to introduce the function $\mathcal{P}$. By symmetry of the problem, we will interesting on the right part of the beam ($\xi \geq 0$). Two cases can be separated as function of the absolute value $|\xi-\bar{\xi}|$ expressing if the evaluated point ξ is in the domain contact or not. Firstly, the zone of out contact is investigated ($\xi > \lambda_c(\bar{\tau})$) . The fast solution can be written as

$$\eta(\xi,\tau) = \tilde{r}\int_0^{\tau}\sqrt{\frac{\tau-\bar{\tau}}{2\pi}}\int_{-\lambda_c(\bar{\tau})}^{\lambda_c(\bar{\tau})}\mathcal{H}\left(\frac{\xi-\bar{\xi}}{\sqrt{\tau-\bar{\tau}}}\right)d\bar{\xi}d\bar{\tau} \tag{A.4.2}$$

$$= \tilde{r}\int_0^{\tau}\frac{\tau-\bar{\tau}}{\sqrt{2\pi}}\int_{\frac{\xi-\lambda_c(\bar{\tau})}{\sqrt{\tau-\bar{\tau}}}}^{\frac{\xi+\lambda_c(\bar{\tau})}{\sqrt{\tau-\bar{\tau}}}}\mathcal{H}(\beta)d\beta \tag{A.4.3}$$

$$= \tilde{r}\int_0^{\tau}\frac{\tau-\bar{\tau}}{\sqrt{2\pi}}\left[\int_0^{\frac{\xi+\lambda_c(\bar{\tau})}{\sqrt{\tau-\bar{\tau}}}}\mathcal{H}(\beta) - \int_0^{\frac{\xi-\lambda_c(\bar{\tau})}{\sqrt{\tau-\bar{\tau}}}}\mathcal{H}(\beta)d\beta\right]d\bar{\tau} \tag{A.4.4}$$

$$= \tilde{r}\int_0^{\tau}\frac{\tau-\bar{\tau}}{\sqrt{2\pi}}\left[\mathcal{P}\left(\frac{\xi+\lambda_c(\bar{\tau})}{\sqrt{\tau-\bar{\tau}}}\right) - \mathcal{P}\left(\frac{\xi-\lambda_c(\bar{\tau})}{\sqrt{\tau-\bar{\tau}}}\right)\right]d\bar{\tau} \tag{A.4.5}$$

with the change variable $\beta = (\xi-\bar{\xi})/\sqrt{\tau-\bar{\tau}}$, $|\xi-\bar{\xi}| = \xi-\bar{\xi}$ and using the definition of the function $\mathcal{P}$. In the case $\xi < \lambda_c(\bar{\tau})$, the same result can be obtained by using the fact that the function $\mathcal{H}$ is symmetrical without absolute value. Now, inside the domain $0 \leq \xi \leq \lambda_c(\bar{\tau})$, the absolute value can be decomposed in two parts as function of the position

$$|\xi-\bar{\xi}| = \begin{cases} \xi-\bar{\xi} & \text{for} \quad \bar{\xi} \in [-\lambda_c(\bar{\tau});\xi] \\ \bar{\xi}-\xi & \text{for} \quad \bar{\xi} \in [\xi;\lambda_c(\bar{\tau})] \end{cases} \tag{A.4.6}$$

Injecting it, in the fast equation

$$\eta(\xi,\tau) = \tilde{r}\int_0^{\tau}\sqrt{\frac{\tau-\bar{\tau}}{2\pi}}\Bigg[\int_{-\lambda_c(\bar{\tau})}^{\xi}\mathcal{H}\Big(\frac{\xi-\bar{\xi}}{\sqrt{\tau-\bar{\tau}}}\Big)d\bar{\xi} + \int_{\xi}^{\lambda_c(\bar{\tau})}\mathcal{H}\Big(\frac{\bar{\xi}-\xi}{\sqrt{\tau-\bar{\tau}}}\Big)d\bar{\xi}\Bigg]d\bar{\tau} \tag{A.4.7}$$

$$= \tilde{r}\int_0^{\tau}\frac{\tau-\bar{\tau}}{\sqrt{2\pi}}\Bigg[\int_0^{\frac{\xi+\lambda_c(\bar{\tau})}{\sqrt{\tau-\bar{\tau}}}}\mathcal{H}(\beta_1)d\beta_1 + \int_0^{\frac{\lambda_c(\bar{\tau})-\xi}{\sqrt{\tau-\bar{\tau}}}}\mathcal{H}(\beta_2)d\beta_2\Bigg]d\bar{\tau} \tag{A.4.8}$$

$$= \tilde{r}\int_0^{\tau}\frac{\tau-\bar{\tau}}{\sqrt{2\pi}}\Bigg[\mathcal{P}\Big(\frac{\xi+\lambda_c(\bar{\tau})}{\sqrt{\tau-\bar{\tau}}}\Big) + \mathcal{P}\Big(\frac{\lambda_c(\bar{\tau})-\xi}{\sqrt{\tau-\bar{\tau}}}\Big)\Bigg]d\bar{\tau} \tag{A.4.9}$$

where the 2 change variables are $\beta_1 = (\xi-\bar{\xi})/\sqrt{\tau-\bar{\tau}}$ and $\beta_2 = (\bar{\xi}-\xi)/\sqrt{\tau-\bar{\tau}}$. For the first term, $\bar{\xi} = -\lambda_c(\bar{\tau}) \rightarrow \beta_1 = \xi + \lambda_c(\bar{\tau})/\sqrt{\tau-\bar{\tau}}$ and $\bar{\xi} = \xi \rightarrow \beta_1 = 0$. For the second integrand, we have $\bar{\xi} = \lambda_c(\bar{\tau}) \rightarrow \beta_2 = (\lambda_c(\bar{\tau})-\xi)/\sqrt{\tau-\bar{\tau}}$ and $\bar{\xi} = \xi \rightarrow \beta_2 = 0$

A.5 Functions $\varphi(\lambda)$

The two functions defined at first leading order $\varphi_\nu(\lambda)$ and $\varphi_\kappa(\lambda)$ can be written in terms of Fresnel and trigonometric functions

$$\varphi_\nu(\lambda) = \frac{4}{\pi}\int_0^{+\infty}\frac{\lambda^3\mathcal{H}(\beta)}{(\beta^2+\lambda^2)^2}d\beta = \cos\Big(\frac{\lambda^2}{4}\Big)\Big[1-2\mathcal{S}\Big(\frac{\lambda}{\sqrt{2\pi}}\Big)\Big] - \sin\Big(\frac{\lambda^2}{4}\Big)\Big[1-2\mathcal{C}\Big(\frac{\lambda}{\sqrt{2\pi}}\Big)\Big] \tag{A.5.1}$$

$$\varphi_\kappa(\lambda) = -\frac{4}{\pi}\int_0^{+\infty}\frac{\lambda\mathcal{H}''(\beta)}{\beta^2+\lambda^2}d\beta = \cos\Big(\frac{\lambda^2}{4}\Big)\Big[1-2\mathcal{C}\Big(\frac{\lambda}{\sqrt{2\pi}}\Big)\Big] + \sin\Big(\frac{\lambda^2}{4}\Big)\Big[1-2\mathcal{S}\Big(\frac{\lambda}{\sqrt{2\pi}}\Big)\Big] \tag{A.5.2}$$

To obtain the results more easily, the idea is to rewritten the others functions in terms of φ_ν and φ_κ. Using *Mathematica* these functions can be expressed in terms of Fresnel and trigonometric functions. For example, with the function $\varphi_q(\lambda)$, we have

$$\varphi_q(\lambda) = \frac{64}{\pi}\int_0^{+\infty}\frac{\beta^2\lambda^3(\beta^2-\lambda^2)^2}{(\beta^2+\lambda^2)^5}\mathcal{H}(\beta)d\beta \tag{A.5.3}$$

$$= \frac{1}{24}\Bigg[24\sqrt{\frac{2}{\pi}}\lambda^3 + \cos\Big(\lambda^2/4\Big)\Big(24-36\lambda^2-14\lambda^4+\lambda^6-2\lambda^2(-36+\lambda^4) \tag{A.5.4}$$

$$\mathcal{C}[\lambda/\sqrt{(2\pi)}] + 4(-12+7\lambda^4)\mathcal{S}[\lambda/\sqrt{2\pi}]\Big) + \sin[\lambda^2/4]\Big(-24-36\lambda^2+14\lambda^4 \tag{A.5.5}$$

$$+\lambda^6 + (48-28\lambda^4)\mathcal{C}[\lambda/\sqrt{2\pi}] - 2\lambda^2(-36+\lambda^4)\mathcal{S}[\lambda/\sqrt{2\pi}]\Big)\Bigg] \tag{A.5.6}$$

$$= \sqrt{\frac{2}{\pi}}\lambda^3 + \frac{\lambda^6-36\lambda^2}{24}\varphi_\kappa(\lambda) + \frac{12-7\lambda^4}{12}\varphi_\nu(\lambda) \tag{A.5.7}$$

In the same way, the others functions can be read as

$$\varphi_p(\lambda) = \frac{8}{\sqrt{2\pi}} \int_0^{+\infty} \frac{\beta\lambda^4}{(\beta^2+\lambda^2)^3} \mathcal{P}(\beta) d\beta = \frac{\sqrt{\pi}}{2\sqrt{2}} \lambda \varphi_\nu(\lambda) \tag{A.5.8}$$

$$\varphi_\alpha(\lambda) = \frac{16}{\pi} \int_0^{+\infty} \frac{\lambda^3\beta^2}{(\beta^2+\lambda^2)^3} \mathcal{H}(\beta) d\beta = \varphi_\nu(\lambda) - \frac{\lambda^2}{2} \varphi_\kappa(\lambda) \tag{A.5.9}$$

$$\varphi_\lambda(\lambda) = -\frac{8}{\pi} \int_0^{+\infty} \frac{\lambda^3\beta^3}{(\beta^2+\lambda^2)^3} \mathcal{H}'(\beta) d\beta = \frac{3}{4}\lambda^2 \varphi_\kappa(\lambda) - \frac{\lambda^3}{2\sqrt{2\pi}} + \frac{\lambda^4}{8} \varphi_\nu(\lambda) \tag{A.5.10}$$

$$\varphi_{\dot{\kappa}}(\lambda) = -\frac{8}{\pi} \int_0^{+\infty} \frac{\beta^2\lambda}{(\beta^2+\lambda^2)^2} \mathcal{H}''(\beta) d\beta = \varphi_\kappa(\lambda) - \sqrt{\frac{2}{\pi}}\lambda + \frac{\lambda^2}{2} \varphi_\nu(\lambda) \tag{A.5.11}$$

$$\varphi_{\dot{\lambda}}(\lambda) = \frac{16}{\pi} \int_0^{+\infty} \frac{\beta^3\lambda}{(\beta^2+\lambda^2)^2} \mathcal{H}'''(\beta) d\beta = 4\lambda\sqrt{\frac{2}{\pi}} - 3\lambda^2 \varphi_\nu(\lambda) + \frac{\lambda^4}{2} \varphi_\kappa(\lambda) \tag{A.5.12}$$

$$\varphi_{\dot{p}}(\lambda) = -\frac{8}{\pi} \int_0^{+\infty} \frac{\lambda^2\beta}{(\beta^2+\lambda^2)^2} \mathcal{H}'(\beta) d\beta = \lambda \varphi_\kappa(\lambda) \tag{A.5.13}$$

$$\varphi_r(\lambda) = \frac{16}{\pi} \int_0^{+\infty} \frac{\beta^3\lambda^2(\beta^4+3\lambda^4)}{(\beta^2+\lambda^2)^5} \mathcal{H}'(\beta) d\beta = \varphi_\nu(\lambda) \frac{\lambda^3(\lambda^4-84)}{192} + \varphi_\kappa \frac{\lambda(3\lambda^4-44)}{32} - \frac{\lambda^2(\lambda^4-60)}{48\sqrt{2\pi}} \tag{A.5.14}$$

$$\varphi_s(\lambda) = -\frac{8}{\pi} \int_0^{+\infty} \frac{\beta^2\lambda(\beta^4+3\lambda^4)}{(\beta^2+\lambda^2)^4} \mathcal{H}''(\beta) d\beta = \varphi_\nu \frac{\lambda^2(36-\lambda^4)}{48} + \varphi_\kappa(\lambda) \frac{4-\lambda^4}{4} + \frac{\lambda(\lambda^4-24)}{12\sqrt{2\pi}} \tag{A.5.15}$$

$$\varphi_t(\lambda) = -\frac{8}{\pi} \int_0^{+\infty} \frac{\beta\lambda^2(\beta^2-\lambda^2)^2}{(\beta^2+\lambda^2)^4} \mathcal{H}'(\beta) d\beta = \varphi_\nu(\lambda) \frac{\lambda^3}{3} + \varphi_\kappa(\lambda) \frac{\lambda(12-\lambda^4)}{24} - \frac{\lambda^2}{\sqrt{2\pi}} \tag{A.5.16}$$

A.6 Shapes function

In Figure A.1, the 3^{th} order Hermitian shape functions is represented with $\xi \in [0; 1]$ having the following form

$$N_1(\xi) = 1 - 3\xi^2 + 2\xi^3; \tag{A.6.1}$$
$$N_2(\xi) = l_e\xi(1 - \xi)^2; \tag{A.6.2}$$
$$N_3(\xi) = \xi^2(3 - 2\xi); \tag{A.6.3}$$
$$N_4(\xi) = l_e\xi^2(\xi - 1) \tag{A.6.4}$$

where l_e is the length element beam.

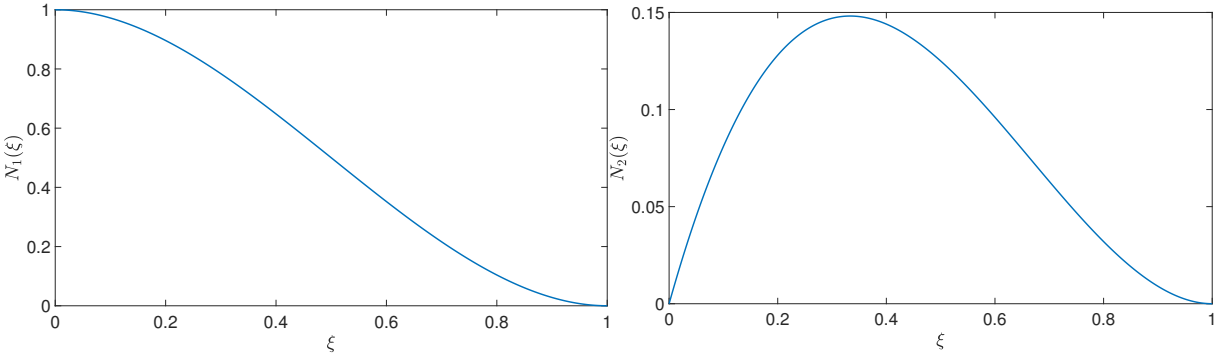

(a) $N_1(\xi)$.

(b) $N_2(\xi)$.

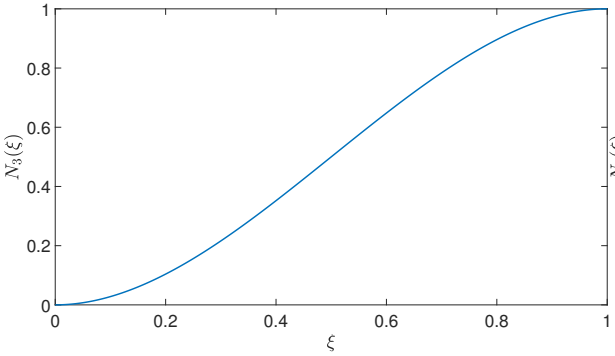

(c) $N_3(\xi)$.

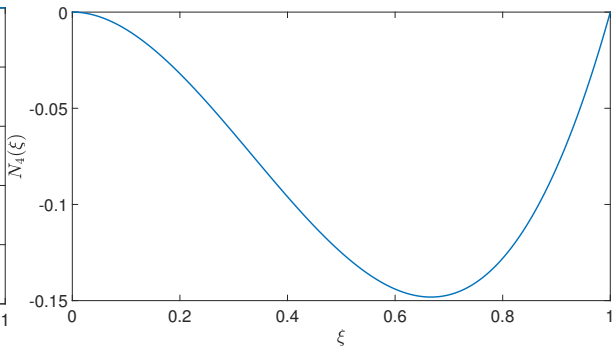

(d) $N_4(\xi)$.

Figure A.1: 3^{th} order Hermitian shape functions.

A.7 Comparison middle and node methods

For $K = 1/80\ [m^{-1}]$, $V_0 = 20\ [m/s]$ and $\Delta x = 2.5 \cdot 10^{-3}\ [m]$, because the curvature is very small, no apparent difference is detected between the 2 methods. An another case is investigated with $K = 1\ [m^{-1}]$ to see if this offset can be observed for continuous contact. The transverse displacement to activate the constraint at the middle of the first element is $1.5 \cdot 10^{-6}$ which is two order bigger than for $K = 1/80\ [m^{-1}]$ with $1.45 \cdot 10^{-8}\ [m]$. Thus, the time needed is $7.5 \cdot 10^{-8}\ [m]$ which is clearly bigger than the time step (three times). In Figure A.2, we can observe that the first jump occurs later for the middle method compared to node method which is due the offset before the constraint is activated. For this simulation, because the ratio κ/ν is bigger the contact evolution evolves slower and need consequently to refine the mesh in the domain contact (Section 3.4).

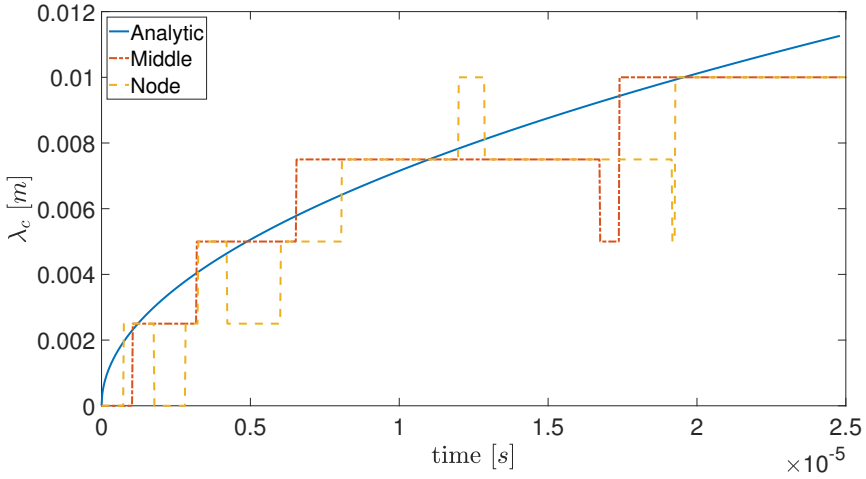

Figure A.2: Contact length evolution.

In Figure A.3, the results of the reaction contact at one side of the beam are shown without filtering. For the contact node, the result seems to be more noisy compared to the middle method. After filtering the solution, in Figure 3.26, the same behavior is found for the two models. Thus, the middle node seems better by the fact that less noise is generated.

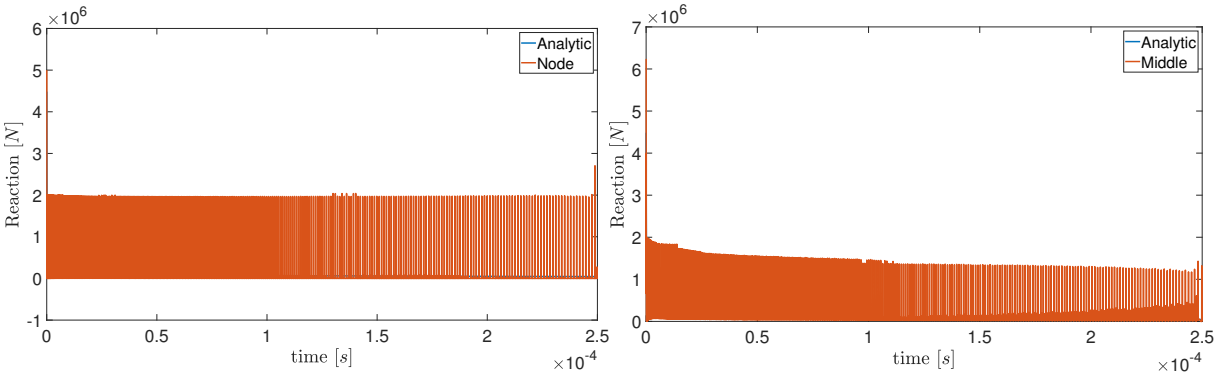

(a) Node method. **(b)** Middle.

Figure A.3: Comparison of the reaction expressed in $[N]$.

References

[1] V. Denoël and E. Detournayl. *On the Nature of Symmetrical Contacts of a Beam Impacting a Rigid Wall*. not publish.

[2] Homer Reid. Lecture notes: Multiple-scales approach to nonlinear oscillators, 2015.

[3] Vincent Denoël. Perturbation methods. University Lecture, 2018-2019.

[4] Karl F.Graff. *Wave Motion in Elastics Solids*. Oxford University Press, 1975.

[5] Moiseev Dimitri. *Multiple Scales Analysis of the Impact of a Vibrating Beam on a Rigid Wall*. 2011-2012.

[6] J.-P. Ponthot. F.e.m. - chapter 12 beam elements and frame structures. University Lecture, 2016.

[7] M. Géradin and D. Rixen. *Théorie des vibrations Application à la dynamique des structures*. Masson, 1996.

[8] Fehmi Cirak. Finite element formulation for beams.

[9] Henri P. Gavin. *Structural Element Stiffness, Mass, and Damping Matrices*. Duke University, 2018.

[10] Lumped and consistent mass matrices. `https://www.google.be/url?sa=t&rct=j&q=&esrc=s&source=web&cd=1&ved=2ahUKEwis57_T77biAhVE_aQKHXzsCB0QFjAAegQIBxAC&url=http%3A%2F%2Fkis.tu.kielce.pl%2Fmo%2FCOLORADO_FEM%2Fcolorado%2FIFEM.Ch31.pdf&usg=AOvVaw1VCM4LlOw6WCO8J6WVrpr4`. Accessed: 2019-04-20.

[11] Vincent Acary Olivier Brüls and Alberto Cardona. *On the Constraints Formulation in the Nonsmooth Generalized-α Method*. Springer International Publishing AG, 2018.

[12] Olivier Brüls. *Normal contact force: Continuous vs nonsmooth models*. University of Liège, 2015-2016.

[13] Olivier Brüls. *Matlab code for the simulation of multibody systems*. University of Liège, 2019.

[14] A.Kissélev M.Krasnov and G. Makarenko. *Equations intégrales problèmes et exercices*. MIR, 1977.